ELECTROCHEMICAL MACHINING

- NEW MACHINING TARGETS AND ADAPTATIONS with
SUITABILITY FOR MICROMANUFACTURING

A thesis submitted for the degree of

Doctor of Philosophy

By

Rebecca Jane Leese

College of Engineering, Design and Physical Sciences

Department of Mechanical, Aerospace and Civil Engineering

Brunel University

March 2016

Abstract

Electrochemical machining (ECM) is a non-conventional machining technique capable of machining any conductive substrate, regardless of its physical properties e.g. hardness. ECM became an attractive method due to its ability to machine substrates without creating a defective surface layer.

ECM utilises electrolysis; a small gap is maintained between two electrodes whilst a favourable potential is applied between them to remove material from the workpiece. The parameters are adjusted to obtain the desired machining results i.e. surface finish, machining resolution and machining rate.

Much work has been conducted for the anodic dissolution of stainless steels and brass but little work outside of these materials is available. This work demonstrates the applicability of ECM for a new range of materials; superconductors and semiconductors, along with the application of ECM for medical needle production and an alteration to the machine set up to anodically dissolve titanium metal at reduced potentials.

Through a series of electrochemical techniques, namely polarisation curves, machining potentials were defined for a cuprate superconductor and a semiconductor. These were then demonstrated as suitable settings by completing tests on an electrochemical machine. Hypodermic needles were created on an electrochemical machine and polarisation curves of titanium with the addition of ultrasonic vibrations were used to demonstrate the anodic dissolution of titanium at much reduced potentials.

Acknowledgement

I would like to express my gratitude to the people who have helped and supported myself to realise this project.

Firstly, I would like to thank my supervisor, Dr Atanas Ivanov, for his guidance, time, effort, encouragement and endless patience to make this project a success. Not forgetting Paul Yates, Qing-Ping Yang, Hari Babu-Nadendla, Ruth Mackay, Angel Naveenathayalan and Alex Spieser for their help and friendship.

Sincere gratitude is also extended to those at pECM Systems Ltd; namely Steve Duffield who allowed the use of their ECM machines and David Moulton who assisted with the day-to-day running of the equipment and set-up.

I would also like to thank Brunel University for financing my Ph.D. studies.

And lastly, I would like to thank my family for their never-ending support, belief and encouragement throughout.

I dedicate this project to those mentioned above.

Table of Contents

List of Figures

List of Tables

List of Abbreviations

BCAST	Brunel Centre for Advanced Solidification Technology
CELT	Confined etchant layer technique
CNC	Computer numerical control
e$^-$	Electron
EBM	Electron beam machining
ECM	Electrochemical machining
ECMM	Electrochemical micromachining
EDL	Electrical double layer
EDM	electro-discharge machining
EDS	Energy-dispersive X-ray spectroscopy
Fe	Iron
Fe(OH)$_2$	Iron hydroxide
GaAs	Gallium arsenide
Gd123	$GdB_2Cu_3O_7$
Gd211	Gd_2BCuO_5
GdBCO-Ag	Gadolium barium copper oxide with silver inclusions
H	Hydrogen
H$_2$SO$_4$	Sulphuric acid
HCl	Hydrochloric acid
HSM	High speed machining
HTS	High temperature superconductor
IEG	Inter-electrode gap
InSb	Indium antimonide
LBM	Laser beam machining
LHC	Large Hadron collider
M	Molar concentration
MEMS	Microelectromechanical systems
MREF-ECM	Modulated reverse electric field electrochemical machining
MRI	Magnetic resonance imaging

MRR	Material removal rate
NaBr	Sodium bromide
NaCl	Sodium chloride
NaClO$_3$	Sodium chlorate
NaNO$_3$	Sodium nitrate
NaOH	Sodium hydroxide
Ni	Nickel
OCP	Over-current protector
PECM	Pulse electrochemical machining
Pt	Platinum
SC	Superconductor
SDSS	Super-duplex stainless steel
SEM	Scanning electron microscopy
SQUIDS	Superconducting quantum interference devices
Ti	Titanium
USM	Ultrasonic machining
USV	Ultrasonic vibrations
WC-Co	Tungsten carbide with cobalt binder
WJC	Water jet cutting
YBCO	Yttrium barium copper oxide

List of Symbols

C	Capacitance
CD	Critical dimension
$\mathbf{c_{DL}}$	Specific electrical double layer capacity
$\mathbf{c_O}$	Concentration of oxidant
$\mathbf{c_R}$	Concentration of reductant
d	Local separation
$\mathbf{E_e}$	Cell potential
$\mathbf{E_e^0}$	Formal potential of the couple O/R
eV	Electron volts
F	Faraday constant (96486 C mol^{-1})
I	Current
K	Kelvin
m	Mass removed
M	Molar mass
n	Number of electrons
NA	Numerical aperture
Q	Charge passed
R	Resistivity
R	Gas constant
t	Time
T	Temperature
T	Tesla - strength of magnetic field
$\mathbf{t_{off}}$	Pulse off-time
$\mathbf{t_{on}}$	Pulse on-time
V	Voltage
z	Valence number
λ	Wavelength of light
ρ	Specific electrolyte resistivity
τ	Time constant for double layer charging

Chapter 1 – Introduction

Electrochemical machining (ECM) is a non-conventional machining technique capable of machining a conductive work piece irrespective of its physical properties e.g. hardness. ECM utilises an electrolysis process called anodic dissolution. It is a non-contact, heat and stress-free material removal process, whereby a DC current is applied between two electrodes submerged in an electrolyte, usually salt water, which is continuously flushed through the gap between the electrodes. Material is removed from the anode, the positively charged electrode, replicating the tool electrode in reverse. (McGeough 1988)

Much work has been conducted in the ECM field using stainless steels, brass and super alloy. However, little work has been published considering less common materials, such as semiconductors and superconductors both of which are hard to machine conventionally due to their brittleness. Titanium alloys have also been machined with ECM but require high potentials due to the chemical resistance of the oxide layer which forms on the surface.

1.1   Aim and Objectives

Electrochemical machining is still a specialised machining technique with niche customers across a range of industries, from aerospace, automotive and medical sectors to name a few. However, ECM only currently targets a few brackets of materials, namely stainless steels and super-alloys which pose difficulties with conventional machining due to their hardness or other physical properties.

Some materials, such as titanium, require high machining voltages to break through the passive surface layer. This makes the process energy intensive, increasing the cost of machining this type of material.

This research aims to expand the range of target materials that can be machined with ECM into superconductor and semiconductor materials, as

well as reducing the machining voltages required for the anodic dissolution of pure titanium metal.

This thesis also proposes to outline a method to electrochemically sharpen hypodermic needles with a single process step at a superior surface finish than that of those currently produced via mechanical grinding.

1.2   Description of Chapters

This section gives a brief summary of what can be found in the chapters to follow:

- Chapter 2 – Literature Review – This chapter gives an overview of the electrochemical machining process along with how each machining parameter, e.g. voltage, electrolyte concentration etc., affects the outcome in terms of resolution and surface finish amongst other things.

- Chapter 3 – Anodic Dissolution of Superconductors – This chapter provides experimental methods and results of the anodic dissolution of gadolinium barium copper oxide (GdBCO) in a non-aqueous electrolyte.

- Chapter 4 – Anodic Dissolution of Semiconductors - This chapter details experimental methods and results for the anodic dissolution of indium antimonide (InSb) and how some machining parameters affected the overall result.

- Chapter 5 –Anodic Dissolution of Titanium with the Addition of Ultrasonic Vibrations – This chapter highlights the importance of titanium metal and discusses the difficulties encountered with conventional and non-conventional machining of this material. This chapter goes on to provide a potential solution to reducing the potentials required for the anodic dissolution of pure titanium metal in ECM.

- Chapter 6 – Electrochemical Production of Hypodermic Needle Tips – This chapter gives an insight into the methods and experimental results obtained from a series of experiments to produce hypodermic needle tips on an ECM machine. It discusses suitable electrolytes and brief details on a tool design.

- Chapter 7 – Conclusions and Further Work – This chapter gives a complete summary of the work covered in this thesis along with details of further work which enhance this body of work.

Chapter 2 – Literature Review

2.1   Introduction

Micro-machining has gained importance in recent years due to a drive towards miniaturisation which has focussed research into many micromachining techniques. Conventional machining techniques, such as drilling and milling are unsuitable for many micro-machining applications due to the stresses imparted on the work pieces. (Leese & Ivanov 2016b)

Non-conventional machining techniques such as electro-discharge machining (EDM), laser beam machining (LBM), electron beam machining (EBM), ultrasonic machining (USM) and electrochemical machining (ECM) have all been utilised in micro-machining. However, EDM, LBM and EBM are all thermal machining processes, creating a heat-affected layer on the work piece surface during machining which then forms micro-cracks at the surface or change the material properties. USM is used primarily to machine brittle materials where conventional machining would cause crack formation. ECM, however, is a heat-free, stress-free machining technique. Whilst ECM theoretically has atomic-scale machining accuracy, it has not been used as commonly as the other methods due to the occurrence of stray erosion and inaccuracies when machining.

Much research has been conducted over the last two decades to understand and develop the ECM process on the micro-scale; from applying nano-second potential pulses to reducing the inter-electrode gap (IEG) to using passivating electrolytes. These changes will be discussed in more detail later in this thesis.

ECM is a technique which utilises an electrolysis process called anodic dissolution. Anodic dissolution is the opposite reaction to electrolytic plating which is used to improve parts properties (e.g. corrosion resistance) or physical appearance (e.g. in the jewellery industry where less expensive metals are plated with smaller amounts of precious metals). ECM has many

advantages over other traditional machining techniques; any conductive material can be machined regardless of its mechanical properties e.g. hardness; it's a virtually stress-free process with very little tool wear; complex shapes can also be obtained in one machining step which wouldn't be ordinarily reached with conventional machining techniques. This work will review research conducted in electrochemical micromachining (ECMM) Figure 2-1 shows a flow diagram for the structure of this chapter.
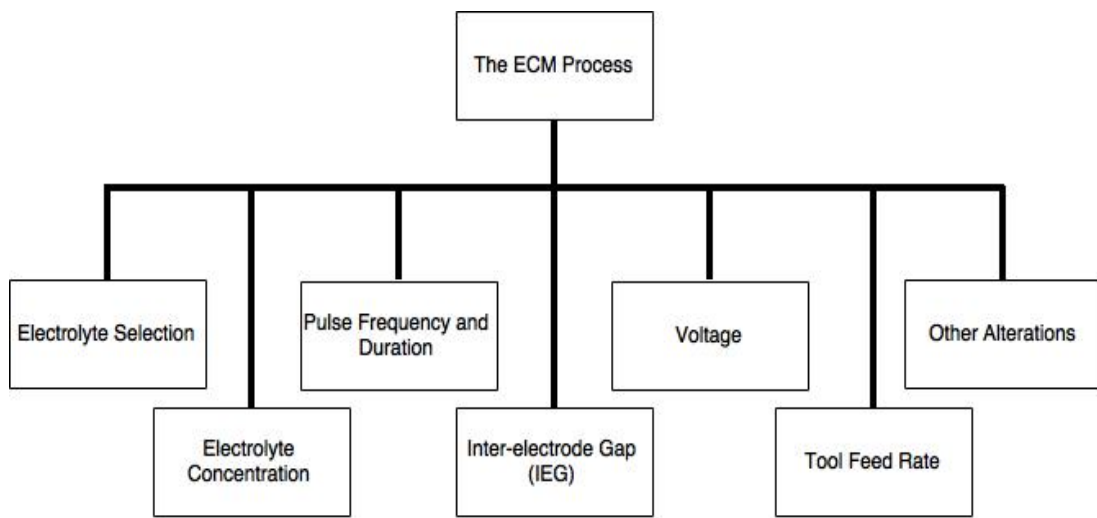
Figure 2-1 Diagram for structure of the chapter

2.2   The ECM Process

Electrochemical machining is a machining technique based on electrolysis. Electrolysis uses the passage of current between two electrodes immersed in a conductive solution, called an electrolyte, to perform chemical reactions at the electrodes. Current is passed between a work piece, which is the positively charged electrode, termed the anode and a tool, which is the negatively charged electrode, termed the cathode. Electrons are carried through the electrolyte in the form of ions. Depending on the potential applied, material can either be deposited or removed from the electrodes.

Anodic dissolution removes material according to Faraday's Law, see Equation 1:

$$m = \left(\frac{Q}{F}\right)\left(\frac{M}{z}\right) \qquad\qquad (1)$$

Where m is the mass removed in g, Q is the charge passed in C ($Q=It$ where I is current and t is time in s), F is Faraday constant (96485 C mol^{-1}), M is the molar mass of the work piece in g mol^{-1} and z is the valence number (number of electrons transferred per ion) which is a dimensionless number.
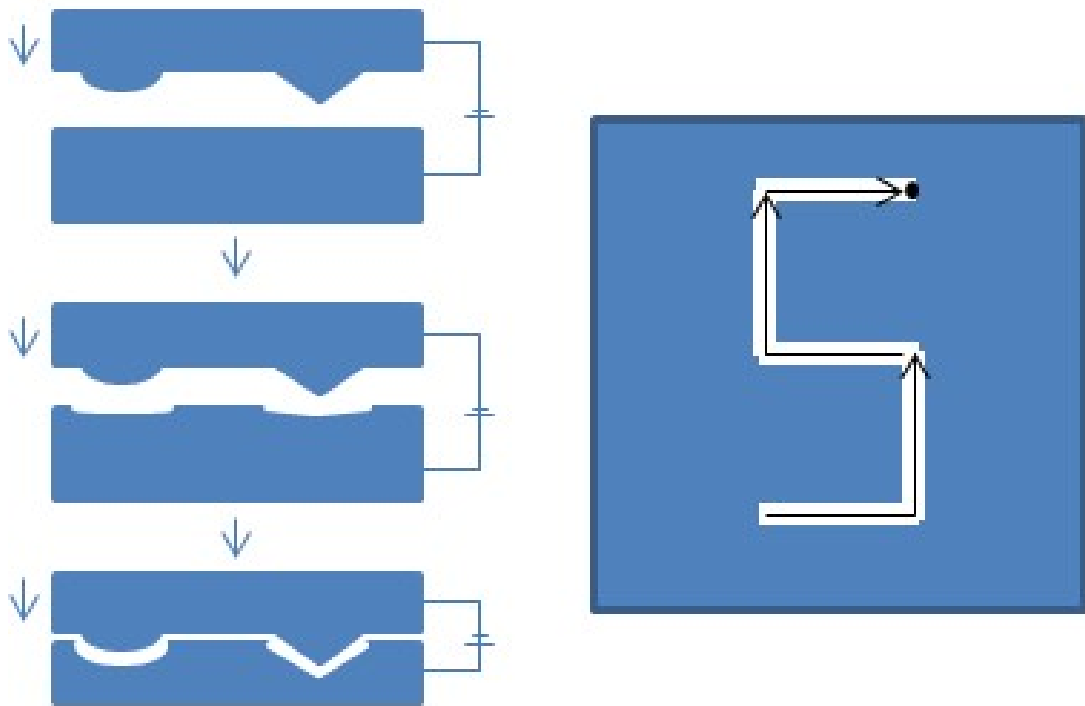
Figure 2-2: ECM Process a) with a complex tool (viewed from the side) and b) with a simple cylindrical tool (viewed from above) The arrow shows the path of the tool. The black dot is the tool.

The tool in ECM is advanced toward the work piece at a constant feed rate to maintain a constant IEG. A steady state gap is formed dependent on a number of factors which will be discussed later in this chapter. A negative copy of the tool is replicated in the work piece. Either a complex tool can be designed or a simple cylindrical tool can be moved in the X-Y plane to create complex features in a way similar to computer numerical control (CNC) milling, as shown in Figure 2-2.

(1)

Using the dissolution of iron in sodium chloride (NaCl) as an example, the dissolution process will be discussed in more detail. Iron is known to actively dissolve in a simple salt solution of NaCl. Ions in the electrolyte are affected by three transport mechanisms; diffusion, convection and migration. Diffusion is the movement of ions from a region of high concentration to a lower concentration. Iron ions are dissolved at the anode surface and diffuse across a thin, stagnant layer of electrolyte at the electrode surface toward the bulk electrolyte where iron ion concentration is much lower. Convection is movement induced by an external force; in the case of ECM the electrolyte is forced through the IEG at high pressure and speed which carries ions away from the IEG. Migration is the movement of ions due to a potential field, i.e. positive ions are electrostatically attracted to a negatively charged cathode tool and vice versa. In this example, iron is dissolved at the anode and hydrogen gas is evolved at the cathode; the reactions are as follows.

Anode: $Fe \rightarrow Fe^{2+} + 2e^-$

Cathode: $2H^+ + 2 e^- \rightarrow H_2\uparrow$
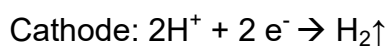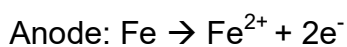
Iron is not deposited on the cathode as the iron ions react with hydroxide ions in the solution to form iron hydroxide ($Fe(OH)_2$) which is insoluble so precipitates to form a sludge. The solid reaction products are filtered from the electrolyte. Figure 2-3 shows a visual representation of the basic reactions occurring during ECM.

The electrolyte is flushed through the IEG to remove reaction products which may cause sparks or short circuits during machining due to increased electrical resistivity in the IEG. The electrolyte also removes heat from the reaction region caused by Joule Heating. If the reaction products are not removed from the machining zone, a metal hydroxide layer could build up at the work piece surface limiting the reaction.
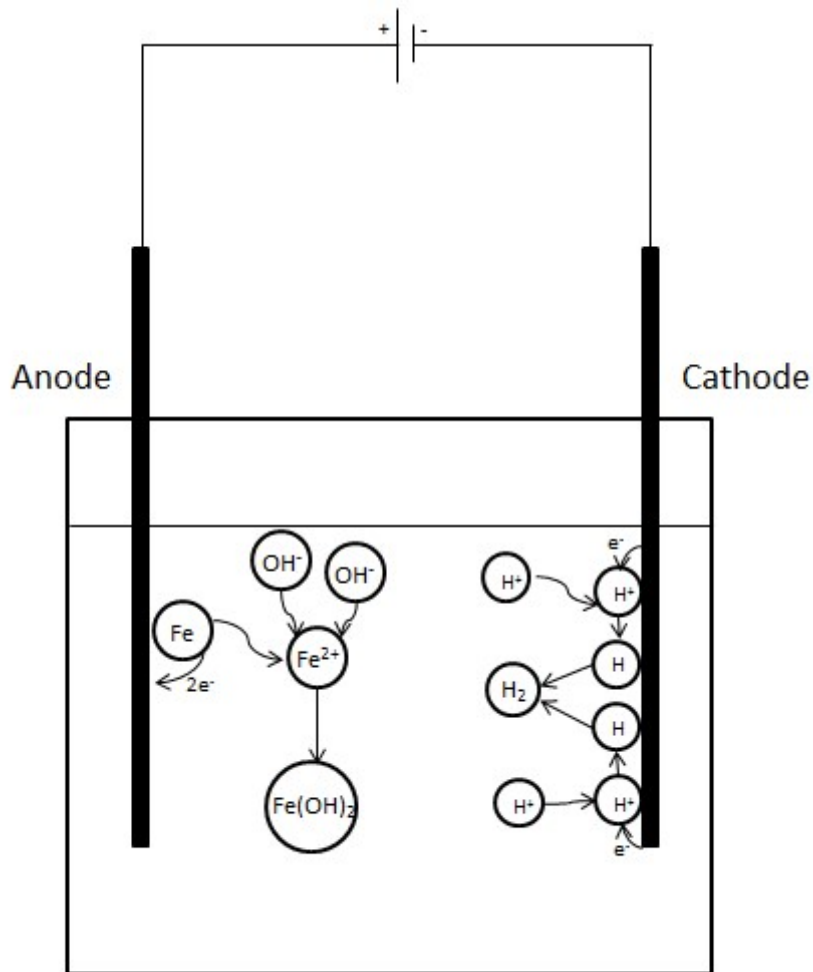
Figure 2-3 Schematic of the basic reactions during ECM (Leese & Ivanov 2016c)

2.3   Electrochemical Micro-Machining

Electrochemical micro-machining (ECMM) is an advanced version ECM where machining is confined to much smaller areas on the work piece to create high aspect ratio holes, shapes and tools on the micro-scale. There are many factors which affect machining accuracy; including electrolyte selection; electrolyte concentration; pulse frequency and duration; IEG size; voltage and feed rate.

2.3.1 Electrolyte Selection

The electrolyte in ECMM is a crucial parameter; it provides the conditions needed for reactions to occur, namely a conductive environment. The ideal electrolyte should have high conductivity, low viscosity, be non-corrosive and inexpensive. The most common electrolytes used are sodium chloride (NaCl) and sodium nitrate ($NaNO_3$) although many others are used.

The electrolyte chosen depends on the work piece material and the desired result, i.e. accuracy, material removal rate (MRR) or surface finish. Table 2-1 shows some electrolytes used for a range of metals commonly machined with ECM (Wendt & Kreysa 2013).

There are two main types of electrolyte; passive and non-passive electrolytes. Passive electrolytes contain oxidising anions such as nitrate. These provide better precision due to the formation of a protective oxide film. Oxygen is usually evolved in the stray current regions. Non-passive electrolytes contain more aggressive anions, such as chloride. (Bhattacharyya et al. 2004) The material removal rate is usually much higher with these electrolytes but the precision is lower in comparison to passive electrolytes (Da Silva Neto et al. 2006).

Acidic electrolytes are sometimes chosen to prevent the build-up of solid machining products which can collect in the IEG slowing machining. Tungsten carbide (WC-Co) is machined with sulphuric acid (H_2SO_4) as tungsten and cobalt can be machined simultaneously. (Choi et al. 2013) Some metals also show enhanced machining in basic electrolytes, e.g. tungsten in sodium hydroxide (NaOH).

All of the electrolyte examples above are aqueous electrolytes. Some materials are water-sensitive so an aqueous electrolyte is inappropriate. In these cases non-aqueous electrolytes are used, such as glycerol based electrolytes. The conductivities of organic-based electrolytes are low in comparison to aqueous electrolytes due to difficulties in dissolving salts in

them. This results in lower machining rates but enhances machining precision. High resistivity electrolytes, such as glycerol-based electrolytes, are commonly used for electro-polishing, another variant of ECM, as the difference in current density between peaks and troughs is greater, resulting in preferential dissolution.(Inman et al. 2011)

2.3.2 Electrolyte Concentration

Electrolyte concentration also plays a role in machining accuracy and machining rates in ECMM. The concentration of the electrolyte determines its electrical conductivity; the higher the concentration, the higher the electrolyte conductivity. Many studies have been conducted researching how electrolyte concentration affects ECM and ECMM machining. (Ayyappan & Sivakumar 2014a; Ayyappan & Sivakumar 2014b; Bannard 1977; Bhattacharyya & Munda 2003; Das & Saha 2014; Datta 1993; Datta & Landolt 2000; Fan et al. 2012; Ghoshal & Bhattacharyya 2013; Jain et al. 2012; Jain & Gehlot 2015; Rathod et al. 2014; Saravanan et al. 2012; Bhattacharyya et al. 2004; M. Wang et al. 2010; Wu et al. 2013; Zhang 2010; Trimmer et al. 2003; De Silva et al. 2003) Accuracy is highly important when machining micro-features as errors appear much larger at this small scale.

Bhattacharyya et al (Bhattacharyya et al. 2004) observed that with a lower concentration, higher voltage and a moderate value for pulse-on time that machining accuracy was improved with a moderate MRR. Ayyappan et al (Ayyappan & Sivakumar 2014a) observed that a higher concentration lead to a higher MRR and better surface finish in an oxygenated electrolyte of NaCl for 20MnCr5 steel . Ayyappan et al (Ayyappan & Sivakumar 2014b) also stated that a higher electrolyte concentration *'allows for more ions for ionization'* which in turn increases MRR. Bannard (Bannard 1977) observed that the dissolution current was higher for higher electrolyte concentrations and the increase in kinetics is why highly concentrated electrolytes are employed in ECM. Bhattacharyya and Munda (Bhattacharyya & Munda 2003) presented results which showed that a lower concentration in combination with a

Table 2-1 Common electrolytes for a range of metals (Wendt & Kreysa 2013)

Metal	Electrolyte	Remarks
Aluminium and its alloys	NaNO$_3$ (100-400 g dm^{-3})	Excellent surface finishing
Cobalt and its alloys	NaClO$_3$ (100-600 g dm^{-3})	Excellent dimensional control, excellent surface finishing
Molybdenum	NaOH (40-100 g dm^{-3})	NaOH consumed and must be added continuously
Nickel and its alloys	NaNO$_3$ (100-400 g dm^{-3})	good surface finishing
	NaClO$_3$ (100-600 g dm^{-3})	good dimensional control, good surface finishing and low metal removal rate
Titanium and its alloys	NaCl (180 g dm^{-3}) + NaBr (60 g dm^{-3}) + NaF (2.5 g dm^{-3})	good dimensional control, good surface finishing and good machining rate
	NaClO$_3$ (100-600 g dm^{-3})	Bright surface finish, good machining rate above 24V
Tungsten	NaOH (40-100 g dm^{-3})	NaOH consumed and must be added continuously
Steel and iron alloys	NaClO$_3$ (100-600 g dm^{-3})	Excellent dimensional control, brilliant surface finish, high metal removal rate, fire hazards when dry
	NaClO$_3$(100-400 g dm^{-3})	Good dimensional control, lower fire hazard, good surface finish and good machining rate
	NaNO$_3$ (100-400 g dm^{-3})	Good dimensional control, fire hazard when dry, low metal removal rates, rough surface finish

larger machining voltage and a *'moderate pulse on time'* produced more accurate shapes at a moderate MRR as the stray current effect is less.

Das and Saha (Das & Saha 2014) were attempting to create cylindrical micro-tools with ECMM and found that the reaction was non-uniform at higher electrolyte concentrations, possibly due to the difficulties in thoroughly cleaning the IEG changing the conductivity of the solution between the electrodes. This lead to shorter cylindrical tools formed in higher concentration electrolytes. Higher concentrations (> 3 M) were detrimental to the surface finish. Datta (Datta 1993) observed that the anion type and concentration affected the MRR. The formation of a salt film on the anode surface may occur more readily at higher salt concentrations leading to a better surface finish. Datta and Landolt (Datta & Landolt 2000) later witnessed that the current distribution is dependent on the electrolyte concentration. This was observed during electrochemical deposition, the process analogous, yet opposite, to ECM. During electrochemical micro-drilling with a mixed electrolyte of hydrochloric acid (HCl) and sodium chloride (NaCl) Fan et al (Fan et al. 2012) showed that the machining overcut increased as the sodium chloride concentration was increased. Although above a certain NaCl concentration (> 0.35 M) the overcut began to decrease when in combination with 0.3 M HCl. It cannot be certain this is a trend which occurs repeatedly in ECM as this was not confirmed for the mixed electrolyte containing 0.1 M HCl.

Ghosal et al (Ghoshal & Bhattacharyya 2013) created micro-channels in S-304 stainless steel with a sulphuric acid electrolyte (H_2SO_4). They found that the channel width varied more with a less concentrated electrolyte. This was thought to occur due to the small number of ions in the solution taking part in ECMM which could cause micro-sparks increasing the standard deviation of the channel width. They also showed that a very low concentration (0.1 M) created a larger overcut than a 0.2 M and 0.3 M electrolyte, yet the 0.3 M electrolyte created a larger overcut than the 0.2 M electrolyte. They

concluded for their application that 0.2 M H_2SO_4 was the optimal concentration.

Jain et al (Jain et al. 2012) found that hole diameter first increased as the concentration increased but then decreases. They attributed this to the reduced ion mobility in solution because of the high concentration. In another case, Jain and Gehlot (Jain & Gehlot 2015) were investigating the effects of several variables on the produced shape with through-mask ECMM. They observed that undercut initially increased with concentration but then began to decrease with an increase in electrolyte concentration. In this case it was explained by an increase in current density which facilitated a shorter machining time in the vertical direction. This also meant the machining time in the lateral direction was reduced and here the effect of the machining time dominated over the increased current density, reducing the undercut.

Rathod et al (Rathod et al. 2014) created micro-grooves in stainless steel using a sulphuric acid electrolyte. Concentrations were only varied between 0.15 and 0.30 M. Up to 0.25 M, they observed an increase in overcut as the concentration was increased. Above 0.25 M the overcut began to reduce in size. This was explained by way of an increase in gas bubbles generated at the micro-tool surface, decreasing machining. Saravanan et al (Saravanan et al. 2012) observed the MRR increased with electrolyte concentration machining a super-duplex stainless steel (SDSS) using a sodium nitrate electrolyte with concentrations ranging between 0.4 and 0.5 M.

Wang et al (M. Wang et al. 2010) stated that the electrolyte concentration affected the current density distribution which in turn affected the current efficiency and accuracy with a higher concentration creating larger overcuts. Wu et al (Wu et al. 2013) created nano-tools with ECM for use in ECMM. They found the tool diameter increased with increased concentration. This is because the material removed per unit of time increases with concentration and the tip was being over-etched at higher electrolyte concentrations causing the tip to drop off.

Zhang (Zhang 2010) stated that high electrolyte concentration increases electrolyte conductivity and therefore a high current efficiency could be achieved. Trimmer et al (Trimmer et al. 2003) indicated a lower concentration lead to higher conductivities which *"necessitates shorter current paths and increases resolution of machining"*. They also stated that there is a lower limit to the concentration that can be used in ECM. This is because the ion content in the gap is not sufficient to completely charge the double layer capacitance.

De Silva et al (De Silva et al. 2003) observed that using a lower concentration increased the Joule heating in the gap which could cause process variations unless steps were taken to avoid this. They also performed experiments to confirm that the current density decreases much more quickly as the gap is increased at lower concentrations, showing that higher accuracy machining can be achieved with lower concentration electrolytes.

Most studies concluded a low electrolyte concentration was more beneficial when machining micro-features as it kept conductivities to a minimum which prevented large machining overcuts even though a compromise was made with respect to the MRR. This is different to macro-ECM operations where an importance is placed on the machining rate and compromises on accuracy and surface finish.

2.3.3 Pulse Frequency and Duration

Pulsed electrochemical machining (PECM) and ECMM utilise a pulsed potential as supposed to the constant potential used in ECM in order to achieve better resolution. Pulses are usually applied as a square wave with variations in amplitude (voltage), frequency and duration. Figure 2-4 shows an example waveform used during PECM.
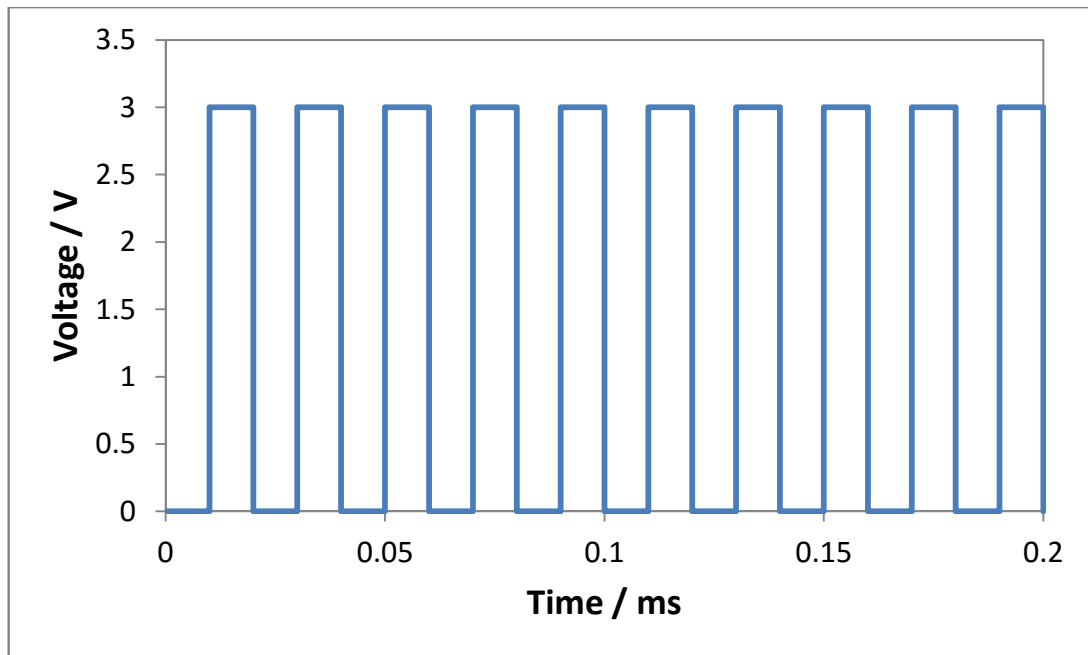
Figure 2-4 Pulsed Potential Wave

During PECM the pulse-off time is not usually equal to the pulse-on-time as shown in Figure 2-4. The pulse-off time is usually longer in duration than the pulse-on time to allow sufficient time for the electrolyte in the IEG to be completely refreshed, taking with it any reaction products. It also allows time for the double layer capacitor to fully discharge.

High frequency pulsed potential during ECM restricts the electrochemical reactions to regions on the work piece in close proximity of the tool. This phenomena is based on the time constant for electrical double layer (EDL) charging which varies with the *"local separation between the electrodes"* (Schuster et al. 2000). During nanosecond duration pulses, the time constant for charging the EDLs is small enough to allow significant charging only at electrode separations in the nano- to micro-meter range. Rates of electrochemical reactions are exponentially dependent on the potential drop in the double layer, resulting in the reactions being confined to the regions of the work piece in close proximity to the tool electrode which is fully polarised.

The EDL, on both electrodes, is a capacitor which becomes charged when a voltage is applied between them. The charging current has to pass through

15

the electrolyte, with the resistance encountered proportional to the length of the current path. Therefore the time constant is locally varied as:

$$\tau = RC = \rho d c_{DL} \tag{2}$$

where R is the resistivity of the electrolyte along the current path, C is the capacitance, ρ is the specific electrolyte resistivity, d is the local separation and c_{DL} is the specific EDL capacity. Due to this *"the electrodes will only be significantly charged where the local τ does not substantially exceed the pulse duration".* (Schuster et al. 2000) Where the electrodes are in close proximity, both the electrode separation and electrolyte resistance are low, whereas regions further away only become weakly polarised. For electrochemical reactions which are exponentially dependent on the potential drop in the EDL, reactions are strongly confined to the regions in close proximity of the tool. See Figure 2-5 for a model of the IEG.

Many researchers have investigated the influence of applying pulsed potential during ECM (Cook et al. 1967; Meijer & Veringa 1984; Van Damme et al. 2006; Zhang et al. 2011; Smets et al. 2010; Jo et al. 2009; Fan et al. 2012; Choi et al. 2013; Schuster et al. 2000; Kock et al. 2003; Bhattacharyya & Munda 2003; Bilgi et al. 2007; Das & Saha 2014; Trimmer et al. 2003; Zhang 2010; Saravanan et al. 2012; Lee et al. 2010; Xu et al. 2015; Cagnon et al. 2003; Bhattacharyya et al. 2002; Rajurkar et al. 1993; Sun et al. 2001; Datta & Landolt 1983; Mathew & Sundaram 2012; Rajurkar et al. 1998; Ghoshal & Bhattacharyya 2013; Rathod et al. 2014).
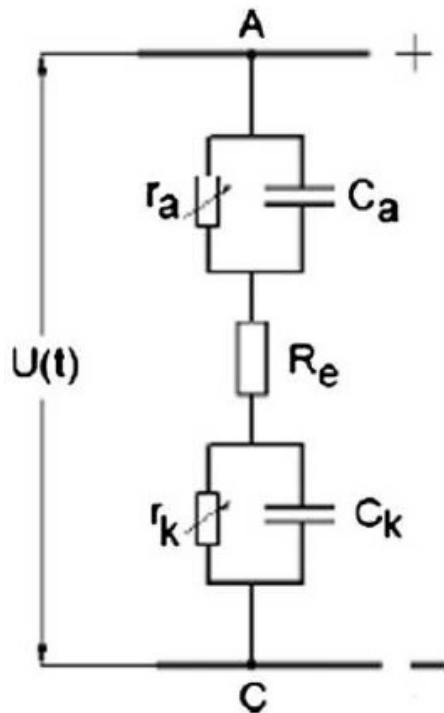
Figure 2-5 Model of the inter-electrode gap (Kozak et al. 2008)

Cook, Loutrel and Meslink (Cook et al. 1967) seem to be the first group to design and apply a pulsed power supply to an ECM system. The intention was to apply a short negative pulse after a positive pulse to remove the passive layer which was forming on the work piece, with the aim to improve material removal rates and allow machining of difficult to machine materials such as tungsten carbide (WC).

Choi et al (Choi et al. 2013) machined a tungsten carbide alloy (WC-Co) using a pulse duration of 100 ns with a pulse period of 1 µs. They noted that the pulse duration must be long enough to dissolve the oxide layer to prevent damage to the tool. Bhattacharyya and Munda (Bhattacharyya & Munda 2003) observed that with pulsed voltage the work piece dissolved uniformly whereas in direct current (DC) ECM when the IEG is very small, deposits can form on the tool leading to non-uniform machining at the work piece surface. Das and Saha (Das & Saha 2014) developed a pulse power supply to create micro-tools from WC-Co. They found that the cylindrical tool length increased

as the pulse on time increased but above 1800 ns spark machining is initiated, causing a deterioration in surface quality.

Fan et al (Fan et al. 2012) observed smaller over cuts and straighter edged holes for higher applied frequencies with the same duty cycle, where the duty cycle is defined as:

$$duty\ cycle = \frac{t_{on}}{t_{on}+t_{off}} \times 100 \qquad (3)$$

The same researchers also reported that over cut increased with increased pulse duration. This they attributed to the increased polarisation of the EDL and an increased production of hydrogen evolution which results in non-uniform machining.

Ghoshal et al (Ghoshal & Bhattacharyya 2013) produced taper-less holes in SS-304 stainless steel with a low concentration sulphuric acid electrolyte and a frequency of 5 MHz and a duty cycle of 40 % which relates to a pulse on time of 80 ns. Saravanan et al (Saravanan et al. 2012) observed that MRR increased as duty cycle was increased but decreased as frequency was increased. In this case they did not consider how these parameters affected the machining over-cut.

Zhang (Zhang 2010) witnessed that a short pulse on time with a long machining time led to a higher current efficiency at the macro-scale. Trimmer et al (Trimmer et al. 2003) utilised short voltage pulses to restrict stray machining to create high aspect ratio holes and complex patterns. They observed that a shorter pulse in combination with a low electrolyte concentration gave the best machining resolution.

Schuster et al (Schuster et al. 2000) are credited with applying pulsed voltages to improve resolution in ECM and take the applicability of ECM into micro- and nano technologies. Their calculations show a pulse of 30 ns should produce machining with a resolution of 1 µm.

Meijer and Veringa (Meijer & Veringa 1984) observed that PECM resulted in a better surface finish and tool reproduction than ECM. Van Damme et al and Smets et al (Van Damme et al. 2006; Smets et al. 2010) created models of the PECM process. They observed an off time > 90 ms allows the electrolyte in the IEG to be completely refreshed to bulk conditions, meaning each pulse is independent of the last pulse. As the pulses increase in length, a viscous salt layer builds on the work piece surface, eliminating water from the electrode surface. This prevents oxygen evolution, increasing the machining efficiency as the pulse length increases because metal dissolution becomes the only reaction.

Zhang et al (Zhang et al. 2011) produced complex shapes in nickel (Ni) sheets using a 40 ns pulse. There was no stray machining observed due to the short length of the voltage pulse applied and large pulse off time (460 ns) in comparison to the on time.

Jo et al (Jo et al. 2009) concluded that the IEG could be controlled by altering the pulse on time which in turn controls the hole diameter. This can be altered during machining, resulting in holes with a smaller entrance hole than inside, see Figure 2-6.
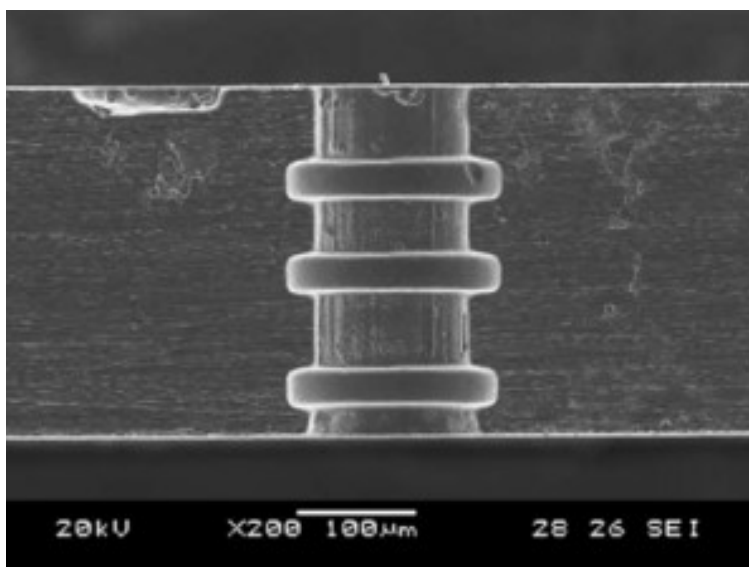
Figure 2-6 Groove array in a micro-hole (Jo et al. 2009)

Kock et al (Kock et al. 2003) showed that PECM can be used to create complex 3D structures down to nanometer precision. The authors used a frequency of 33 MHz with 3 ns pulses of 2.0 V to machine 3D micro-structures into a nickel work piece. Bilgi et al (Bilgi et al. 2007) utilised PECM for deep hole drilling. The pulses, along with an insulated tool, ensured there was no tapering of holes at the entry hole.

Lee et al (Lee et al. 2010) used PECM to machine a nickel-titanium shape memory alloy. The authors saw an increase of machining inaccuracy when the duty cycle was raised above 50 % with a pulse on time varying between 10 and 75 µs. Xu et al (Xu et al. 2015) observed that as the pulse duration was increased from 25 ns to 40 ns the surface roughness remained low but above 40 ns the surface roughness increased.

Cagnon et al (Cagnon et al. 2003) performed PECM with two steps; a fast rough cut, followed by a slower fine cut. This was achieved by varying the pulse on time from 143 ns for the rough cut to 50 ns for the fine cut. The authors created several complex, 3D micro-structures in stainless steel. Bhattacharyya (Bhattacharyya et al. 2002) reported that PECM results in more accurate machining as it eliminates reaction products, including heat, from the IEG during the pulse off time maintaining a consistent electrolyte conductivity and therefore an equal MRR across the machining profile.

Rajurkar et al (Rajurkar et al. 1993) produced a model to ascertain the IEG characteristics. They observed that for very short pulse times the localisation was improved. Sun et al (Sun et al. 2001) modified a PECM process to include a very short cathodic pulse in order to remove the anodic film that can form at the work piece surface. This would allow an improved surface finish. They called this *"modulated reverse electric field ECM (MREF-ECM)"*. This process also benefits from the improved dimensional accuracy observed with PECM.

Datta and Landolt (Datta & Landolt 1983) developed an electrochemical saw with a pulsed voltage. They report that the use of a pulsed voltage negates

the use of a complex electrolyte pumping systems whilst applying extremely high current densities as the off time allows removal of reaction products and effects of Joule heating from the inter-electrode gap. Mathew and Sundaram (Mathew & Sundaram 2012) created micro-tools with PECM starting with a diameter of 50 µm which was reduced to 13.7 µm; achievable due to the high control of the machining process seen in PECM.

Rajurkar, Zhu and Wei (Rajurkar et al. 1998) created a model which confirmed the effectiveness of using short pulses to enhance localisation. In this case a pulse duration of 1-3 ms with a duty cycle of 50 % was sufficient for the desired accuracy. Rathod et al (Rathod et al. 2014) applied the same frequency pulses but varied the duty cycle, which changes the pulse on time and the pulse on/off time ratio. A higher duty cycle resulted in a larger over cut but surface roughness and width variation along the length of the machined channel improved with increased frequency and decreased duty cycle.

2.3.4 Inter-Electrode Gap (IEG)

As discussed in the above section, the IEG is a critical parameter and maintaining a constant gap during machining is a challenge many researchers have tried to combat through modelling and in-line measurement systems. (Rajurkar et al. 1995; Bilgi et al. 2007; Muir et al. 2007; Kozak et al. 2004; Bhattacharyya et al. 2004; Schuster et al. 2000; Rajurkar et al. 1993; Jain & Rajurkar 1991; Fang et al. 2014; Clifton et al. 2003; Kozak et al. 2008; Jain & Pandey 1979; Bhattacharyya & Munda 2003; Jo et al. 2009; Zhang et al. 2011; Bhattacharyya et al. 2002; Y. Wang et al. 2010; Zeng et al. 2012; Das & Saha 2014; Mathew & Sundaram 2012; Jain & Pandey 1980; Da Silva Neto et al. 2006; Jain & Pandey 1982; Labib et al. 2011; Zhang 2010; Kozak et al. 1998; Sharma et al. 2002; Kock et al. 2003; Rajurkar et al. 2006) The gap maintained in PECM and ECMM is much smaller than in DC-ECM, in the range of 5-50 µm compared to 100-600 µm. (Bhattacharyya et al. 2004; Zhang 2010) This is because a smaller IEG leads to better resolution, crucial from ECMM.

Figure 2-7 shows how the potential varies across the IEG. The smaller the IEG the smaller the applied potential has to be to reach the machining potential as the ohmic drop caused by the electrolyte resistance is reduced. This is used to the researchers' advantage. There is preferential dissolution of material which is closer to the tool electrode due to the higher potential creating a higher current density at that point.

Researchers investigated how the IEG size affected several factors during machining. Bilgi et al (Bilgi et al. 2007) observed that a smaller IEG led to a higher MRR. Jo et al (Jo et al. 2009) realised the working gap varied with the pulse voltage and duration. They used this observation to create complex internal shapes, Figure 2-6. Bhattacharyya et al (Bhattacharyya et al. 2002) reduced the IEG to micrometer scale by lowering the voltage and electrolyte concentration, resulting in higher resolution machining. Zhang et al (Zhang et al. 2011) found it much easier to control the IEG when nanosecond voltage pulses were applied due to the small amount of material removed with each pulse.
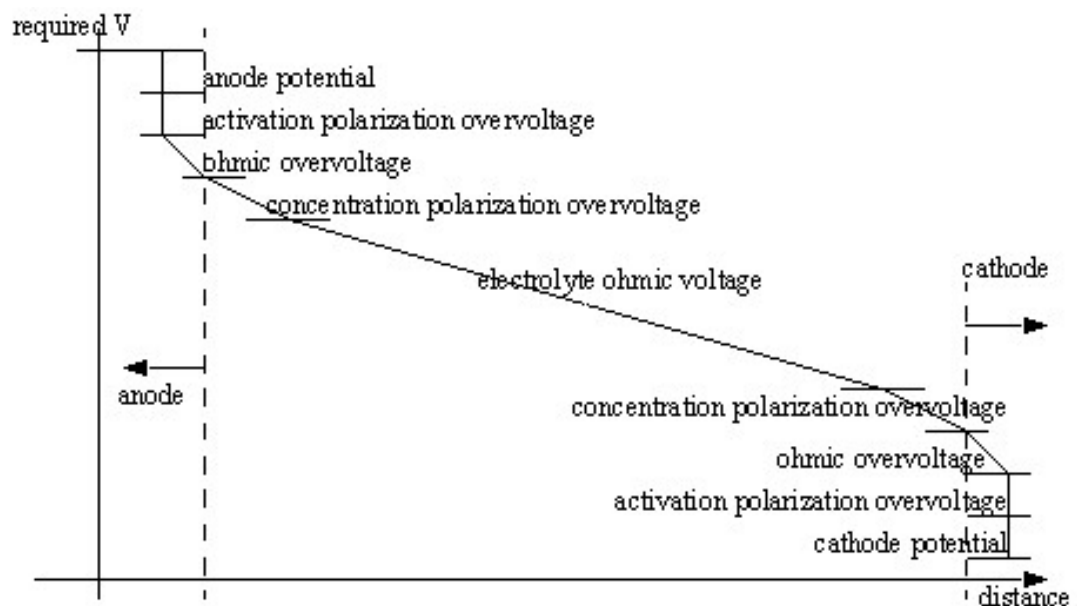
Figure 2-7: Potential profile within the IEG (Engineer on a Disk n.d.)

Zeng et al (Zeng et al. 2012) observed a better surface finish with a smaller IEG. Kock et al (Kock et al. 2003) showed that with very short pulses, the

IEG increased linearly with pulse duration and Sharma et al (Sharma et al. 2002) observed that a relatively high feed rate with a low applied voltage resulted in a small IEG. Kozak et al (Kozak et al. 1998) proposed that using smaller surface area tools facilitated smaller IEG which in turn improved machining resolution.

Rajurkar et al (Rajurkar et al. 1995) created a model to determine the minimum IEG with the onset of electrolyte boiling being the limiting factor. The same author (Rajurkar et al. 1993) had previously modelled the IEG and the development of bubbles in the IEG and how this affected machining. They reported a very thin layer of bubbles or an even distribution of bubbles throughout the gap resulted in equal machining across the whole electrode interface.

Jain and Pandey (Jain & Pandey 1982) suggested the IEG acted as a pure ohmic resistor. Kozak et al and Fang et al (Kozak et al. 2004; Fang et al. 2014) created models which predicted the IEG shape and size with Fang modelling the current distribution lines within the IEG too. Clifton (Clifton et al. 2003) also modelled the IEG but used C-functions to *"map out parameter interdependence, resulting from non-ideal conditions"*.

Jain et al (Jain & Rajurkar 1991; Jain & Pandey 1980) and Mathew et al (Mathew & Sundaram 2012) created models of the IEG to design an ideal tool shape based on predictions for the resulting anode shape, see Figure 2-8 for a flow diagram demonstrating all considerations in the model. Jain and Pandey (Jain & Pandey 1979) developed a model of the IEG in ECM. They noted a decrease in the IEG resulted in a greater temperature and conductivity rise in the electrolyte. Kozak et al (Kozak et al. 2008) developed a model calculation whereby the electric field within the IEG is described by Laplace's equation to define the limiting gap size for a given pulse length, voltage and electrolyte concentration.
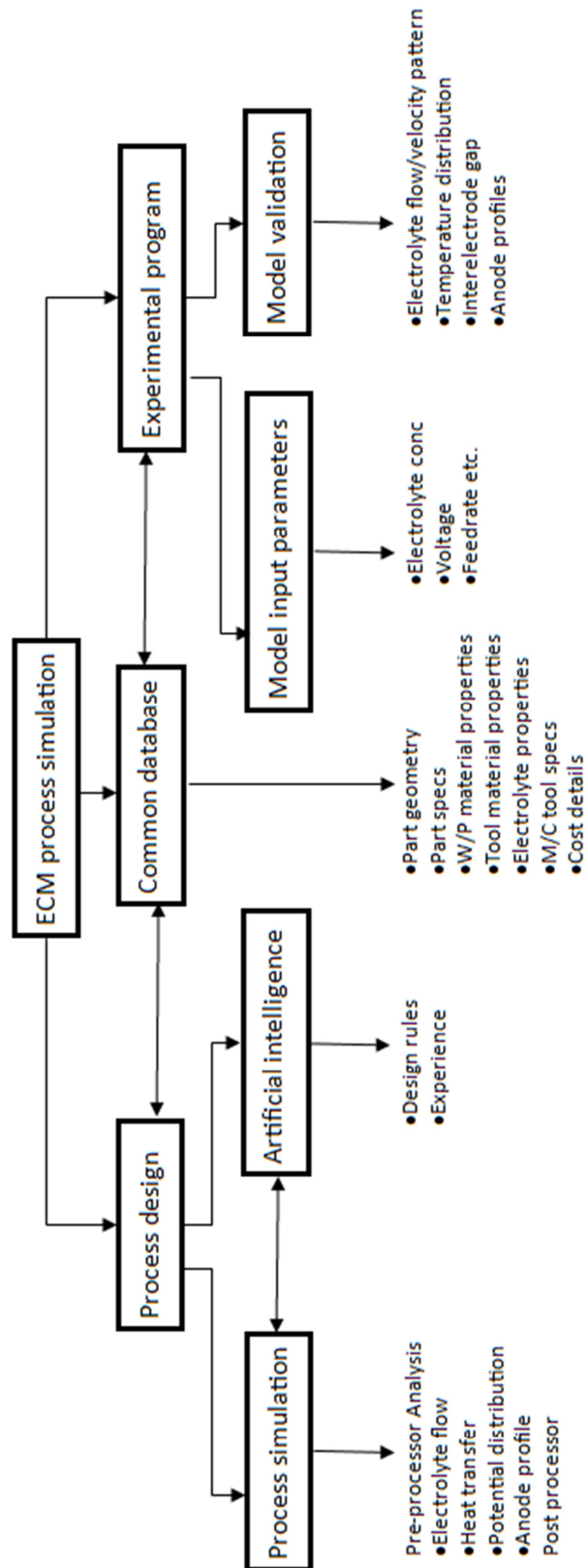
Figure 2-8 Process Simulation Parameters (Jain & Rajurkar 1991)

Other researchers developed methods to maintain the chosen IEG distance during machining. Da Silva Neto (Da Silva Neto et al. 2006) noted improper control of the IEG led to poor tool replication; in their case the surface finish was negatively affected and Rajurkar et al (Rajurkar et al. 2006) noted it was important for proper control of the IEG to prevent short circuits or arcing occurring during machining. Schuster et al (Schuster et al. 2000), Bhattacharyya and Munda (Bhattacharyya & Munda 2003) and Das and Saha (Das & Saha 2014) all used a current detection method to maintain the IEG. A small voltage was applied between the tool and work piece; the tool was slowly moved towards the work piece, monitoring the current. When it is registered that electrodes are in contact, the tool is stopped and retracted by the chosen IEG distance.

Wang et al (Y. Wang et al. 2010) developed a soft-computer numerical control system which monitored the process and automated functions such as gap detection and adjustment. Labib et al (Labib et al. 2011) developed a fuzzy logic control system, whereby the short circuit situation could be avoided which the researchers thought could ultimately lead to a better surface finish. Muir et al (Muir et al. 2007) utilised an ultrasonic method which would measure the IEG without disrupting the machining process.

2.3.5 Voltage

From Faraday's Law, see Equation 1, one can predict that the applied voltage in ECM will affect the amount of material removed through the relationship $V = IR$ where V is the voltage and R is the resistance. (De Silva et al. 2003) In this case R is the resistance of the electrolyte. With these two equations, it is possible to presume that a higher voltage will result in a higher current passing which would increase the amount of material removed during the same time period with a lower voltage. Many researchers have demonstrated this to be true. (Fan et al. 2012; Datta & Landolt 1983; Bhattacharyya & Munda 2003; Bilgi et al. 2004; Rathod et al. 2014; Kozak et al. 2008; Saravanan et al. 2012; Xu et al. 2015; Jain & Pandey 1980; Acharya et al. 1986; Tandon et al. 1990; Ayyappan & Sivakumar 2014b; De

Silva et al. 2003; Cook et al. 1967; Bilgi et al. 2007; Wu et al. 2013) Wagner and Wang (Wagner 2002; M. Wang et al. 2010) also stated the current density is a function of the applied voltage. However, when the potential is raised above a particular voltage (dependent on the work piece material and electrolyte combination) the MRR decreased. They explained this by an increase in hydrogen gas generation at the tool electrode. These bubbles, trapped in the IEG, increased the resistivity of the electrolyte, decreasing the current density at the work piece, decreasing MRR. (Bhattacharyya & Munda 2003; Rathod et al. 2014; Bilgi et al. 2007)

Although a higher voltage leads to a higher MRR it has other effects which may be detrimental to machining. Cook (Cook et al. 1967), Cagnon (Cagnon et al. 2003), Datta (Datta & Landolt 1983) and Bilgi (Bilgi et al. 2004) all noted that damage to the tool occurred when high voltages were used caused by sparking which affected machining accuracy. Tandon (Tandon et al. 1990) was investigating electrochemical spark machining but observed that a higher voltage increased the rate of tool wear.

Machining resolution also decreased as the machining voltage was increased, illustrating that lower voltages are more appropriate for ECMM to keep over cut to a minimum. Bhattacharyya (Bhattacharyya & Munda 2003), Fan (Fan et al. 2012), Ghoshal (Ghoshal & Bhattacharyya 2013), V. Jain (Jain et al. 2012; Jain et al. 2007), Rathod (Rathod et al. 2014), Kozak (Kozak et al. 2004; Kozak et al. 2008), Datta (Datta & Landolt 1983),Fang (Fang et al. 2014), Bilgi (Bilgi et al. 2004; Bilgi et al. 2008; Bilgi et al. 2007), Tandon (Tandon et al. 1990), N. Jain (Jain et al. 2007), Rao (Rao et al. 2008) all observed an increased overcut when machining with a higher voltage, which resulted in more rounded edges. Sharma (Sharma et al. 2002) stated *"good holes can be obtained by a combination of low voltage and comparatively high feed rate".* Acharya (Acharya et al. 1986) stated that the optimum voltage for a high MRR was higher than the optimum voltage required for geometrical accuracy.

Several authors also observed improved surface finish with a higher applied voltage. (Cagnon et al. 2003; Inman et al. 2011; Xu et al. 2015; Zeng et al. 2012; Ayyappan & Sivakumar 2014a) Xu (Xu et al. 2015) noted an initial improvement in surface finish as the voltage increased. However, in their case, as the voltage was increased above 6 V the surface roughness increased. Sjöström (Sjöström & Su 2011) stated that a lower applied voltage may lead to a better surface finish but at the cost of a lower MRR.

Choi (Choi et al. 2013), Bhattacharyya (Bhattacharyya & Munda 2003; Bhattacharyya et al. 2002), Kozak (Kozak et al. 2008), Cook (Cook et al. 1967) and Jo (Jo et al. 2009) all stated that the IEG could be lowered by the application of a lower machining voltage, which in turn increased the machining accuracy. Kozak (Kozak et al. 2008) showed that the limiting gap becomes smaller with a smaller applied voltage. Jo (Jo et al. 2009) took advantage of this knowledge to create complex internal structures, see Figure 2-6.

Inman (Inman et al. 2011) and Zhang (Zhang 2010) realised a higher machining voltage was necessary to break through passive layers at the work piece surface. Bhattacharyya (Bhattacharyya & Munda 2003) recognized an increase in Joule heating upon the application of a higher voltage. This caused changes in the local electrolyte conductivity, leading to an inaccurate tool replication in the work piece. Das (Das & Saha 2014) noted an increased cylindrical length, when fabricating cylindrical micro tools, with increased voltage up to 21 V. Above 21 V, the authors suspected the end of the micro tool was falling away due to increased machining at the electrolyte air interface.

The direction of the reaction at the work piece (deposition or dissolution) at a given potential can be predicted by the Nernst equation, see Equation 4.

$$E_e = E_e^0 + \frac{2.3RT}{nF} \log \frac{c_O}{c_R} \qquad\qquad (4)$$

Where E_e^0 is the formal potential of the couple O/R, R is the gas constant, T is the temperature, n is the number of electrons involved, F is the Faraday constant and c_O and c_R are the concentrations of the oxidant and reductant respectively. (Pletcher 2009) The equation can be used to determine the ratio of oxidant to reductant species in the system at a given potential by using the equilibrium potential as a starting point. The equilibrium potential is the potential at which there are equal concentrations of both oxidant and reductant species. Datta (Datta 1993) observed that at potentials above the limiting current density new anodic reactions could occur, notably a change in dissolution valency or oxygen evolution at the work piece.

2.3.6 Tool Feed Rate

The too feed rate is a crucial parameter in ECMM to minimise overcut and maximise MRR and maintain constant IEG. Cook et al (Cook et al. 1967) first observed that the feed rate was dependent on the current density, with Singh (Singh et al. 2008) also stating that the feed rate influences the IEG. More material is removed per unit time when the current density is higher which facilitates a higher tool feed rate.

Many papers report the use of a constant feed rate during ECM. The aim was to use a feed rate which matched the dissolution rate so the IEG could be kept constant throughout machining. (Muir et al. 2007; Jain & Jain 2007) Researchers found if too high a feed rate was used the IEG would rapidly decrease in width, eventually causing a short circuit which creates sparks and damages the tool or work piece. (Bilgi et al. 2004; Datta & Landolt 1983; Zhang et al. 2011; Cagnon et al. 2003; Jain & Pandey 1979; Rathod et al. 2014) Ghoshal (Ghoshal & Bhattacharyya 2013) realised the optimum feed rate was the maximum feed rate which did not induce sparking between the electrodes.

Authors observed that the MRR increased with feed rate (Da Silva Neto et al. 2006; Ayyappan & Sivakumar 2014a; Jain & Pandey 1980; Rao et al. 2008; Acharya et al. 1986; Jain & Pandey 1979; Zeng et al. 2012) but it could lead

to non-uniform dissolution as reported by Jain (Jain & Pandey 1979). This could be due to the increased temperature rise when the feed rate is increased. The increase in feed rate can lead to electrolyte boiling or choking. (Jain & Pandey 1979; Jain & Pandey 1980)

Many researchers studying the effect of feed rate on the ECM process noted a decrease in the machining overcut as the tool feed rate was increased. (Kozak et al. 2004; Jain et al. 2012; Da Silva Neto et al. 2006; Bilgi et al. 2004; Fan et al. 2012; Datta & Landolt 1983; Jain & Pandey 1982; Zeng et al. 2012) This is probably due to the observation that a higher feed rate decreased the IEG (Kozak et al. 2004; Singh et al. 2008; Clifton et al. 2003; Bilgi et al. 2007), which, as previously discussed, increases machining resolution. Some also reported a decrease in surface roughness with an increase in feed rate. (Da Silva Neto et al. 2006; Zeng et al. 2012) In a couple of papers, authors reported an increase in dimensional inaccuracy with an increase in feed rate (Jain & Jain 2007; Rao et al. 2008). Kozak (Kozak et al. 2004) also reported above a certain feed rate, 63 mm/min, the sharpness of the edges decreased.

Whilst most authors reported the use of a fixed feed rate during machining, Labib (Labib et al. 2011) and Jain (Jain & Jain 2007) maintained a constant IEG by adjusting the feed rate accordingly. This prevented the equilibrium IEG becoming established, possibly allowing a smaller IEG to be maintained throughout machining.

2.3.7 Other Alterations to ECM

Having discussed all of the common parameters controlled for precise ECM above, other alterations to the ECM process will now be explored. All of the alterations aimed to improve MRR or decrease machining overcut.

One of the most common alterations made to ECMM was the addition of ultrasonic vibrations (USV) to either the work piece or the tool. (Huaiqian et al. 2008; Bhattacharyya et al. 2002; Xu et al. 2015) Observations were made

that the application of USV enhanced ion transport and improved surface roughness both when amplitude and frequency were increased.

Qu et al (Qu et al. 2013) pulsated the electrolyte instead of vibrating one of the electrodes. The authors reported an improvement in the surface roughness and increased MRR when the electrolyte pulsating frequency was increased. A maximum frequency of 20 Hz was applied.

Trying to improve machining precision, researchers began investigating ways to restrict and control the potential field between the tool and the work piece. Tools were insulated which prevented machining in the side gap. Another alteration was the development of a dual-pole tool. The cathodic tool was initially insulated and then an insoluble anodic layer was added on top. This reduces the chances of over-cut due to stray machining by changing the electric field within the gap. (Zhu & Xu 2002; Bhattacharyya et al. 2004)

A similar technique, termed the confined etchant layer technique (CELT), was developed in 1992 (Tian et al. 1992). This technique utilised the electrochemical generation of corrosive chemicals in the vicinity of the electrodes. The machining was confined by the use of a micro-electrode and an excess of a sequestering ion was employed in the electrolyte to prevent a build-up of the corrosive ions away from the tool electrode.

2.4   Conclusion

A vast amount of research has already been conducted, observing the effects of electrolyte choice, concentration, pulse frequency and duration, IEG, voltage, tool feed rate and other alterations such as the application of ultrasonic vibrations to one of the electrodes.

Very little work has also been conducted on ECM machining of semiconductor materials outside of doped silicon materials. A wide range of semiconductor materials are being used more commonly in electronic equipment, some of which are brittle and difficult to machine with conventional machining processes. It is proposed to determine whether ECM

is a suitable machining method for some of these semiconductors, including indium antimonide (InSb) and gallium arsenide (GaAs).

Another interesting field is the machining of superconductors. Most high temperature superconductors are based on the perovskite crystal structure with internal layers throughout the structure which are crucial to the superconductivity of the material. Traditional, contact machining techniques can damage these layers through the application of physical pressure on the material. ECM is an ideal technique for machining superconductors as it is a non-contact, stress-free and heat-free technique.

Also, there has been no work, to the author's knowledge, investigating the effect of crystal structure, comparing the results obtained in ECM for polycrystalline, monocrystalline and amorphous materials. This would be of interest with the aim to developing more precise machining results and manufacturing of microelectromechanical systems (MEMS) devices as well as testing the boundaries of achievable roughness and feature size.

Chapter 3 – Anodic dissolution of Superconductors

3.1   Introduction

3.1.1 What is Superconductivity?

Figure 3-1 Meissner Effect in action: A magnet levitating above Yttrium barium copper oxide ($YBa_2Cu_3O_7$) cooled to -196°C (Bobroff & Bouquet 2010)

Superconductivity is a quantum mechanical phenomenon whereby certain materials exhibit zero electrical resistance when cooled below a critical temperature, close to absolute zero (0 Kelvin) in most cases (Anon n.d.). This means superconductive materials can carry a current indefinitely without the loss of energy (Vortex Business Solutions 2013). Metallic superconductive materials also exclude an applied magnetic field from their core when cooled below the critical temperature of the material in question, termed the Meissner Effect (Hyperphysics n.d.). This property is observed by the levitation of small permanent magnet above a superconducting material, as shown in Figure 3-1. It does this by setting up electric currents near the

surface, creating a magnetic field which cancels the applied magnetic field within the bulk of the superconductor.

3.1.2 Brief History of Superconductivity

Superconductivity was first discovered in 1911 by Dutch physicist Heike Kamerlingh Onnes. (Anon n.d.) The earliest superconductors were only superconductive when cooled to near absolute zero which was reached by dousing the material in liquid helium. The first observation of superconductivity was of solid mercury at a temperature of 4.2 K.

In 1986, Bednorz and Müller discovered a material which became superconductive at just 35 K (Bednorz & Müller 1986), something that physicists thought impossible due to BCS theory (Bardeen-Cooper-Schreiffer theory), which forbade superconductivity above 30 K (Bristol n.d.).

BCS theory describes electron pairing into Cooper pairs, at energies close to the Fermi level at low temperatures, through the interaction with the crystal lattice. Cooper pairs are electron pairs which are coupling over a range of hundreds of nanometres, three orders of magnitude larger than the lattice spacing. Electron pairs can behave differently to single electrons and can condense into the same energy level. The electron pairs have a slightly lower energy level, leaving a band gap on the order of 0.001 eV which prevents collision interactions which leads to ordinary resistivity. At temperatures where the thermal energy is smaller than the band gap, zero resistance is observed.

Just a year later, M K Wu, Torng and Ashburn and Paul Chu with his students from the University of Houston discovered the first so-called 'high temperature superconductor' (HTS), yttrium barium copper oxide (YBCO) with a critical temperature of 92 K (Wu et al. 1987). This was an important step forward as it was the first material that became superconductive above the boiling point of liquid nitrogen, 77 K, making superconductors more

accessible due to the high availability of liquid nitrogen in comparison to liquid helium. Liquid nitrogen is also less expensive than liquid helium.

3.1.3 Superconductor Applications

Superconductors, both high and low temperature, have applications in many fields outside of research; including transport, physics, military, electronics/power and medical industries(Vortex Business Solutions 2013).

Maglev (magnetic levitation) trains employ superconductors to reduce friction between the train and the tracks making transportation more energy efficient. The first commercial Maglev train was in Birmingham, England, but closed in 1995 after 11 years of service. Their wider use has been restricted by political and environmental concerns as strong magnetic fields are a potential bio-hazard, thought to effect the immune system (Eck n.d.).

Superconductors are also used in particle colliders to accelerate charged particles to near the speed of light (Eck n.d.). The most renowned use of a particle collider is the large hadron collider (LHC) at CERN in Switzerland, where the Higgs-Boson particle was first discovered in July 2012 (CERN n.d.).

Military uses for SCs include the use of superconducting quantum interference devices (SQUIDs), for the detection of land mines, and 'E-bombs' which deliver a large electromagnetic pulse that can disable the enemies' electronic equipment. The 'E-bomb' was first used in warfare in 2003 when US troops attacked an Iraqi broadcast facility. SQUIDs also show potential to image the body to a certain depth without the high magnetic fields associated with MRI imaging (Eck n.d.).

Magnetic resonance imaging (MRI) scanners used routinely in hospitals to aid diagnosis, also require superconductors; sensitivity and resolution are increased with an increase in the magnetic field (Stafford 2003). Commercial MRI scanners are available from 0.2 T up to 7 T at present. MRIs have

reduced the need for exploratory surgery (Vortex Business Solutions 2013). T is the symbol for Tesla, the unit for the strength of a magnetic field.

Superconductors also have beneficial uses within the electronics industry, as might be expected, due to zero electrical resistance under certain conditions. Electric generators using superconductors have an efficiency of over 99% (Eck n.d.). Their physical size is also around half of that of a standard generator.

3.1.4 Structure of Superconductors

High temperature cuprate superconductor structures are based on the perovskite structure; layers of copper oxide are separated by metals (in the case of YBCO these would be Yttrium and Barium). The perovskite structure is the unit cell, the simplest repeating unit, of the compound. Figure 3-2 shows the unit cell of YBCO superconductor. The more copper oxide layers, the higher the critical temperature.(Arteche n.d.) Electric currents are carried by oxygen holes in the copper oxide sheets; due to this the conductivity parallel to the copper oxide sheets is much higher than that of the perpendicular direction.

Another commonly used superconductor is magnesium diboride (MgB_2). The critical temperature for MgB_2 is 39 K, below the boiling point of liquid nitrogen, but it is an inexpensive material making it an attractive alternative to the cuprate perovskite superconductors (READE n.d.). Its structure is also a layered formation but it behaves more like a metallic superconductor than a cuprate superconductor.
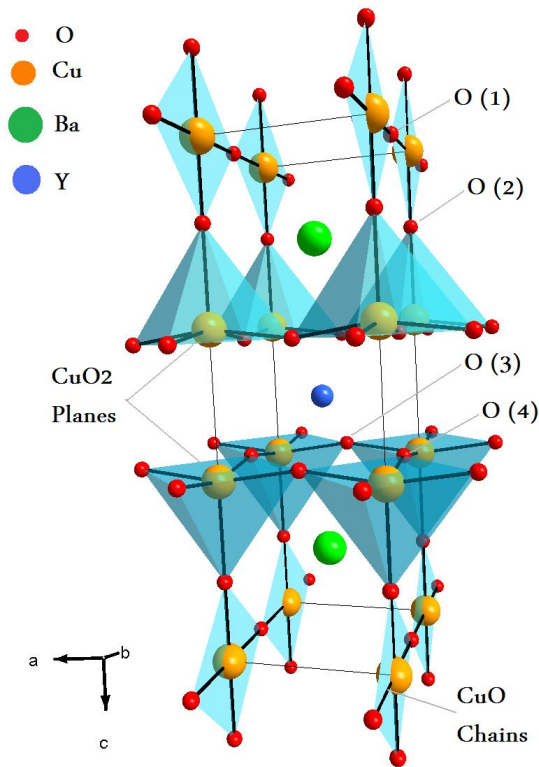
Figure 3-2 YBCO Perovskite Structure (Haj33 2009)

3.1.5 Benefits of Single Crystal Superconductors

Single crystal superconductors have a very high critical current density whilst poly-crystals have a very low critical current density meaning only a small current can be passed while maintaining superconductivity (Hilgenkamp & Mannhart 2002). Current density is the amount of current that can be carried per unit area of cross section. The problem is due to grain boundaries within the material. When the angle or orientation between grains is greater than 10° the supercurrent cannot cross the boundary (Graser et al. 2010) resulting in high resistances within the structure, diminishing the maximum current flow. It is for this reason that single crystal superconductors are beneficial.

As previously explained, superconductors exhibit the Meissner Effect which sees magnetic fields excluded from the bulk. In type II superconductors (e.g. YBCO) raising the applied magnetic field sees the magnetic field penetrate into the superconductor bulk but resistivity remains zero as the current is not

too high. Raising the magnetic field higher destroys the material due to massive internal strains due to the repulsion of the lines of magnetic flux within the material. Single crystals are beneficial here as they allow higher magnetic fields to be applied, as higher currents can be accommodated than in polycrystalline materials.

3.1.6 Processing Superconductors

Superconductors, such as YCBO, are brittle ceramics; this poses processing problems. Micro-cracks occur during the sample preparation due to the mechanical stresses from cooling and the unit cell rearrangement from tetragonal to the superconducting orthorhombic phase. (Isfort et al. 2003; Diko et al. 1995; Richardson & De Jonghe 1990) These micro-cracks can crack further with post-formation drilling which disrupts the superconductive properties of the material. (Kósa & Vajda 2007) Drilling has to be done slowly, applying little pressure with low rotational speeds to prevent cracks forming in the structure.

This chapter aims to propose an alternative method for post-formation drilling or shaping of superconductive materials, mainly gadolinium barium copper oxide ($GdBa_2Cu_3O_7$) doped with silver (Ag), through the application of electrochemical machining techniques. GdBCO-Ag is a superconductive material comparative to YBCO. The Ag inclusions add strength to the material. As far as this research is aware, no attempts have been made to use electrochemical machining methods to process superconductive materials.

3.1.7 Gadolinium Barium Copper Oxide (GdBCO)

The gadolinium barium copper oxide samples are monocrystalline material with silver inclusions to increase the mechanical strength of the material. The sample contains 70 % Gd123, 20 % Gd211 and 10 % Ag. Gd123 is GdBCO with the following chemical formula $GdB_2Cu_3O_7$ whereas Gd211 has the chemical formula Gd_2BCuO_5. Only Gd123 is superconducting. Gd123 forms

the crystal with silver and Gd211 particles are trapped in the Gd123 matrix, see Figure 3-3.

Gd123 is a black material whilst Gd211 is green in colour. As Gd211 is dispersed within Gd123 the green is not visible. The spherical Ag particles are not visible individually by eye but they do give the material a slight shimmer.
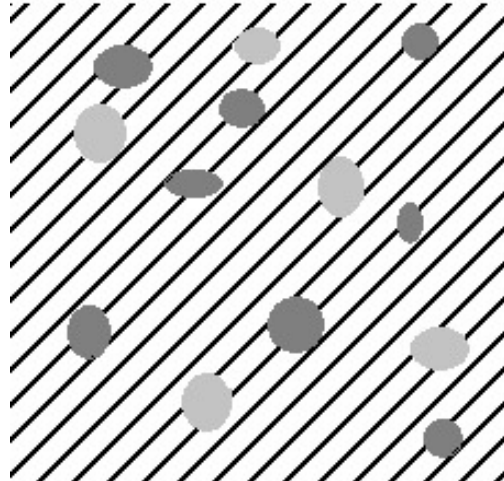
Figure 3-3 Gd123 matrix with trapped Ag (pale grey) and Gd211 (dark grey) particles

Cuprate superconductors, GdBCO-Ag included, are water sensitive. The presence of water causes changes in stoichiometry, e.g. $YBa_2Cu_3O_7$ in the presence of water forms $Y_2Ba_4Cu_8O_{16}$ (Günther et al. 1996) which is not a superconductive compound.

3.1.8 Motivation for the Work

A colleague at Brunel University, Dr Hari-Babu Nadendla, working within the Brunel Centre for Advanced Solidification Technology (BCAST), approached the Ivanov research group about processing their single crystal cuprate superconductors. They had difficulties when trying to cut thin tubular shells from cylindrical samples. Due to the fragile nature of the material, cracks along the ac-plane (see Figure 3-2) propagate, connecting small cracks that

lie along the ab-plane. (Gombos et al. 2012) Cracks along the ab-plane do not interrupt the material's superconducting properties but cracks along the ac-plane diminish the material's superconducting capabilities.

3.2   Method

3.2.1 Polarisation Curves

Polarisation curves are used in the ECM to determine the ideal machining potential. A potential is scanned across a voltage range and the current response in monitored. From the current response, the electrochemical behaviour at the work piece surface can be described.

3.2.1.1   Attaching GdBCO-Ag Samples to Copper Wires

Small samples of GdBCO-Ag pre-prepared by University of Cambridge but received from BCAST at Brunel University were attached to insulated copper wires with silver-loaded epoxy and left to cure in an oven at 55 °C for ten minutes.

3.2.1.2   Preparing the Electrolyte

3.0 M sodium chloride (NaCl) was used as the electrolyte. The electrolyte was made with ACS grade NaCl from Sigma Aldrich and deionised water from an ELGA PURELAB Option Q water purifier.

3.2.1.3   The Cell Setup

A 3-electrode set up was used for the polarisation curve experiment, see Figure 3-4. The reference electrode was a Sigma Aldrich double junction silver/silver chloride reference electrode and a homemade platinum flag as the counter electrode. The working electrode was the GdBCO-Ag sample attached to a copper wire. Care was taken to ensure the silver epoxy on either the counter electrode or the working electrode was not in the electrolyte so as to avoid mixed potentials. This was to guarantee the current response was only from the dissolution of the working electrode and other

associated reactions e.g. hydrogen evolution at the counter electrode surface. The solution was not subjected to any external convection forces.
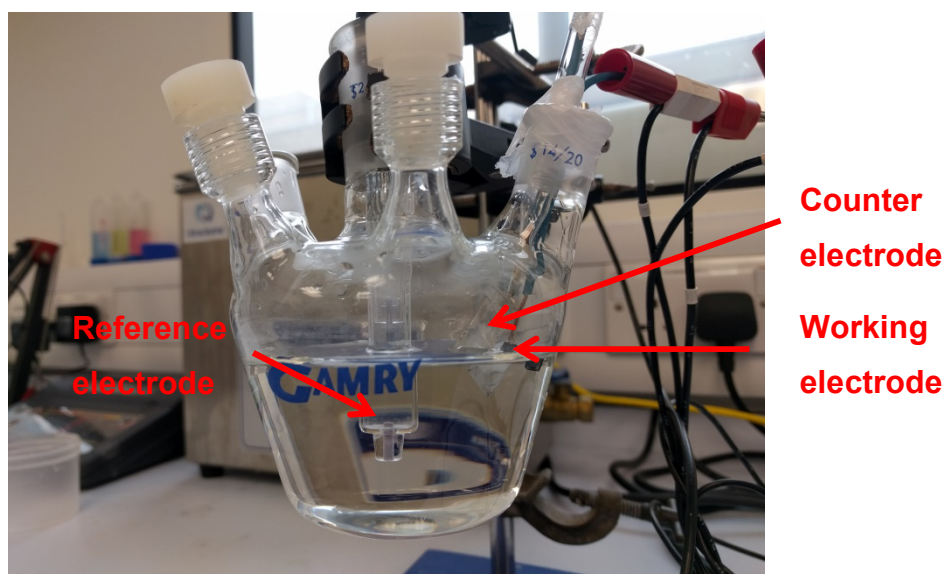
Figure 3-4 Electrochemical cell set up

3.2.1.4 The Polarisation Curve Experiment

The potential was applied using an IviumStat potentiostat. The potential was scanned from -0.5 V to 10.0 V at a scan rate of 2 mV s^{-1}. The counter electrode and working electrode were held close together (approximately 5 mm) to replicate the ECM conditions as closely as possible. The electrodes were connected to the potentiostat via banana plugs to ensure a good electrical connection. The counter and working electrodes were not inserted into the electrolyte until the potential had been applied to minimise the length of time the superconductor was in contact with the aqueous electrolyte. Polarisation curves allow the determination of the dissolution potential that would be used on the electrochemical machine.

3.2.2 Using the ECM Machine to cut GdBCO-Ag samples with Aqueous Electrolytes

3.2.2.1 Placing GdBCO-Ag samples in the ECM Machine

A brass plate was created that could be held in the ECM machine with screws to allow electrical connection to the GdBCO-Ag sample. The GdBCO-Ag samples were attached to the brass plate with silver-loaded epoxy which was cured in the oven at 55 °C for ten minutes. The brass plate set up is show in Figure 3-5.
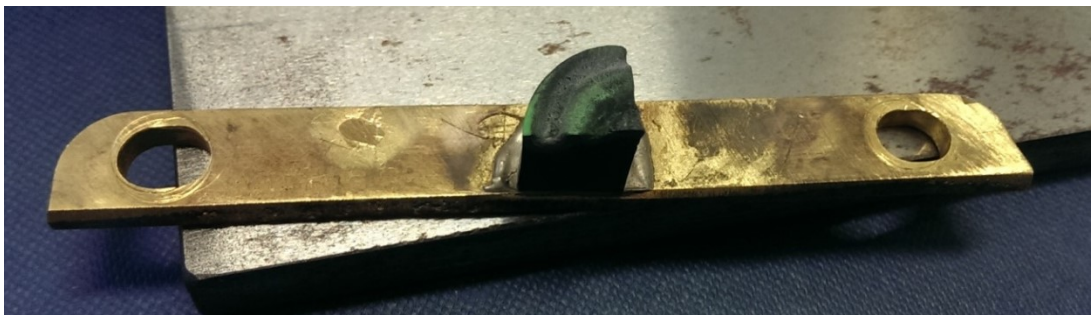
Figure 3-5 Brass plate connected to GdBCO-Ag sample with silver-loaded epoxy

3.2.2.2 The Tool

The tool used for machining the GdBCO-Ag samples was platinum wire (Pt) due to the chemical stability of the metal. The Pt wire was formed into a circular shape with a vertical strut to allow connection to the tool holder on the ECM machine. This shape was chosen as experiments were planned to cut thin shells of material from GdBCO-Ag cylindrical samples, see Figure 3-6, which cannot currently be done by any known method due to the brittleness and fragility of the material. The tool had an internal diameter of 18 mm. This allowed for a 2 mm shell to be cut from a 20 mm diameter GdBCO-Ag sample.

3.2.2.3　　　Touch-n-Go Operation

One of the crucial parameters in electrochemical machining is the IEG. Before machining can commence, the gap must first be established. To do this the ECM machine makes small movements of the tool towards the work piece surface along the z-axis. A small voltage (< 2 V) is applied at a frequency of 50 kHz and a 50 % duty cycle whilst the tool is moved towards the work piece. When a short circuit is detected the tool retracts and continues to descend using increments half the size previously used. This is repeated until an accuracy of 0.1 μm or better is achieved. (Spieser 2015) An initial IEG of 5 μm was used.

3.2.2.4　　　ECM Machine Settings for Machining

Once the gap had been established machining could begin. The control algorithm for the tool movement during machining was set to 'adaptive feed-rate' which monitors the number of times the over-current protector (OCP) is triggered and adjusts the feed-rate accordingly, i.e. the feed rate is adjusted to reduce the number of times the OCP is triggered.
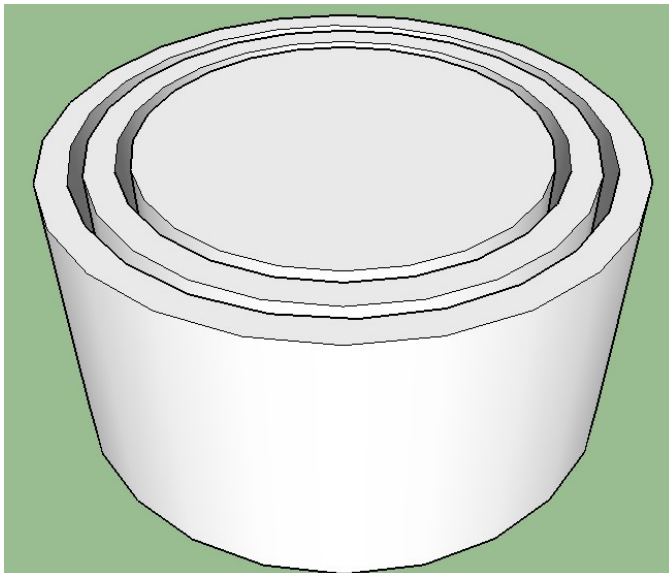
Figure 3-6 Target geometry

To begin with a constant potential was applied to confirm the ideal potential shown in the polarisation curves was suitable for machining.

Once the potential was shown to be suitable for the anodic dissolution of GdBCO-Ag, machining was carried out under pulsed-potential conditions. The frequency, duty cycle and maximum/minimum pulse current were varied in order to improve machining precision whilst maintaining a high machining rate.

3.2.3 Polarisation Curves in Non-Aqueous Electrolytes
3.2.3.1 Attaching the GdBCO-Ag Samples to Copper Wire

Small samples of GdBCO-Ag pre-received from BCAST at Brunel University were attached to insulated copper wires with silver-loaded epoxy and left to cure in an oven at 55 °C for ten minutes.

3.2.3.2 Preparing the Electrolytes

Sodium chloride, sodium bromide and sodium chlorate were used as the electrolytes at differing concentrations with methanol, glycerol, formamide or formic acid as the solvent. Sodium chlorate was only dissolved in glycerol. All chemicals were ACS Grade from Sigma Aldrich, apart from the glycerol which was food grade from Classikool.

3.2.3.3 The Cell Set Up

A 3 electrode set up was used for the polarisation curves in methanol electrolytes. The reference electrode used was a homemade platinum flag electrode due to the Ag/AgCl reference electrode being an aqueous electrolyte which would add uncertainty to the applied potential due to unknown measurements. The counter electrode was also a homemade platinum flag electrode. The working electrode was the small samples of GdBCO-Ag attached to the copper wires. Care was taken to ensure the silver epoxy on all the electrodes was not inserted into the electrolyte to avoid mixed potential readings. The silver epoxy could also dissolve in the

methanol electrolyte, detaching the GdBCO-Ag sample from the wire before the experiment was finished.

3.2.3.4   The Polarisation Experiment in Non-Aqueous Electrolytes

The potential was applied using an IviumStat potentiostat. The potential was scanned from -2.0 V to 10.0 V at a scan rate of 2 mV s^{-1}. The counter electrode and working electrode were held close together (approx. 5 mm at the closest point) to replicate the ECM process as closely as possible. The electrodes were connected to the potentiostat via banana plugs for a strong electrical connection. Polarisation curves allow the determination of the dissolution potential that would be used on the electrochemical machine. Polarisation curves were carried out using a combination of solvents and solutes, which can be seen in Table 3-1, in order to determine the best solvent-electrolyte combination for the anodic dissolution of gadolinium barium copper oxide with silver inclusions.

Table 3-1. Experiment Design for Non-Aqueous Polarisation Curves

Salt	Solvent	Concentration (M)
NaBr	Methanol	1.50
NaBr	Methanol	1.00
NaBr	Methanol	0.25
NaBr	Methanol	0.10
NaBr	Formic Acid	2.25
NaBr	Formic Acid	1.50
NaBr	Formic Acid	0.75
NaBr	Glycerol	4.50
NaBr	Glycerol	2.25
NaBr	Glycerol	1.50
NaBr	Glycerol	0.75
NaBr	Formamide	2.25
NaBr	Formamide	1.50
NaBr	Formamide	0.75
NaCl	Methanol	0.25
NaCl	Methanol	0.10
NaCl	Formic Acid	1.00
NaCl	Formic Acid	0.75
NaCl	Formic Acid	0.50
NaCl	Glycerol	1.75
NaCl	Glycerol	1.00
NaCl	Glycerol	0.75
NaCl	Glycerol	0.50
NaCl	Formamide	1.75
NaCl	Formamide	1.00
NaCl	Formamide	0.75
NaCl	Formamide	0.50
$NaClO_3$	Glycerol	0.40
$NaClO_3$	Glycerol	0.20

3.2.4 Electrochemical Machining of GdBCO-Ag with Non-Aqueous Electrolytes

3.2.4.1 Attaching the GdBCO-Ag sample to the ECM Machine

The electrochemical machining experiments were carried out at pECM Systems Ltd in Barnsley as the machine there is more powerful than the machine built in-house at Brunel University and has a controllable z-feed rate.

A custom made work piece holder was created from a piece of copper to mount the GdBCO-Ag sample to the ECM machine. The GdBCO-Ag sample is a 2 cm diameter section of a cylinder so a 2 cm diameter hole was created in the copper into which the work piece was placed and clamped using a screw as can be seen in Figure 3-7. The electrical connection was made through the copper holder.
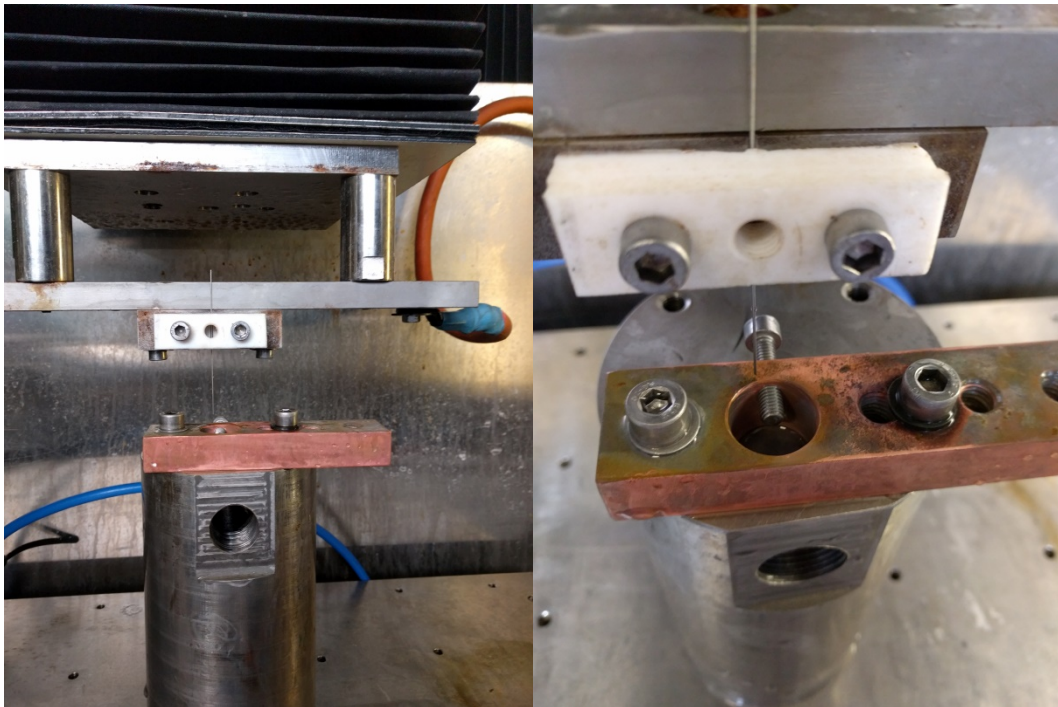
Figure 3-7 ECM machine set up for GdBCO-Ag machining

3.2.4.2   The tool

A platinum ring with upstand was used as the tool as shown in Figure 3-8. Platinum was chosen due to its chemical inertness. The tool had an internal diameter of 18 mm. This allowed for a 2 mm shell to be cut from a 20 mm diameter GdBCO-Ag sample.

3.2.4.3   The Electrochemical Machining Experiments

Once the work piece and tool had been placed into the ECM machine the inter-electrode gap needed to be established. A multimeter was attached between the tool and the work piece to detect when physical contact had been made between the two electrodes. Once contact had been established, the z-axis was moved 0.1 mm away from the contact point. The initial IEG was therefore set at 0.1 mm.
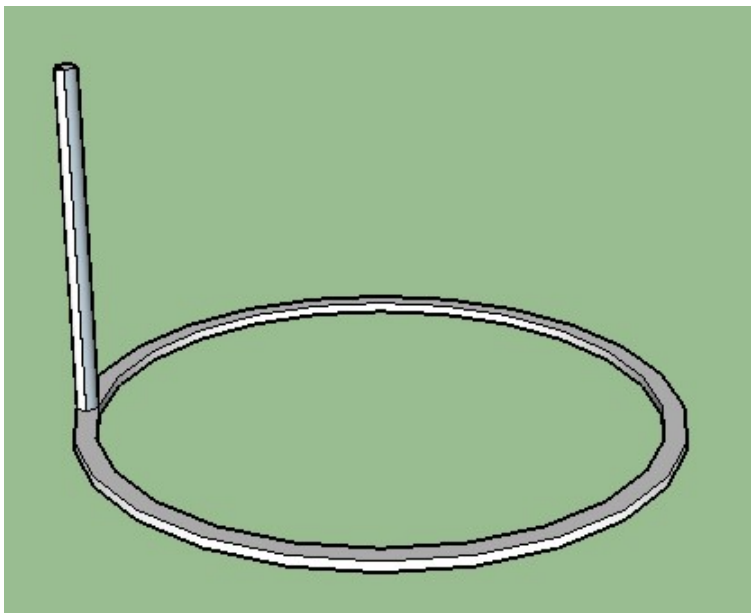
Figure 3-8 Platinum Tool used for ECM experiments with GdBCO-Ag

The aim was to create a 1 mm deep groove in the sample, closely replicating the tool diameter of 0.25 mm. The voltage and maximum current were altered during the experimentation whilst the feed rate was set at 0.5 mm

min^{-1} for all tests. The voltage was varied between 8.5 and 20.0 V whilst the maximum current was varied between 10 and 30 A.

3.3 Results & Discussion

3.3.1 Polarisation Curves in Aqueous Electrolytes

Polarisation curves were used here to determine if common aqueous electrolytes used in commercial electrochemical machining processes were also suitable to machine GdBCO-Ag; and if suitable to define the potential at which dissolution is achievable. Although GdBCO-Ag is a water sensitive material, water has been used as a coolant to machine these materials conventionally. (Kósa & Vajda 2007; Habisreuther et al. 2001) If the GdBCO-Ag sample was exposed to water for only a short period of time it would not necessarily have detrimental effects to the material's superconductive properties by affecting the delicate chemical balance. Habisreuther et al (Habisreuther et al. 2001) did not observe any negative effects of water on the SC sample and the parts were dried immediately after each step.

A low scan rate (2 mV s^{-1}) was chosen to gain as much detailed information as possible regarding Faradaic current by minimising the charging or capacitive current observed. The capacitive current is current associated with charging/discharging the electrode and does not contribute to any electrochemical change at the electrode surface (Pletcher 2009). When charging the electrode, the electrolyte molecules near the electrode surface rearrange themselves to balance the charge from the metal. Using high scan rates increases this non-Faradaic current as the potential of the electrode is changing at a high speed which can 'mask' some Faradaic information, i.e. the non-Faradaic current can become much higher than the Faradaic current, swamping the useful information.

Figure 3-9 shows the polarisation curve for a GdBCO-Ag sample with approximately 8 mm^3 (2 x 2 x 2 mm) of material in the electrolyte when first inserted. Current began flowing around 1.25 V vs Ag/AgCl, this is the

activation potential. The energy required to dissolve material from the anode is reached and as a result, current begins to flow. A peak is observed at around 3.3 V. This is due to the decreasing surface area as material is dissolved. By 4.5 V vs Ag/AgCl the sample that was in contact with the electrolyte was completely dissolved. This sees the current response drop to zero as the electrical circuit has been broken.

The suggested electrochemical reactions taking place at the anode are:

$$Gd \rightarrow Gd^{3+} + 3e^- \tag{5}$$

$$Ba \rightarrow Ba^{2+} + 2e^- \tag{6}$$

$$Cu \rightarrow Cu^{2+} + 2e^- \tag{7}$$

along with oxygen evolution due to the breakdown of water at the anode:

$$2H_2O \rightarrow O_2 \uparrow + 4H^+ + 4e^- \tag{8}$$

Evidence of oxygen evolution is seen in the polarisation curve by the variation in current over the peak in Figure 3-9. Oxygen bubbles temporarily block the work piece surface, resulting in a drop in observed current. Once the bubbles reach a critical diameter, the bubbles either burst or release from the electrode surface and float to the electrolyte surface, exposing the work piece surface to the electrolyte, increasing the current response. A single experiment is shown in Figure 3-9 which represents a typical result but replications of the experiment will not yield identical results due to the stochastic nature of the bubble formation at the electrode surface.
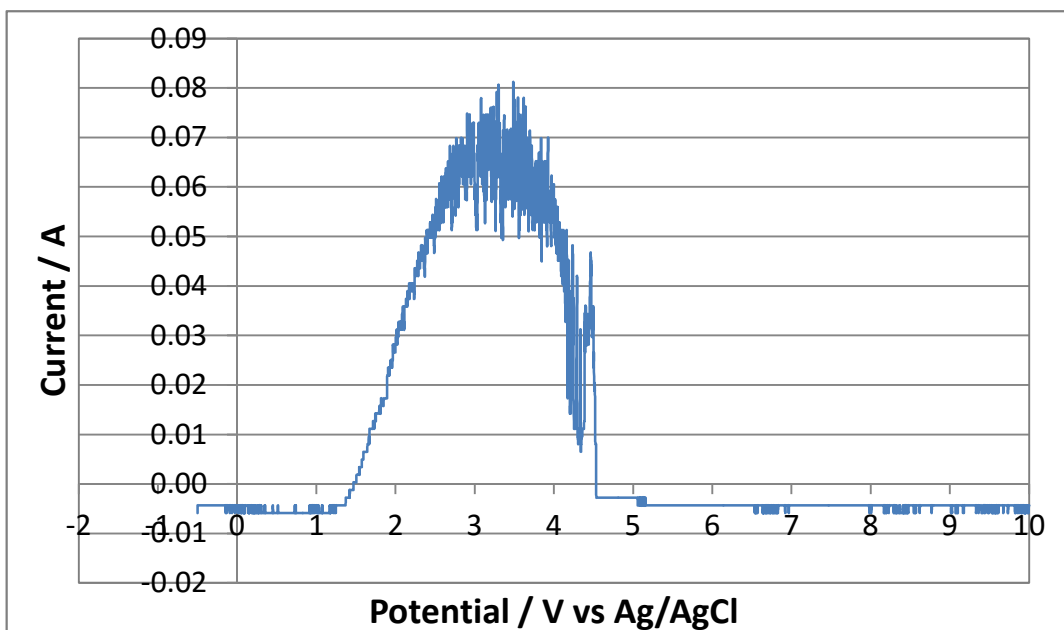
Figure 3-9 Polarisation Curve for GdBCO-Ag in 3.0 M aqueous NaCl at a scan rate of 2 mV s^{-1} (2 x 2 x 2 mm working electrode, 8 x 15 x 0.25 mm counter electrode) solution not degassed, natural levels of oxygen present

Images of the sample surface were taken before and after the polarisation experiment using a JEOL 6000 table top scanning electron microscope (SEM) machine with an inbuilt energy dispersive X-ray spectroscopy (EDS) function. EDS can reveal elemental information. High energy electrons are directed at the sample which excites an electron from an inner shell of an atom creating an electron hole. An electron from a higher energy shell then fills this hole. The difference in energy between the inner and outer shell can then be released as an X-ray. The energy of the released X-ray is characteristic of a certain element. This allows for elemental composition analysis of the sample. Figure 3-10 shows SEM images of the GdBCO-Ag sample before and after the polarisation curve in 3.0 M NaCl.
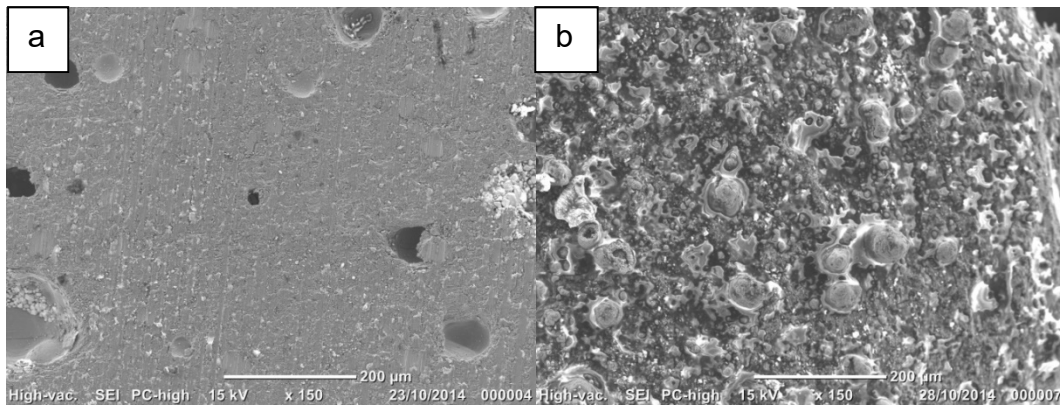
Figure 3-10 SEM Images of GdBCO-Ag sample a) before polarisation curve in 3.0 M NaCl b) after polarisation curve in 3.0 M NaCl

The surface of the GdBCO-Ag sample, before the polarisation curve was conducted, is relatively uniform with some air pockets and areas where small particles are trapped in the matrix. This is expected as there is a small amount of Gd211 particles trapped within the Gd123 single crystal as well as silver particles.

After the polarisation curve experiment the surface looks radically different with small round protrusions from the surface. This suggests one or more components of the sample were not machined at the same rate as the others. Energy-dispersive X-ray spectroscopy (EDS) analysis was conducted to determine the composition of these small protrusions. It was found that the silver inclusions had not been machined at the same rate as the bulk superconductor material; Figure 3-11 shows an EDS map of an area on the surface after the polarisation experiment. The silver inclusions are known to improve the superconducting properties and the mechanical behaviour of the material (Konstantopoulou et al. 2014). There are dark areas on the EDS map where the electron source cannot reach due to the uneven surface as EDS is a 'line-of-sight' technique. However, it is still possible to say the small round protrusions are silver from the EDS map produced in Figure 3-11. The ideal situation would see all components machined at the same rate.
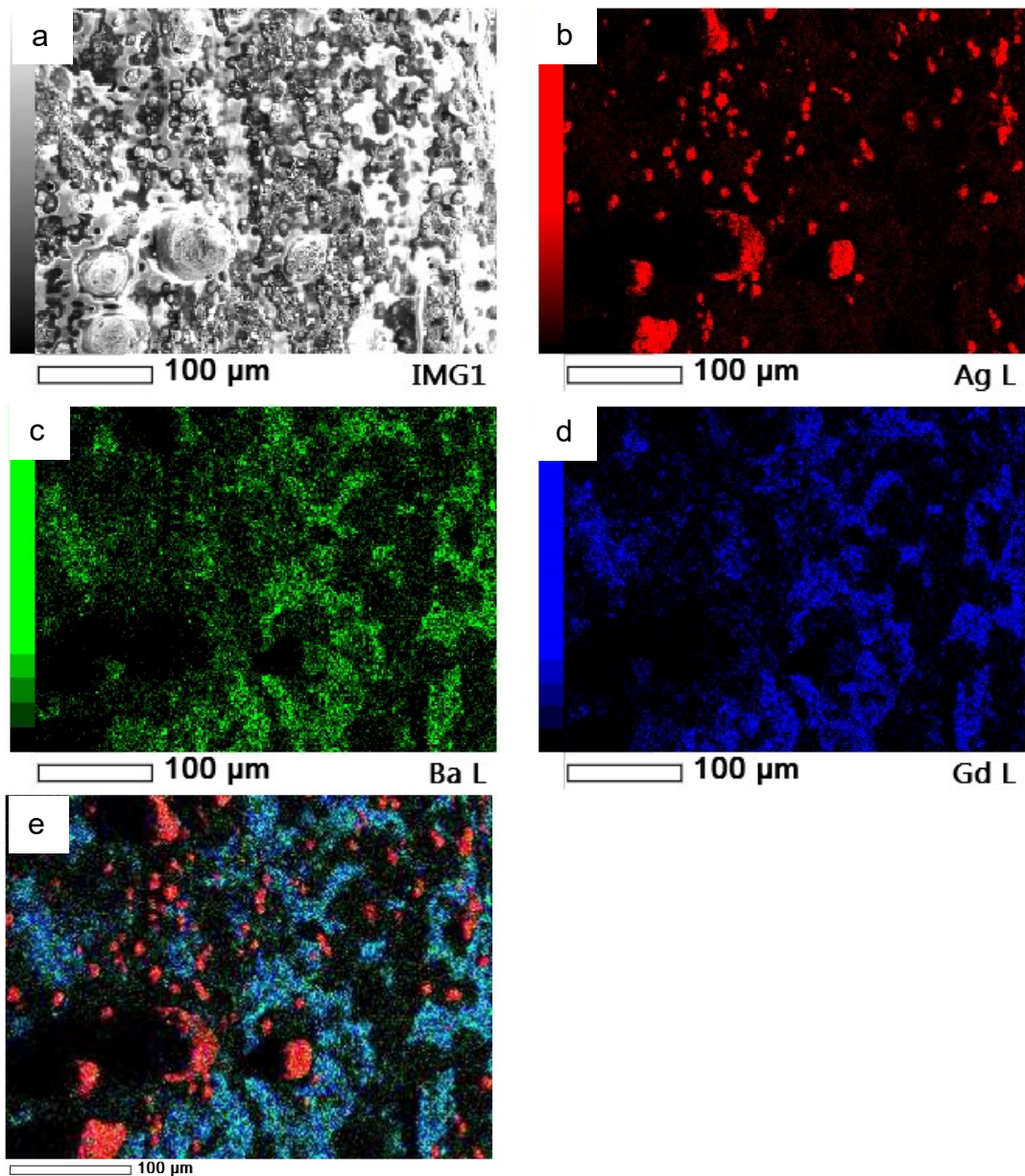
Figure 3-11a) SEM image corresponding to the mapped area b) EDS map image of GdBCO-Ag after polarisation curve mapping the silver distribution (red) c) the barium distribution (green) d) the gadolinium distribution (blue) e) overlaid images b, c and d.

The barium and gadolinium occupy the same space on the map; as a result the colours have mixed giving a turquoise colour in Figure 3-11e. Oxygen has not been included in the analysis.

Sodium chloride did successfully machine GdBCO-Ag although not ideally as silver was not dissolved at the same rate at the remaining elements. This is because silver chloride is insoluble so it is unlikely that silver was being anodically dissolved. The addition of sodium nitrate to the electrolyte may assist in the dissolution of silver as silver nitrate is one of the very few soluble silver salts.

3.3.2 Electrochemical Machining with an Aqueous Electrolyte

The electrolyte used for the electrochemical machining in aqueous electrolyte was 1.0 M NaCl after it was demonstrated NaCl was able to anodically dissolve GdBCO-Ag, although it did not remove the Ag particles electrochemically. A lower concentration was chosen than used in the polarisation curves with the aim of high resolution machining.

The machining potential was chosen to be 7.0 V. This potential should allow a reasonable MRR and should give a high quality surface finish providing the silver particles are small.

Initial ECM experiments, using a constant potential of 7.0 V, demonstrated relatively fast machining rates; but little localisation was to be expected due to the natural evolution of the current distribution over time. The composition of the material is 70 % superconducting Gd123 (that is $GdBa_2Cu_3O_{6-7}$) and 20 % non-superconducting Gd211 (that is Gd_2BaCuO_5) with 10 % silver inclusions to improve the strength of the material. As machining progressed a green colour began to appear at the surface, this can be observed in Figure 3-12. Gd211 naturally has a green colour so it is believed the Gd123 component was being machined at a higher rate than the Gd211 component. This is undesirable, as stated earlier, Gd123 is the superconductive phase. Ideally, all three components (Gd123, Gd211 and Ag) would be machined at the same rate, inducing no colour, nor overall chemical change in the material.

Figure 3-12 GdBCO-Ag sample after ECM machining in 1.0 M NaCl

It was decided it would be best to use non-aqueous electrolytes as the SC sample was being exposed to the aqueous environment for extended periods of time which could cause loss of SC properties in the sample. Also, the green colour indicates preferential dissolution of the SC component over the other components in an aqueous electrolyte.

3.3.3 Polarisation Curves in Non-Aqueous Electrolytes

Non-aqueous solvents have been demonstrated in ECM with metal workpieces with the aim to prevent passivation (Sjöström & Su 2011; Landolt et al. 2003; Fushimi et al. 2009; Fushimi & Habazaki 2008) so stretching the idea to SCs was not a difficult decision to make. Non-aqueous solvents do not allow for such high solute concentrations due to the lower dielectric constants and as such the currents drawn during polarisation experiments are much lower than those observed in aqueous electrolytes. (Pletcher 2009) With lower currents the material removal rate will be proportionally lower but this is something that has to be accepted due to the susceptibility of the SC to aqueous environments.

Glycerol was expected to dissolve high salt content in comparison to the other solvents being studied (methanol, formamide and formic acid).

However, glycerol is a viscous solvent (1.41 Pa s at 20 °C, compared to 0.001 Pa s for water at 20 °C) resulting in low diffusion rates of ions through the electrolyte. With low diffusion rates both to and from the work piece the reaction is limited; this is confirmed by the low currents observed in polarisation curves using glycerol as the solvent, see Figure 3-13. The polarisation curve in Figure 3-13 uses the highest concentration of any of the salts studied, which resulted in the highest observed currents amongst the glycerol-based electrolytes. The current was too low to observe any significant anodic dissolution. Also, in a viscous, non-polar electrolyte, charging the EDL takes a longer time due to reduced ion mobility
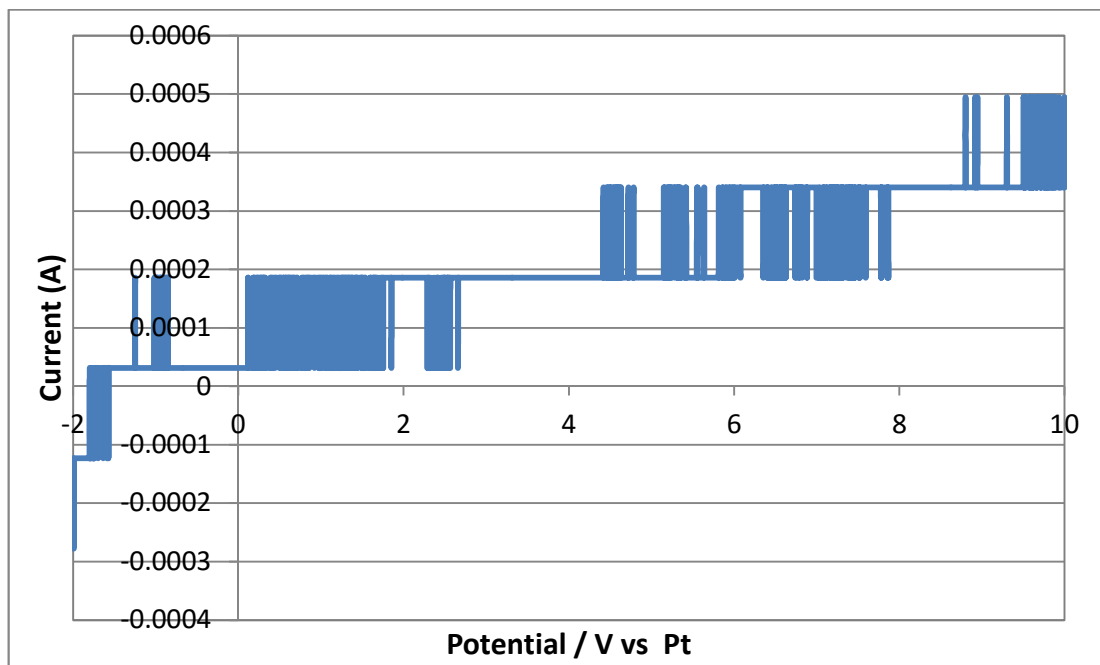
Figure 3-13 Polarisation Curve of GdBCO-Ag in 2.25 M NaBr in Glycerol scan rate 2 mV s^{-1}, 2 x 2 x 2 mm GdBCO-Ag sample, 8 x 10 x 0.25 mm platinum counter electrode, electrolyte not degassed.

Unfortunately this showed that glycerol-based electrolytes were not suitable for the anodic dissolution of GdBCO-Ag at room temperature due to the viscosity.

As sodium chlorate was only paired with glycerol in the experimental plan, sodium chlorate will not be discussed further with respect to the anodic dissolution of GdBCO-Ag in non-aqueous electrolytes.

The viscosities of the three remaining solvents did not pose the same difficulties and the results of the polarisation experiments will be discussed below.

Sodium chloride and sodium bromide were dissolved in methanol to study their suitability as electrolytes for the anodic dissolution of GdBCO-Ag. Methanol allowed the least amount of salt to be dissolved of all of the solvents studied; with a maximum concentration of 1.3 mol dm^{-3} for NaBr and only 0.19 mol dm^{-3} for NaCl. With low electrolyte concentrations, it was expected that the conductivity of the solution would be low also. Low electrolyte conductivity does not facilitate high currents to be passed due to an increase in resistance. As a result, polarisation curves in methanol showed a low current response; a maximum of 110 mA was observed when using saturated NaBr, as can be seen in Figure 3-14.

Current begins to flow around 1.5 V in the polarisation experiments for both NaBr and NaCl in methanol, indicating similar activation potentials for both salts. For both 0.1 M NaBr and 0.1 M NaCl there is a sudden current drop between 4.3 and 4.7 V. For 0.1 M NaCl the current doesn't begin to rise until 6.3 V suggesting the SC surface becomes passivated and unresponsive. As this drop is not observed for the saturated NaCl electrolyte or for the higher concentrations of NaBr, it is suspected the methanol is complexing, or bonding, to the surface preventing further reaction with the salt. At higher concentrations there are fewer methanol molecules at the surface in comparison, as such fewer methanol molecules will complex to the surface and the higher salt concentration facilitates dissolution over passivation. The current begins to drop linearly with potential for saturated NaBr suggesting material removal and the decrease in surface area of the sample. There is a
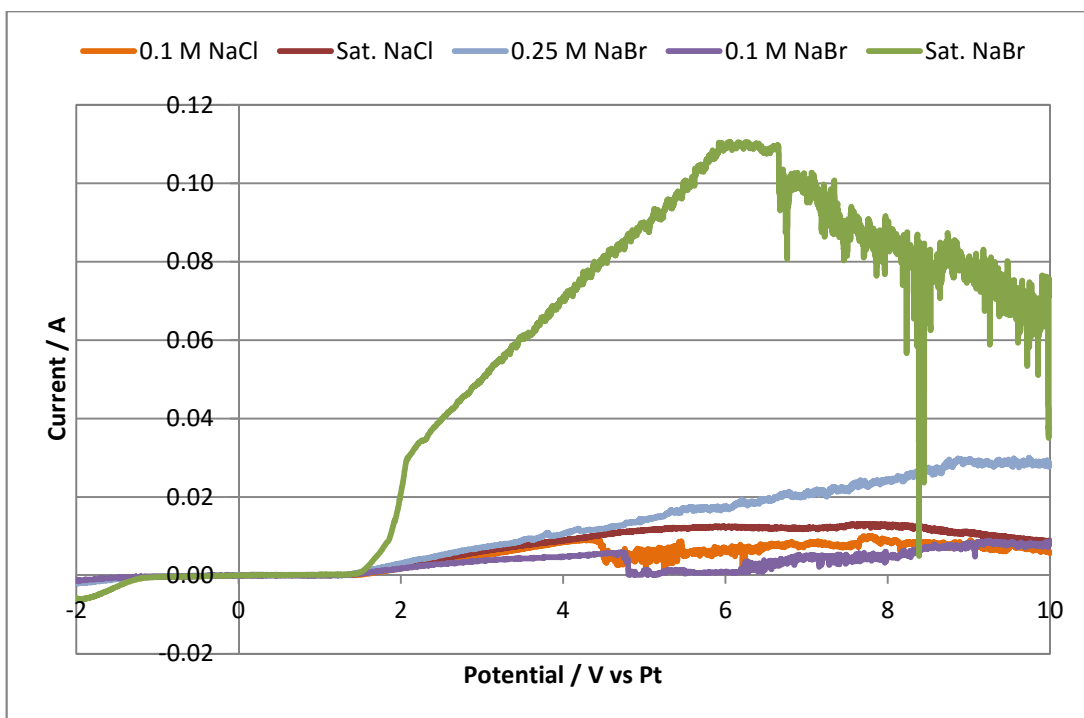
Figure 3-14 Polarisation curve of GdBCO-Ag in various concentrations of NaBr and NaCl in Methanol at a scan rate of 2 mV s^{-1} at room temperature, working electrodes dimensions of 2 x 2 x 2 mm and a counter electrode with dimensions 8 x 10 x 0.25 mm.

large fluctuation in current in this region, between 6.5 V and the end of the experiment, which is associated with the removal and instant reformation of a surface film. This surface film could be a metal bromide film or a metal oxide. The surface film would need to be analysed for chemical composition to determine this.

Overall, using methanol as a solvent did not provide electrolytes with conductivity high enough to facilitate levels of anodic dissolution which would make ECM a suitable method to machine SCs.

Sodium bromide in formic acid resulted in total or near-total dissolution of the sample at all concentrations. This can be seen in Figure 3-15; the current of each curve drops to zero or near-zero indicating there has been complete removal of the sample in contact with the electrolyte; this breaks the electrical circuit preventing further current flow. There is a small peak evident

in all curves shown in Figure 3-15 at around 0 V. This is evidence of the formation of a passive layer. As the passive layer forms, the current drops to zero until a potential is reached that can break down the protective layer and current begins to flow once more.

The current response for 0.75 M NaBr in formic acid becomes unstable between 6.5 and 8.5 V. This is thought to be because of the removal and instant formation of a passivating surface layer. The current profile for all curves appears slightly 'fuzzy'; this is due to the evolution of carbon dioxide from the breakdown of the formic acid solvent. The suggested reaction is shown in Equation 9.

$$CH_2O_2 \rightarrow 2H^+ + CO_2 + 2e^- \hspace{3cm} \text{(9)}$$
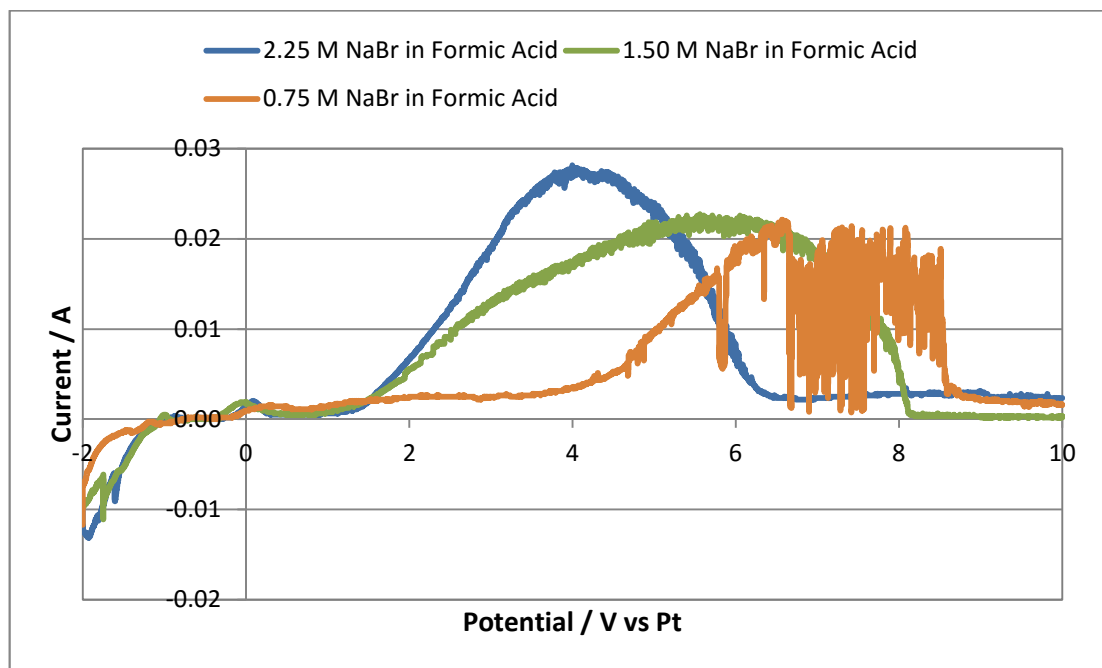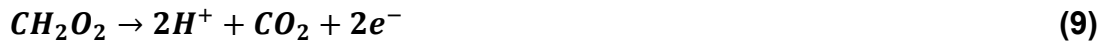
Figure 3-15 Polarisation curve of GdBCO-Ag in various concentration of NaBr in Formic Acid at a scan rate of 2 mV s^{-1}, working electrode dimensions of 2 x 2 x 2 mm and counter electrode with 8 x 10 x 0.25 mm platinum sheet (Leese et al. 2016)

At lower electrolyte concentrations the reaction in Equation 9 could become competitive with the dissolution reaction as there is insufficient salt at the anode surface to prevent carbon dioxide evolution.

At higher concentrations there are proportionally fewer formic acid molecules at the surface, suppressing the evolution of carbon dioxide. The formic acid molecules within the surface layer are likely to be coordinated to metal ions which prevent them from being electrically decomposed. A similar effect has been observed in aqueous media where oxygen evolution is diminished at higher concentrations. (Van Damme et al. 2006)

The initial current response is negative, as seen in Figure 3-15. This is due to the working electrode being polarised as the cathode intially. The current drawn is likely due to the evolution of hydrogen, demonstrated by Equation 10.

$$nH^+ + ne^- \rightarrow \frac{n}{2} H_2 \uparrow \tag{10}$$

The hydrogen ions present in the electrolyte originates from the dissociation of the formic acid solvent, as seen in Equation 11 below.

$$\tag{11}$$
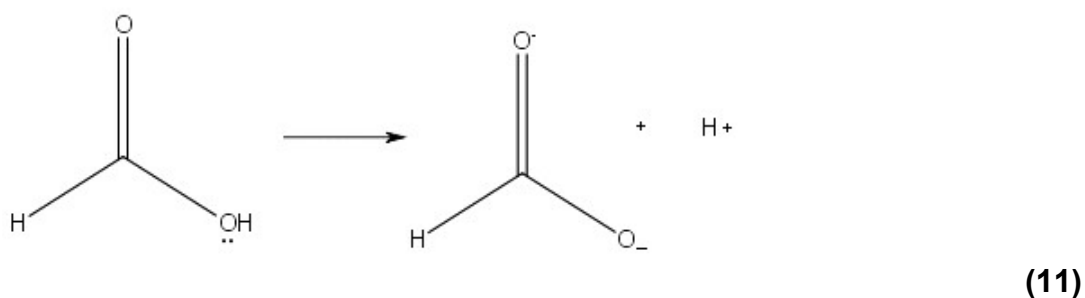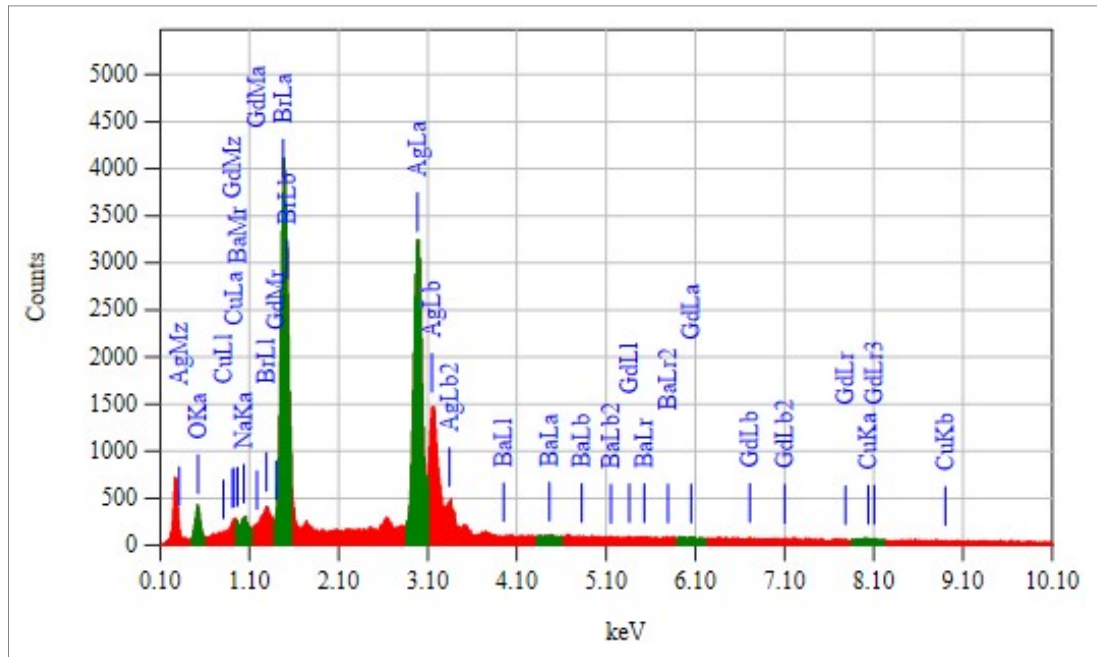
Figure 3-16 EDS spectrum of GdBCO-Ag after polarisation experiment in 2.25 M NaBr in formic acid

Figure 3-16 shows the EDS spectrum of the GdBCO-Ag sample after the polarisation experiment in 2.25 M NaBr in formic acid. EDS probes the surface layer and gives information regarding the elemental composition. Typically X-rays are emitted from a depth between 2 μm and 0.5 μm. In this spectrum there is a large peak assigned to the presence of silver and another large peak assigned to bromine. This indicates the silver component has not been dissolved at the same respective rate in order to keep the composition the same. If the sample composition has not been altered by the polarisation experiment the following atomic percentages should remain true; Gd 10.0 %, Ba 14.6 %, Cu 20.9 %, O 53.6 % and Ag 0.9 % based on the Gd123:Gd211:Ag ratio 7:2:1 respectively. The quantitative analysis, shown in Table 3-2, shows the surface is covered with a high percentage of silver and bromine. Ideally there should be very little bromine on the sample surface after polarisation as this should be washed off to leave a clean surface. Due to the very low atomic percentages of the other components it can be said the AgBr salt layer is thicker than at least 0.5 μm which is the minimum

probing depth of the electron beam for EDS. This was to be expected as AgBr is insoluble.

Table 3-2 Quantitative Analysis from EEDS of sample after polarisation experiment in 2.25 M NaBr in Formic Acid

Element	Atomic Percentage
O	5.00
Na	0.86
Cu	1.73
Br	42.89
Ag	49.37
Ba	0.07
Gd	0.09
Total	100.01

Interestingly, sodium bromide in formamide does not lead to complete dissolution over the period of the polarisation experiment, yet the total charge passed is comparatively higher. The current becomes limited; observed by the current plateau as the potential is increased for each concentration in Figure 3-17. The electrolyte concentration limits the current density achievable at the electrode surface. During the initial linear region, varying between 1.3 V and 7.1-8.1 V, the reaction is activation controlled; the rate of reaction is limited by the electrode potential. The limited current in the higher potential regions is dependent on electrolyte concentration.

The more alkaline electrolyte appears to be less efficient for the anodic dissolution of GdBCO-Ag; a higher charge was passed during the polarisation experiment yet the material was not completely dissolved. The sample sizes were all very similar, approximately 2 mm x 2 mm x 2 mm (8 mm^3), which suggests other reactions are occurring at the electrode alongside the dissolution reactions suggested in Equations 5, 6 and 7. Other reactions could include oxidation of the electrolyte, e.g. chlorine gas

generation, salt film formation or dissolution at a higher valency due to higher stability of the ions at higher valence in alkaline solutions.
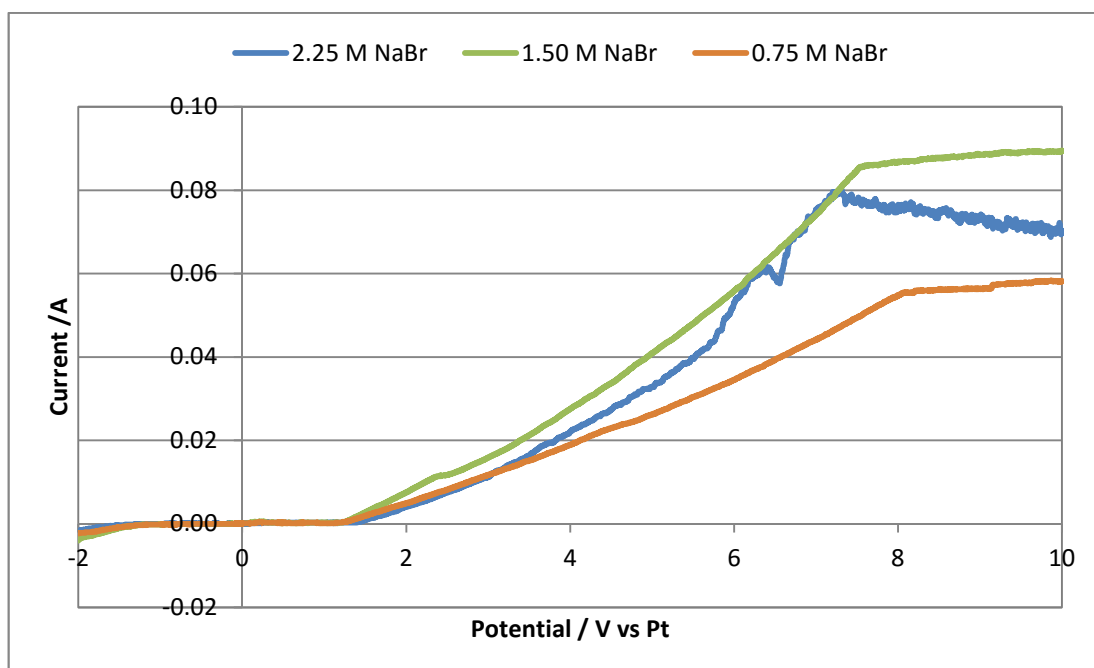
Figure 3-17 Polarisation Curve of GdBCO-Ag samples in various concentrations of NaBr in Formamide with a scan rate of 2 mV s^{-1} and a working electrode dimension of 2 x 2 x 2 mm and a counter electrode 8 x 10 x 0.25 mm

Due to the higher current being drawn in the experiment with a formamide solvent compared to the formic acid solvent, yet the sample sizes being the same, another reaction must be occurring simultaneously at the SC surface. There are several orientations the formamide molecule can approach the anode surface; the oxygen atom has a partial negative charge, as seen in the second structure in Equation 12. The nitrogen atom also has an electron pair which could coordinate to the SC surface. The lone pair can be seen on the nitrogen (N) atom in the first figure in Equation 12; it is represented by the double dots on the nitrogen atom. The orientation the molecule approaches the surface could affect the reaction mechanism and/or reaction products.

(12)
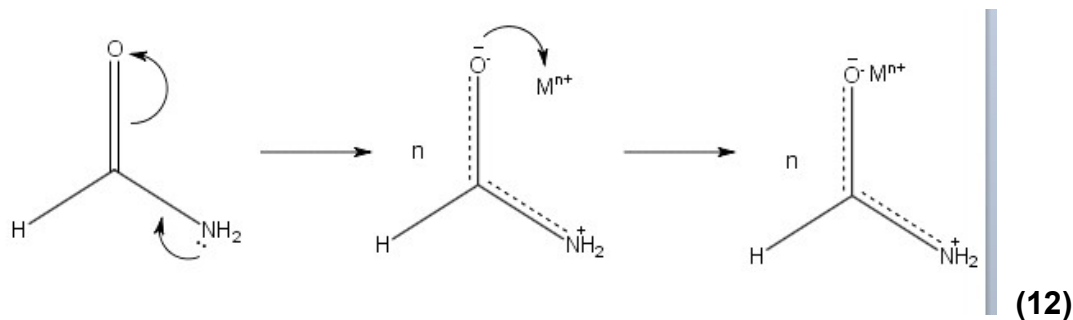
Parmeter et al (Parmeter et al. 1988) studied the interaction of formamide with ruthenium. They reported several decomposition products of formamide on metal surface, which are shown in Figure 3-18.
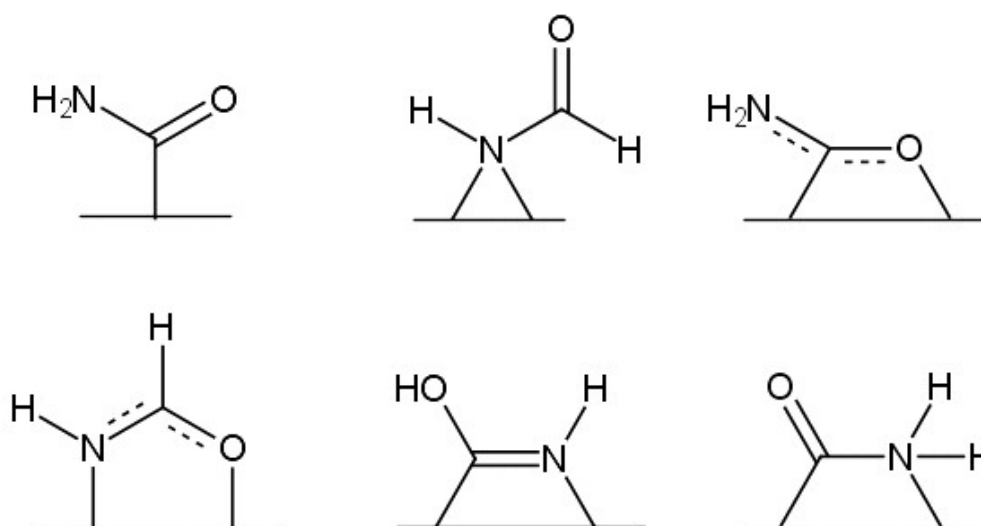
Figure 3-18 Possible decomposition products of formamide on metal surfaces reproduced from (Parmeter et al. 1988)

As the potential was raised, the SC began to dissolve into the solution, visible by the diffusion of a soluble violet compound away from the anode surface. As the experiment progressed, the violet compound diffused throughout the whole solution. A black solid was observed at the bottom of the electrochemical cell, this is probably SC material which has been mechanically removed from the surface due to the dissolution of surrounding material as seen in Figure 3-19.
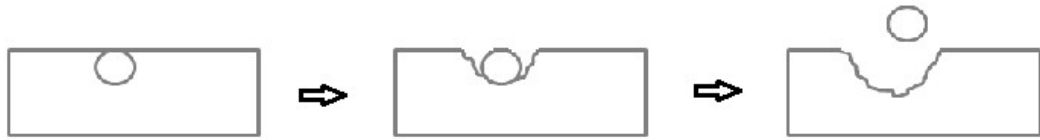
Figure 3-19 Pictorial representation of material removed without undergoing electrochemical change

Nelson (Nelson 1953) studied the anodic dissolution of copper in a saturated ammonium bromide solution of formamide, a similar solution to the one used in this study. The author initially observed a blue solution upon electrolysis, which is expected due to the use of a pure copper anode; he also observed the formation of a few violet crystals on the cathode upon the second use of the electrolyte for electrolysis. The purple crystals were found to be tetraformamide copper (II) bromide ($Cu[HCONH_2]_4Br_2$). It is possible the same compound is formed upon dissolution of GdBCO-Ag in NaBr with formamide where the formamide molecules form a complex with $CuBr_2$ solvating the compound. Similar complexes for the other elements in GdBCO-Ag can be expected to form also. The suggested complexes are $Ba[HCONH_2]_4Br_2$ and $Gd[HCONH_2]_3Br_3$.

It is also possible for the copper within the SC material to react with the solvent in the following reaction, Equation 13. This was observed by Nelson. (Nelson 1953)

$$(13)$$
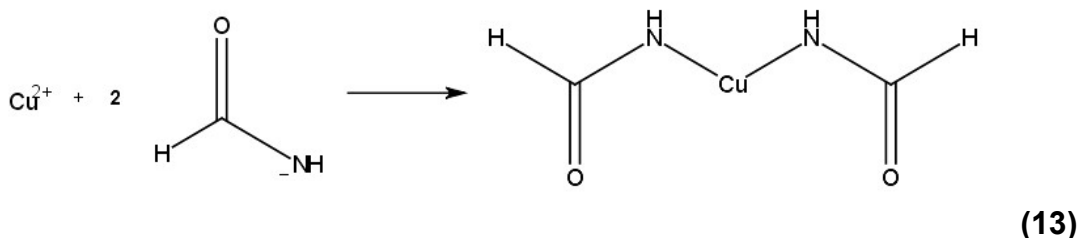
For this reaction to happen, a hydrogen ion first has to be lost from the amide group to create the negative charge on the nitrogen. This reaction is expected at the cathode, evolving hydrogen gas in the process. Again, one can expect similar reactions and products with the other metallic components

64

of the SC material, as shown in Equation 13, forming $Gd(NHCHO)_3$ and $Ba(NHCHO)_2$.

Gas bubbles were also seen to form on the anode as the voltage was increased; this has been attributed to bromine gas generation from the oxidation of bromide in the electrolyte. This is also observed in the polarisation curve where the current fluctuates slightly over the peak, appearing to thicken the current line.

At the highest concentration, 2.25 M, there is a slight decrease in the current drawn at the anode at approximately 6.4 V vs Pt. This would suggest the surface become less reactive for a time; this could be due to the formation of a salt layer e.g. $CuBr_2$, $BaBr_2$ and $GdBr_3$, which is quickly removed. It is possible this only formed in 2.25 M NaBr in formamide due to the higher concentration of salt which means the saturation concentration is reached more quickly. The salt film has the effect of blocking the active surface, reducing the current that can be passed.
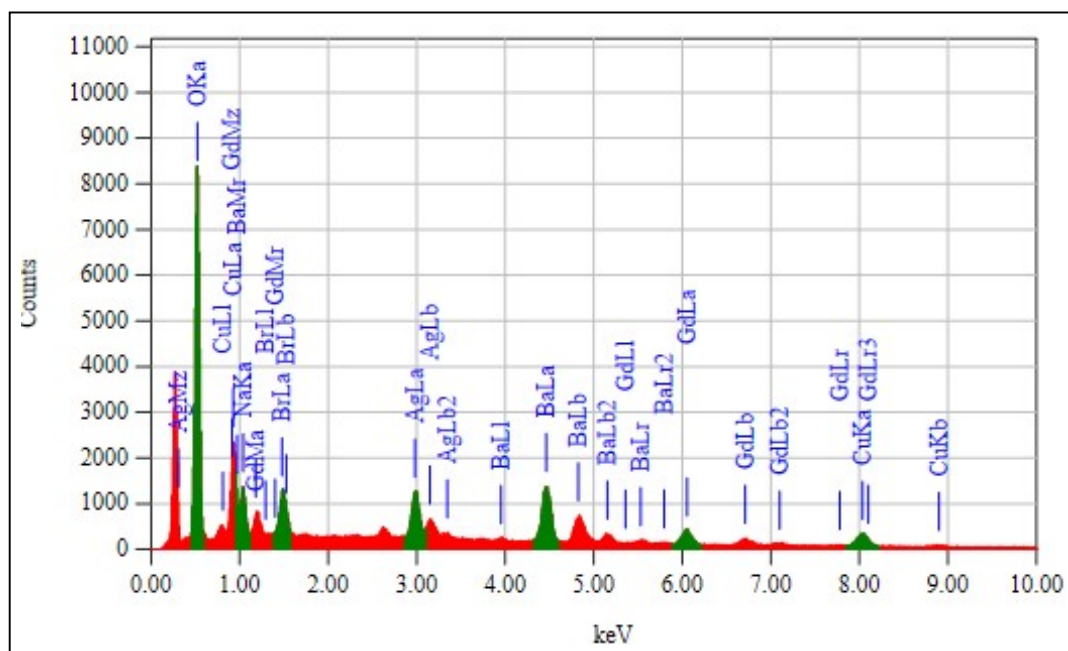
Figure 3-20 EDS spectrum of GdBCO-Ag after polarisation experiment in 2.25 M NaBr in formamide

As explained above there are several possible reactions which could take place at the anode which does not lead to anodic dissolution; if these reactions take place simultaneously alongside the dissolution process the efficiency would decrease from 100 %, seeing a higher current but less total anodic dissolution. Full analysis of gas products, sample surfaces and the electrolyte after the experiment needs to be conducted in order to uncover the true reactions occurring during these experiments.

Comparing the EDS spectrum of a sample after the polarisation experiment in 2.25 M NaBr in formamide in Figure 3-20 to Figure 3-16, the oxygen peak is much larger and the silver peak is proportionally smaller. This is confirmed by the quantitative analysis in Table 3-3. The oxygen concentration is still lower than expected from a pure sample; however, there is little evidence of a salt layer, consistent with the polarisation curves, so it can be said the oxygen content from the surface layer has been diminished. This is not necessarily a problem; it is possible to adjust the oxygen concentration post processing to achieve the correct stoichiometry to ensure the material is superconductive.

Table 3-3 Quantitative Analysis from EDS of sample after polarisation experiment in 2.25 M NaBr in Formamide

Element	Atomic Percentage
O	34.03
Na	0.61
Cu	24.42
Br	2.28
Ag	1.89
Ba	24.78
Gd	11.99
Total	100.00

As a result, NaBr in formic acid is preferred over NaBr in formamide for the anodic dissolution of GdBCO-Ag due to higher dissolution efficiencies but the

surface needs to be washed more thoroughly to remove AgBr from the surface or even the addition of sodium nitrate to the electrolyte to encourage the dissolution of the silver particles through the formation of the soluble silver nitrate salt.

Polarisation curves of GdBCO-Ag with NaCl in both formic acid and formamide behaved in much the same way as with NaBr in these solvents. Sodium chloride is less soluble in both formic acid and formamide than sodium bromide. However, 0.75 M NaCl in formic acid facilitated higher dissolution currents than 0.75 M NaBr in formic acid as shown in Figure 3-21. The period of unsteady current response between 6 and 8 V is thought to be due to the removal and rapid reformation of a film on the electrode surface. Again only single experiments are represented in the figure due to the stochastic nature of the film removal and reformation.
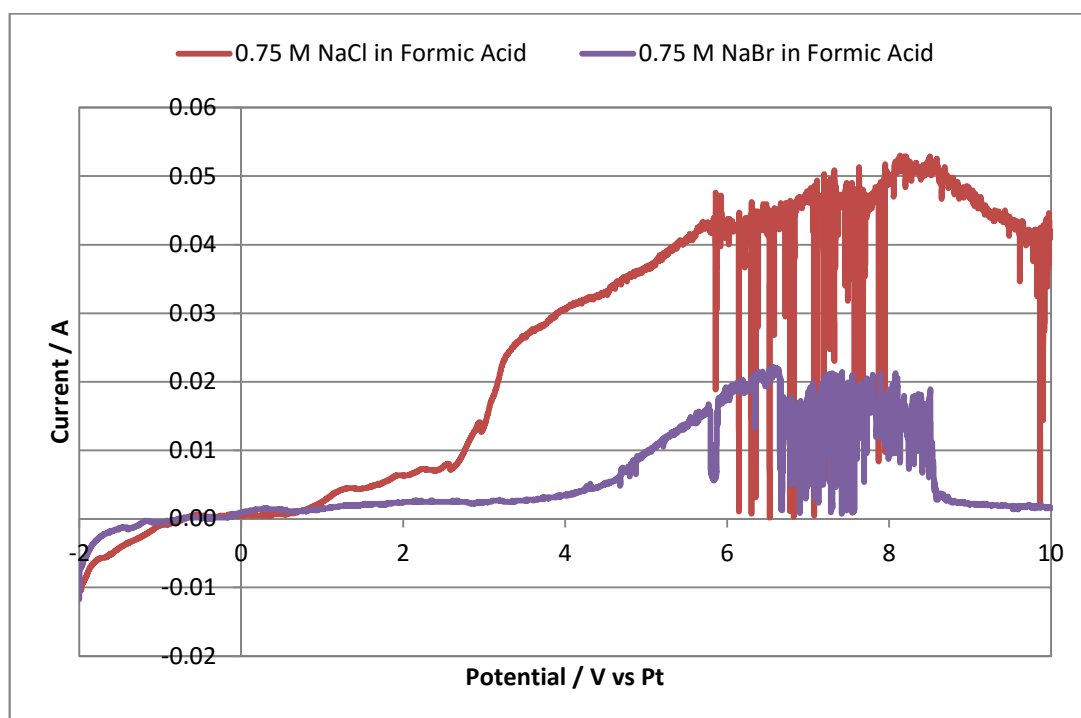
Figure 3-21 Polarisation curve of GdBCO-Ag in 0.75 M NaBr and 0.75 M NaCl in formic acid with a scan rate of 2 mV s^{-1}, working electrode dimensions 2 x 2 x 2 mm and counter electrode dimensions 8 x 10 x 0.25 mm, room temperature

The chlorine ionic radius (181 pm) is smaller than the bromine ionic radius (196 pm) (Clark n.d.) which results in a higher diffusion coefficient for the smaller ion. Smaller ions generally increase the conductivity of a solution compared to larger ions as they experience less resistance moving through the solution. Chlorine is also more reactive than bromine due to its higher electronegativity. Due to the comparatively higher electronegativity, there are stronger forces and attractions between the chlorine ion and oppositely charged ions. This would mean the metal ions would be coordinated to the halide ion at higher rates in NaCl than in NaBr, and hence the metal ions are solvated at higher rates.

Polarisation curves of GdBCO-Ag conducted in NaCl with formic acid resulted in the total or near total dissolution of the material submerged in the electrolyte, apart from for the lowest concentration; this is shown by the current dropping to zero in Figure 3-22. For 0.50 M NaCl in formic acid the total charge passed is very low and the sample appears to be completely dissolved by 4.5 V when the current drops to zero. However, when the experiment was finished, the sample was still attached to the copper wire which allowed electrical connection. This suggests the surface became passivated preventing the passage of current. This passivation is most likely to be the adsorption of the formic acid solvent molecules or the formation of an oxide layer consisting of various metal oxides (CuO, Gd_2O_3, BaO) preventing further reaction. It is suspected this is the case as the initial chloride concentration in the solution is low which does not favour the formation of a salt layer as reaching the saturation concentration would take a considerable length of time.

As with NaBr in formic acid, there is a region of unsteady current in the polarisation experiment for 0.75 M NaCl in formic acid. This is attributed to removal and reformation of a surface layer on the SC sample. There is evidence of gas formation at the anode surface, most probably carbon dioxide as shown by Equation 9, by the small variation of current over the peak. For 1.00 M NaCl in formic acid there is a small peak around 2.5 V

followed by a larger peak which is present in the polarisation experiment for 0.75 M NaCl also. The smaller peak is likely to be the formation of a salt layer which increases the resistance of the anode causing the current to drop slightly. The salt layer is removed and current begins to rise again at 3.6 V.
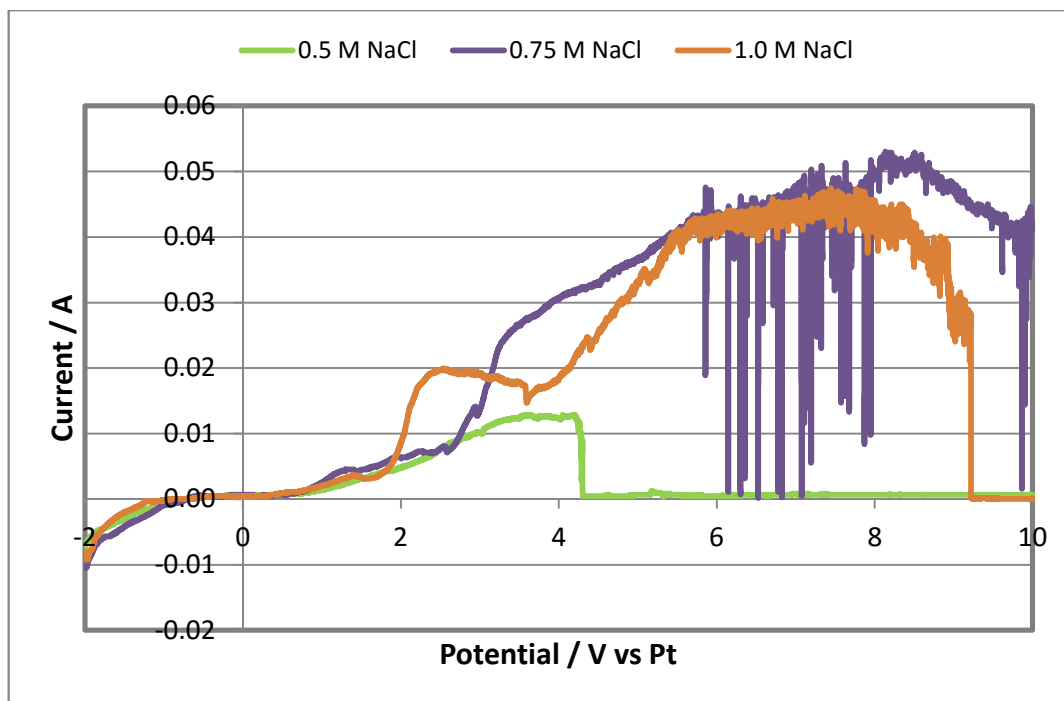

Figure 3-22 Polarisation curves of GdBCO-Ag in various concentrations of NaCl in formic acid with a scan rate of 2 mV s^{-1}, working electrode dimensions 2 x 2 x 2 mm and counter electrode dimensions 8 x 10 x 0.25 mm, room temperature

The EDS (energy-dispersive X-ray spectroscopy) spectrum in Figure 3-23 shows minimal chloride presence on the GdBCO-Ag surface but shows a relatively high O peak and Cu peak, indicating the propensity to form copper oxide over copper chloride.

Using the quantitative data in Table 3-4 it is possible to see the atomic percentages of Ag and Cl are very similar, suggesting the compound AgCl has formed. This is confirmed via an EDS map showing Ag and Cl clustered together, this is shown in Figure 3-24. The atomic percentage of Cu is in line with the expected value of 20.9 % but the percentages of Gd and Ba are

69

higher than expected by 4-5.5 % and the oxygen percentage is over 15 % lower than expected. Oxygen from the SC matrix is likely to react with other oxygen ions to form oxygen gas at the anode decreasing the overall oxygen atomic percentage in the material's surface layer.
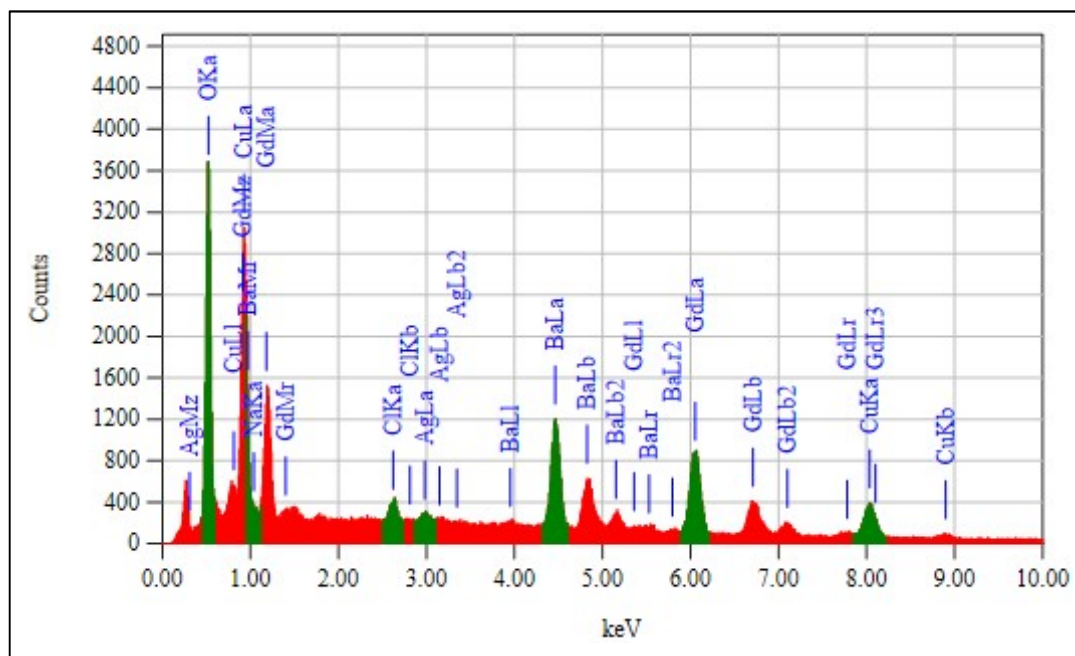
Figure 3-23 EDS Spectrum of GdBCO-Ag sample after polarisation experiment in 1.00 M NaCl in formic acid

Table 3-4 Quantitative Analysis from EDS of sample after polarisation experiment in 1.00 M NaCl in formic acid

Element	Atomic Percentage
O	36.48
Na	0.85
Cl	4.72
Cu	19.29
Ag	5.14
Ba	19.96
Gd	13.57
Total	100.01
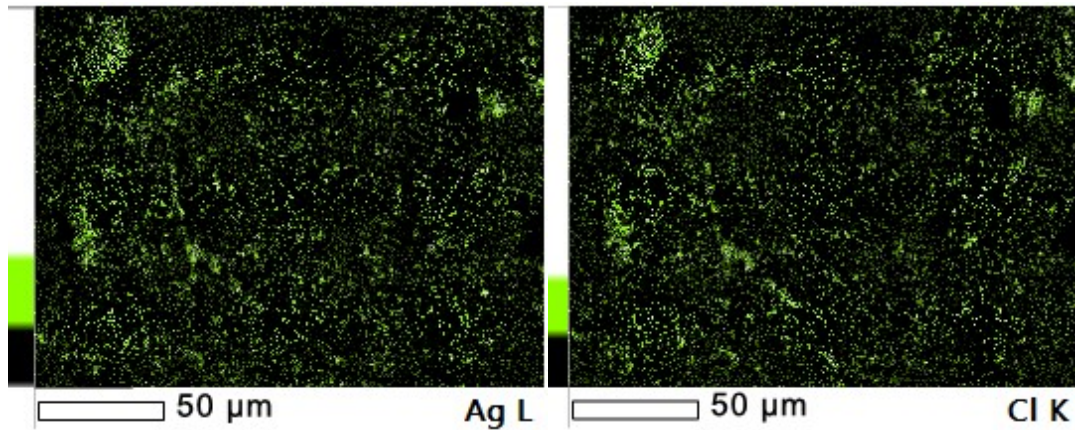
Figure 3-24 EDS map of GdBCO-Ag sample after polarisation experiment in 1.00 M NaCl in formic acid showing the distribution of a) Ag and b) chlorine

Polarisation experiments with NaCl in formamide, again produced similar results to NaBr in formamide, see Figure 3-25, with lower machining efficiencies than seen in formic acid as the sample was not completely dissolved.

There are two periods where the current fluctuates during the polarisation experiment in 0.75 M NaCl in formamide; it is likely both of these periods are gas evolution as the overall current does not drop which would indicate passivation. It appears the gas evolution is suppressed for a period between the two regions of current fluctuation. However, both NaCl and NaBr in formamide did not facilitate total dissolution of GdBCO-Ag during the experiment time period as was seen when formic acid was used as the solvent.
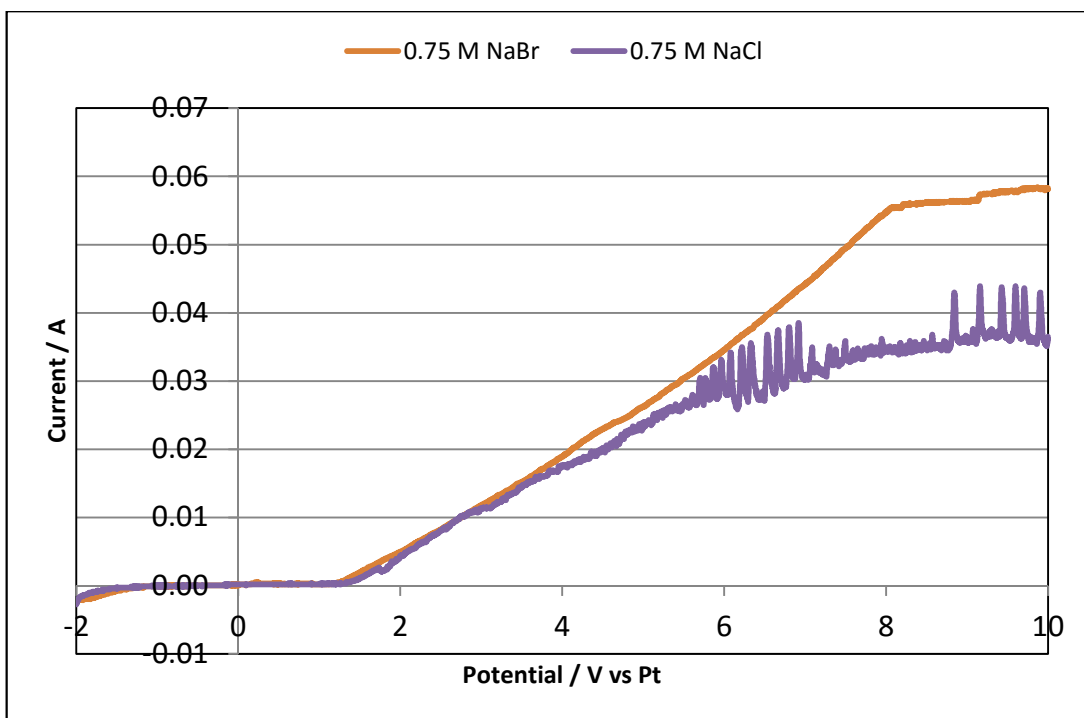
Figure 3-25 Polarisation curves of GdBCO-Ag in 0.75 M NaCl and NaBr in formamide with a scan rate of 2 mV s^{-1}, working electrode dimensions 2 x 2 x 2 mm and counter electrode dimensions 8 x 10 x 0.25 mm at room temperature with natural gas levels

Figure 3-26 shows the polarisation curves for the various concentrations of NaCl in formamide studied. As expected the lowest concentration exhibits the lowest current during the experiment. There is also a small period where gas appears to be evolved from the surface between 6.0 and 6.5 V.

At the highest concentration studied, 1.00 M NaCl in formamide, the high concentration of salt suppressed gas evolution at all potentials. The suppression of gas evolution was also seen for NaBr in formic acid and by Van Damme et al (Van Damme et al. 2006) using aqueous electrolytes.
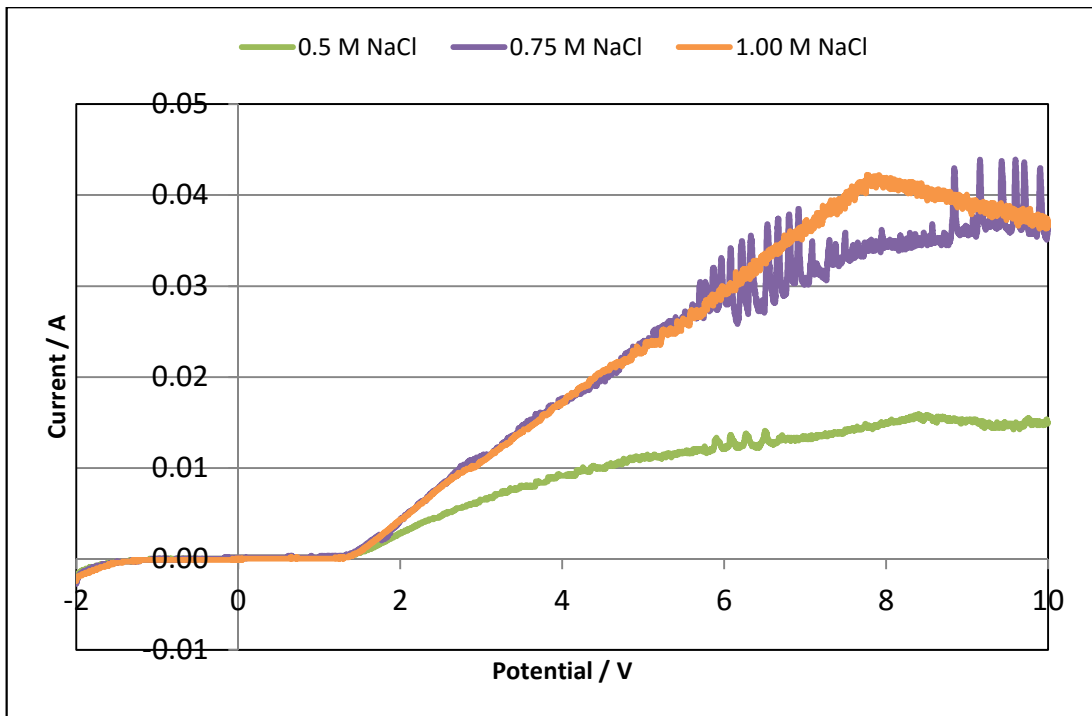
Figure 3-26 Polarisation curves of GdBCO-Ag in various concentrations of NaCl in Formamide with a scan rate of 2 mV s^{-1}, working electrode dimensions 2 x 2 x 2 mm and counter electrode dimensions 8 x 10 x 0.25 mm at room temperature with natural gas levels

A thick green layer was observed on the SC surface for all concentrations of NaCl in formamide; this is consistent with the formation of a salt layer consisting of predominantly copper (II) chloride and copper oxide (CuO) as this is the most abundant element in the matrix. Gadolinium (III) chloride and gadolinium oxide (Gd2O3) forms white crystals; barium (II) chloride and barium oxide (BaO) also form white crystals. Energy-dispersive X-ray spectroscopy was conducted on the GdBCO-Ag sample after the polarisation experiment. The spectrum, in Figure 3-27, shows all of the elemental components present in the surface layer. Comparing the spectrum to Figure 3-23, the peak height ratios appear very similar, indicating the two electrolytes behave in an approximately similar way to each other, removing components at the same ratio irrespective of the solvent used but not necessarily at the same rate.
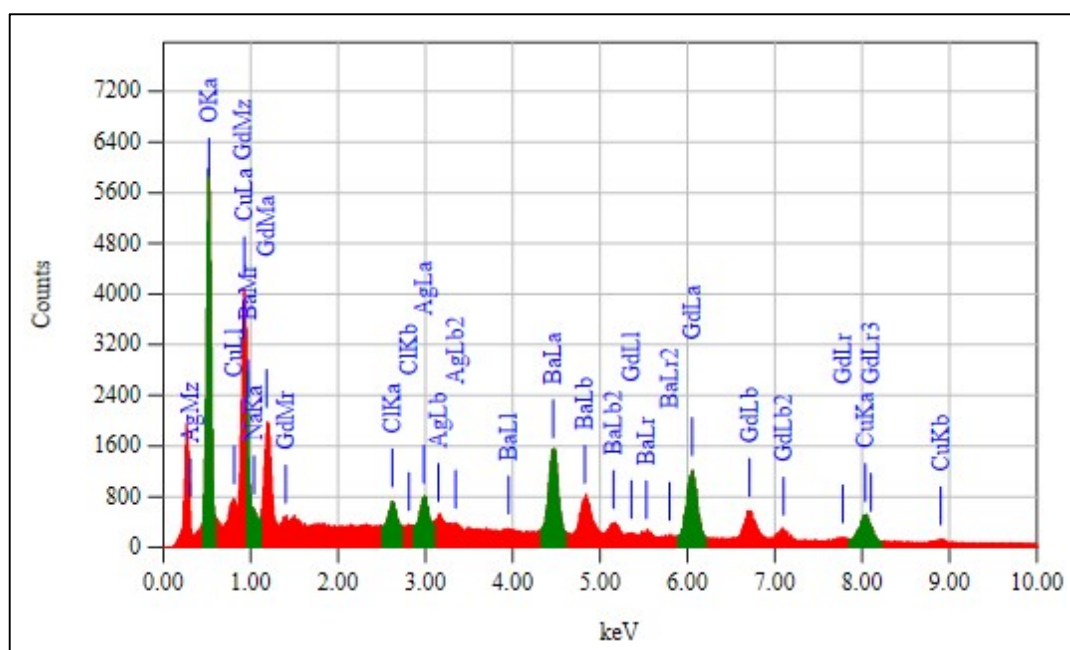
Figure 3-27 EDS Spectrum of GdBCO-Ag sample after polarisation experiment in 1.00 M NaCl in formamide

Table 3-5 shows the quantitative data regarding the atomic percentages of elements at the SC surface after the polarisation experiment in 1.00 M NaCl in formamide. This most closely represents the ideal composition across all tests. Again, Ag has not been machined at the same relative rate as the other elements to maintain the original stoichiometry but this it to be expected due to its stability. Silver is not known to corrode easily. The oxygen content is less than 4 % from the expected value and the EDS map reveals an even distribution of oxygen across the surface, see Figure 3-28. There is also oxygen present in the solvent which may have reacted with the SC surface which would increase the oxygen atomic percentage within the surface layer. The values for gadolinium are slightly increased from the ideal values of 10.00 %, whilst the copper value is lower than the ideal value of 20.9 %. The barium atomic percentage is as expected.

Table 3-5 Quantitative Analysis from EDS of sample after polarisation experiment in 1.00 M NaCl in formamide

Element	Atomic Percentage
O	49.96
Na	1.55
Cl	2.95
Cu	13.29
Ag	4.49
Ba	14.34
Gd	13.42
Total	100.00

Whilst polarisation experiments with NaCl in formamide results in a surface containing the closest to the ideal ratio, the material removal rate was low and a thick green layer was seen to form on the surface. This layer was easily removed with a short washing cycle using an ultrasonic bath.
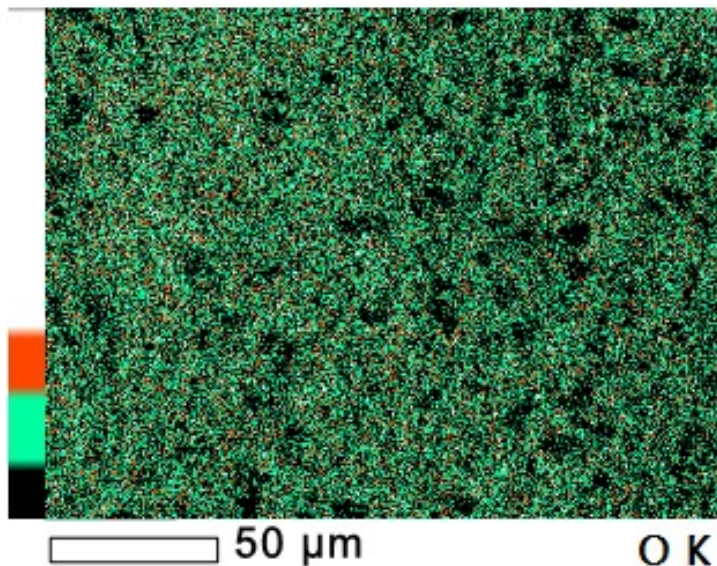
Figure 3-28 EDS map of GdBCO-Ag sample after polarisation in 1.00 M NaCl in formamide showing oxygen distribution at the surface

The surface finish of the machined sample is also important; the superconductive properties rely on good alignment of grains and a continuous structure. If cracks or gaps are introduced into the material the superconductive properties will be damaged. Figure 3-29 compares SEM images of the GdBCO-Ag sample after polarisation experiments in 0.75 M NaCl or NaBr in formic acid and formamide.
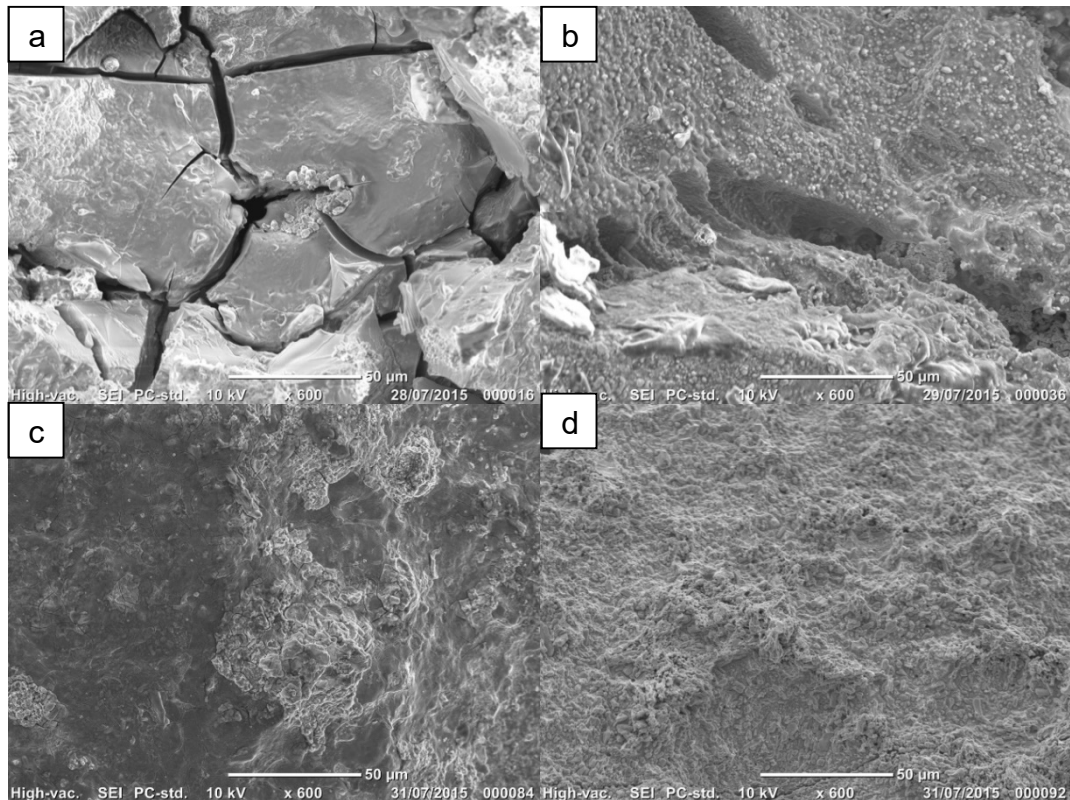
Figure 3-29 SEM images of GdBCO-Ag sample after polarisation experiment in a) 0.75 M NaBr in formic acid b) 0.75 M NaBr in formamide c) 0.75 M NaCl in formic acid and d) 0.75 M NaCl in formamide

There are large cracks visible in the sample after polarisation in 0.75 M NaBr in formic acid; this is undesirable and the very thing this study is attempting to avoid. However, this was using the lowest concentration salt where gas was seen to be evolving at the anode. As the oxygen atomic percentage is lower than expected it can be assumed this is released from the matrix and forms pockets of gas which build in pressure until the material cracks

releasing the gas. This does not happen at the higher concentrations as the gas generating mechanism is out-competed by the dissolution mechanism. This is confirmed when studying the SEM image of the GdBCO-Ag sample after the polarisation experiment in a higher concentration NaBr formic acid electrolyte, see Figure 3-30; there are no cracks in the sample, but the sample is covered with a porous film.
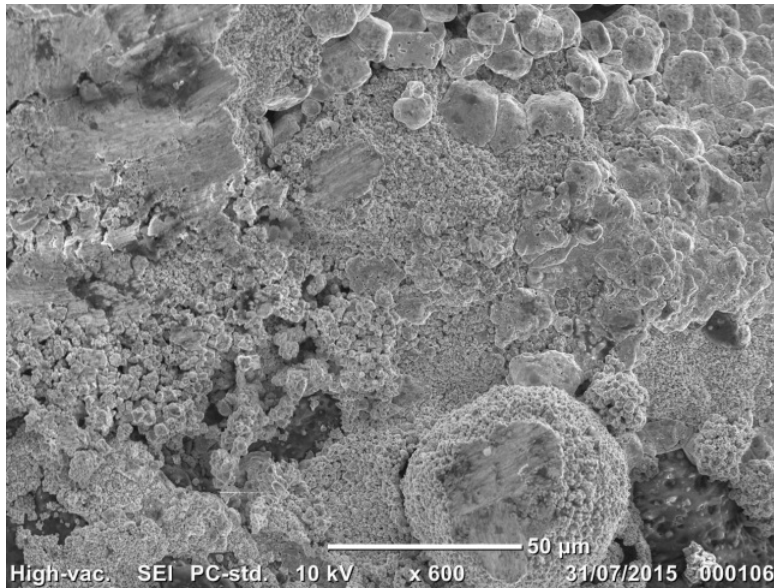
Figure 3-30 SEM image of GdBCO-Ag sample after polarisation experiment in 2.25 M NaBr in formic acid

There are no cracks in the sample after polarisation in 0.75 M NaBr in formamide, shown in Figure 3-29b, but there are deep pockets which run across the image.

The surfaces of the samples in Figure 3-29 c and d are the most uniform although there are still peaks and valleys present. There is a porous surface layer on the sample after polarisation in 0.75 M NaCl in formamide, Figure 3-29d, which is not present in Figure 3-29c after polarisation in 0.75 M NaCl in formic acid. This agrees with the observations from the polarisation experiments that using formic acid as the solvent facilitates more efficient material removal as there is no passivation of the surface; this is in part due to the acidic environment which facilitates a higher concentration of dissolved

anions to remain within the solution rather than precipitate which could occur at the anode surface creating a salt layer.

Overall, a formic acid based electrolyte provides the most efficient anodic dissolution mechanism. A 1.00 M sodium chloride electrolyte in formic acid will be used for the electrochemical machining experiments.

3.3.4 Electrochemical Machining of GdBCO-Ag with Non-Aqueous Electrolytes

The polarisation experiments conducted in non-aqueous electrolytes showed NaCl in formic acid was the best choice. Sodium chloride is less expensive than sodium bromide which was a factor that also influenced the salt choice.

Care had to be taken when using formic acid as it is an irritant, corrosive and it is also volatile so the working area has to be extremely well ventilated and full personal protective equipment had to be worn at all times.

Initially a voltage of 20 V was applied with the machine's standard setting for maximum current of 10 A. The maximum current however limited the machining and after the test had ended, no visible evidence of machining could be seen on the GdBCO-Ag sample. The machine aims to work at the set potential but will reduce the voltage when the maximum current is reached.

The next test saw the maximum current raised to 30 A whilst the potential was reduced to 15 V as a precaution to prevent sparking. The IEG and the feed rate were kept constant. These settings resulted in the creation of a groove almost 2 mm wide, as can be seen in Figure 3-31 marked by the red lines.
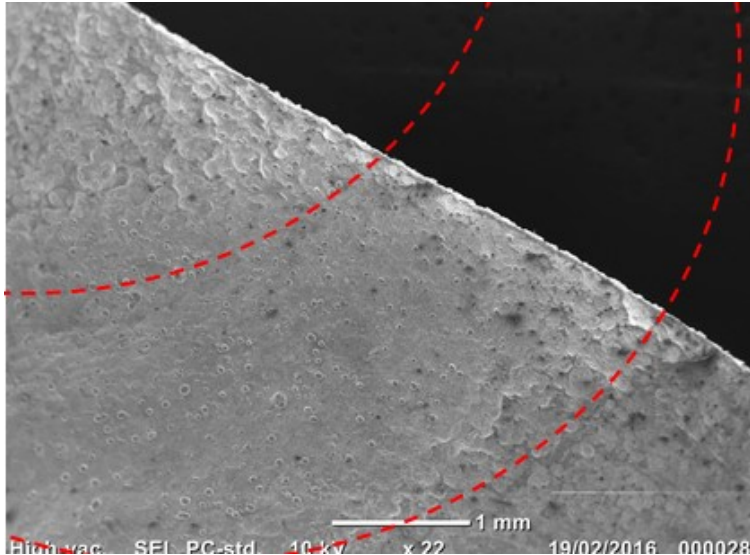
Figure 3-31 SEM image of GdBCO-Ag sample after ECM experiment at 15 V with a maximum current allowance of 30 A

Previous research has shown that the applied voltage affects the machining resolution, with a higher voltage producing a larger overcut. The maximum current of 30 A proved appropriate as the limit was not reached which would have reduced the applied potential; the maximum current remained at 30 A for the remaining tests. The potential was reduced to 8.5 V as this was the potential indicated by the polarisation experiments which would facilitate dissolution and this would reduce the machining overcut.

As the tool was made solely from 0.25 mm diameter platinum wire it was very flexible. As a result, the tool was not 100 % parallel with the work piece causing a variance in the IEG. The IEG was set from the closest point. Figure 3-32 shows the effect of the non-constant IEG with more significant machining at places which were in closer proximity to the tool. The machining overcut has also been reduced by decreasing the machining voltage, with the groove being less than 0.5 mm in width.
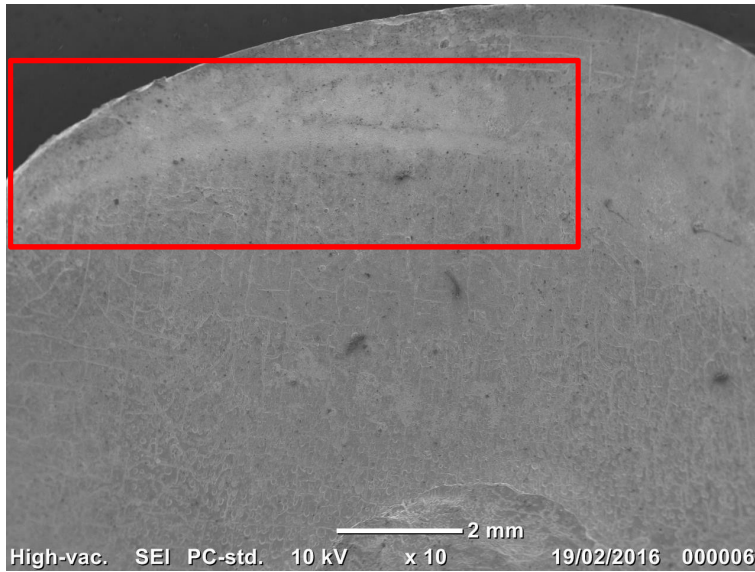
Figure 3-32 SEM image of GdBCO-Ag sample after ECM experiment at 8.5 V with a maximum current allowance of 30 A. Red box highlights machined area.

Unfortunately, the tool came into contact with the work piece during machining at 8.5 V which caused a large spark destroying the tool. The platinum wire melted onto the GdBCO-Ag sample, which can be seen in Figure 3-33.

It is still unclear whether the superconductive properties of the GdBCO-Ag material has been affected by the anodic dissolution process, this is something which needs to be done in future.

3.4   Conclusion

ECM has been demonstrated as a suitable technique for machining ceramic cuprate superconductors, namely GdBCO-Ag. A non-aqueous electrolyte of sodium chloride in formic acid proved to be the most suitable electrolyte to use for the anodic dissolution of the material. Aqueous electrolytes did facilitate anodic dissolution; however, there appeared to be a preference for machining the Gd123 portion of the sample. Machining was also very slow

which made an aqueous electrolyte an unsuitable choice due to GdBCO-Ag being water sensitive.
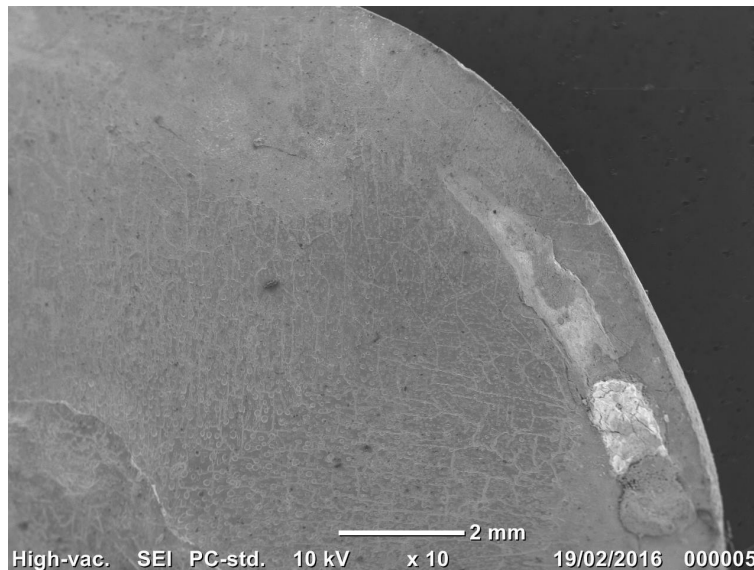
Figure 3-33 SEM image of GdBCO-Ag sample after ECM experiment at 8.5 V with a maximum current allowance of 30 A showing the platinum melt from the destruction of the tool

A voltage of only 8.5 V with a maximum current of 30 A, a feed rate of 0.5 mm min^{-1} and an IEG of 0.1 mm gave the best machining results using the non-aqueous electrolyte with the Impulse ECM machine at pECM Systems Ltd.

3.5 Further Work

Firstly, the tool needs to be developed further. The tool was made from platinum wire which was overly flexible causing difficulties establishing the IEG and maintaining this throughout machining. Whilst the machining resolution was improved by reducing the machining voltage, the overcut was still larger than desired. To combat this overcut, pulsed electrochemical machining should be investigated.

Chapter 4 – Anodic Dissolution of Semiconductors

4.1 Introduction

4.1.1 What is a semiconductor?

A semiconductor is a material, usually a crystalline solid, which has higher resistance than a conductor but lower resistance than an insulator. (Semiconductor n.d.) Their resistivity decreases as their temperature is increased; behaviour opposite of that seen in metals. Their properties can be altered by doping the material with other elements which lowers the resistance, but also allows the formation of semiconductor junctions within the crystal. The behaviour of electrons at these junctions forms the basis of modern electronics.

Group 14 metalloid elements, silicon, germanium and indeed carbon, are semiconductors; crystalline and amorphous silicon is a cheap semiconducting material which is widely used in electronic devices. (Shriver et al. 2006) Aluminium, gallium and indium react with phosphorus, arsenic and antimony to form semiconductor materials. Gallium arsenide (GaAs) is the most widely used of these compound semiconductors. It is superior to silicon as it has higher electron mobility as well as generating less electronic noise than silicon devices. However, GaAs is known to decompose in air so needs to be kept under an inert atmosphere or encapsulated. Silicon wafers are also stronger than GaAs wafers meaning processing is easier.

4.1.2 Why are semiconductors important?

Semiconductors form the basis of modern electronics, being used in everything from integrated circuit boards to individual electrical components. The electronics industry was worth over 2 trillion euros in 2012 (Statista 2014) and it is an ever expanding industry. As such, the industry for semiconductors is constantly growing with the electronics sector, estimated to be in excess of 300 billion Euros (Technische Universitat Munchen 2015).

The electrical conductivity of semiconductors can be controlled by the application of electric currents, electromagnetic fields and light. This makes it possible to create a range of devices which can *'amplify, switch, convert sunlight to electricity or produce light from electricity'*. (Engineering and Technology Wiki 2015)

The electrical properties of semiconductors are exploited for use in many products from integrated circuits, to phones, to energy technologies e.g. solar panels, to solid state lighting. (Technische Universitat Munchen 2015)

4.1.3 Semiconductor machining techniques

Semiconductors used in the electronics industry are commonly made from single crystals so care must be taken not to create any defects in the material when shaping them to a suitable form.

Silicon (Si) and gallium arsenide (GaAs) are the most commonly used semiconductor and are processed through a technique called photolithography. Photolithography uses a template mask and a photoresist to mark areas on the wafer which are to be etched. The method's resolution is limited by the wavelength of light used with the mask to remove the selected areas of the photoresist to allow the semiconductor underneath to be exposed to a chemical etchant. The minimum feature size is given approximately by Equation 1:

$$CD \; \alpha \; \frac{\lambda}{NA} \tag{14}$$

Where *CD* is the critical dimension i.e. the minimum feature size, λ is the wavelength of light used and *NA* is the numerical aperture of the lens as seen from the wafer. (Mack n.d.)

Semiconductors have also been machined with laser beam machining (LBM) (Simon & Ihlemann 1996), diamond based milling (Hurley 1997), ultrasonic machining (USM) (Sato 1962), as well as spark erosion (Powell 1967). Powell et al (Powell 1967) found that indium antimonide (InSb) cracked

under the forces created by the sparks due to the materials very brittle nature. LBM creates a recast layer, regardless of the laser pulse length employed; Simon et al (Simon & Ihlemann 1996) observed the presence of a recast layer when using a laser pulse length of just 500 fs. This is an undesirable feature when single crystal materials have been used and creates inaccuracies in the machined feature size. This means that alternate methods can be used but an allowance for extra material removal via etching has to be considered to remove the defective layer. If small features are required, it may be best to use ECM directly.

4.1.4 Motivation for the work

Silicon based technology accounts for an overwhelming portion of the semiconductor sector and as such the machining processes are well established and fast moving. However, techniques for handling other semiconductor materials are not as well established.

Figure 4-1 InSb detector mounted on a quartz substrate

QMC Instruments Limited use indium antimonide in a bolometer. A bolometer is a device for measuring the power of electromagnetic radiation via the heating of a material with a temperature-dependent electrical resistance. Initially, electrical discharge machining (EDM) was used to create the specialised shape for the bolometer from the indium antimonide (InSb) wafer but QMC Instruments Ltd wished to find an alternative method to

create this device, shown in Figure 4-1. For the device to function correctly, the physical and electrical properties of the material must remain unaltered by the machining process. Using EDM creates a recast layer on the surface which can negatively affect the device's function.

Electrochemical machining (ECM) would be an attractive alternate machining method for the InSb bolometer if InSb could be anodically dissolved. As far as this research is aware, the anodic dissolution behaviour of InSb has not previously been studied. As such, this research proposes to investigate the anodic dissolution behaviour of doped and un-doped InSb because ECM provides a heat and stress-free machining process for electrically conductive materials, leaving the work piece properties unaltered by the process.

4.2 Methodology

4.2.1 Polarisation Experiments

4.2.1.1 Attaching the InSb samples to copper wires

Fragments of InSb wafer were fractured from a larger InSb wafer and attached to a copper wire using silver loaded epoxy. The silver loaded epoxy was cured for ten minutes at 55 °C in an oven.

4.2.1.2 Preparing the electrolyte

Molar concentration sodium chloride (NaCl) and sodium nitrate (NaNO$_3$) electrolytes were prepared using ACS grade salts from Sigma Aldrich with deionised water from an ELGA PURELAB Option Q water purifier. The pH of the solution was not altered from its natural pH.

4.2.1.3 The cell set up

A standard 3 electrode cell set up was used with a Sigma Aldrich double junction Ag/AgCl as the reference electrode, a homemade platinum flag was used as the counter electrode and the InSb sample was the working electrode.

4.2.1.4 The Polarisation Experiment

The potential in the polarisation experiment was applied using an IviumStat potentiostat. The potential was scanned from -0.5 to 10.0 V vs Ag/AgCl at a scan rate of 20 mV s^{-1}. The electrodes were connected to the potentiostat via banana plugs to ensure a good electrical connection was made. Care was taken to ensure the silver epoxy holding the InSb sample to the copper wire was not inserted into the electrolyte to avoid any reactions taking place at the epoxy.

4.2.2 Electrochemical Machining Experiments
4.2.2.1 The electrochemical machine set up

The electrochemical machining experiments were conducted at pECM Systems Ltd in Barnsley on an 'Impulse ECM' machine manufactured at pECM Systems Ltd. The sample was clamped to the z-axis of the ECM machine with a Tufnol paper laminate bar and screws, as can be seen in Figure 4-2. The tool was held in a V block connected to the negative terminal. The tool was a copper wire with a diameter of 1 mm. The tool was insulated on the sides with some electrical tape to prevent over machining.

A multimeter was used to determine when contact had been made between the two electrodes and then the work piece was moved away 0.1 mm to establish the IEG. This position was defined as the starting position and machining could commence from this point. The end position was reached when the z-axis had travelled 1.0 mm from the starting point.

The sample was machined close to where it was clamped to prevent the sample from snapping so easily. It could not be clamped with too much force either or the sample cracked.
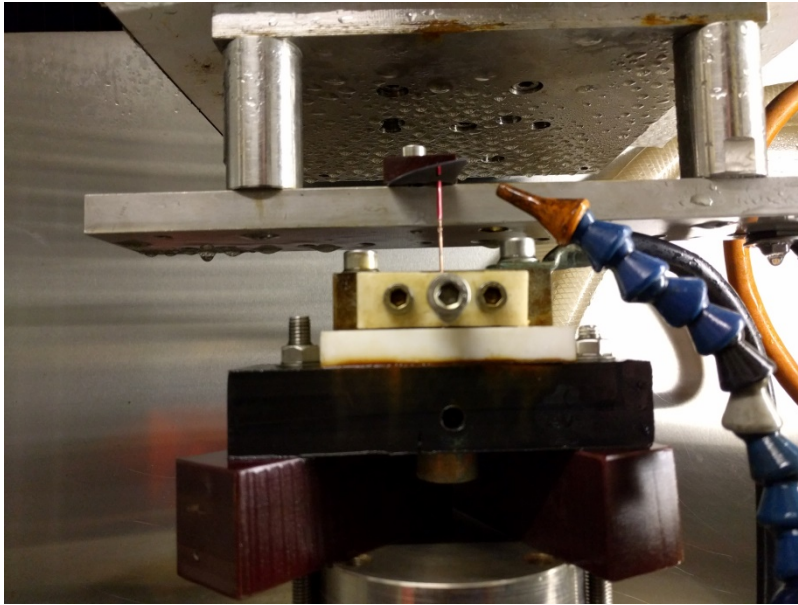
Figure 4-2 ECM machine set up for InSb machining

4.2.2.2 Machining Parameters

A 1.7 M sodium nitrate electrolyte was used for the electrochemical machining experiments with the InSb samples. Sodium nitrate was chosen as during the polarisation experiments, $NaNO_3$ resulted in complete dissolution of the sample which was inserted into the electrolyte. The machining voltage and electrode feed rate were altered to determine machining settings. A constant IEG of 0.1 mm was maintained for all experiments.

The samples were very fragile so a moderate frequency of 12 Hz was used on the electrolyte pump to prevent the force of the electrolyte from snapping the sample.

4.3 Results and Discussion

4.3.1 Polarisation Experiments

Polarisation experiments are utilised in electrochemical machining research to determine electrolyte-work piece interactions and suitable machining

conditions, i.e. the machining voltage. A polarisation curve shows the potential-current relationship.

In this research, polarisation curves were conducted in 1.0 M NaCl and $NaNO_3$. In both cases the InSb wafer was first rinsed in nitric acid (HNO_3) to remove a thin aluminium layer on one side of the wafer. The wafer was then rinsed with deionised water and dried.

Sodium chloride is a very common electrolyte choice for electrochemical machining applications as it contains aggressive chloride ions which help to prevent passive layers from forming on the electrode surface.

The expected anodic reactions occurring during anodic dissolution of InSb are outlined in Equations 15 and 16.

$$In \rightarrow In^{3+} + 3e^{-} \tag{15}$$

$$Sb \rightarrow Sb^{3+} + 3e^{-} \tag{16}$$

Antimony is most commonly found in its 3+ oxidation state although it can also be seen in its 5^{+} oxidation state, but rarely.

Hydrogen evolution is expected at the cathode, as shown in Equation 17.

$$nH^{+} + ne^{-} \rightarrow \frac{n}{2}H_2 \uparrow \tag{17}$$

Indeed, the sodium chloride electrolyte facilitated the anodic dissolution of InSb during the polarisation experiment; the polarisation curve can be seen in Figure 4-3.

Current begins flowing early in the experiment at approximately 0.2 V vs Ag/AgCl. At 8.5 V the current begins to drop as the surface area is decreased due to the anodic dissolution of the sample. There is a slight reduction in the current at 6.75 V; it was observed during the polarisation experiment that a black layer formed at this potential which indicates this film was mildly passivating. As the potential was raised, the black film also began

to dissolve, which can be seen when the observed current again begins to rise.
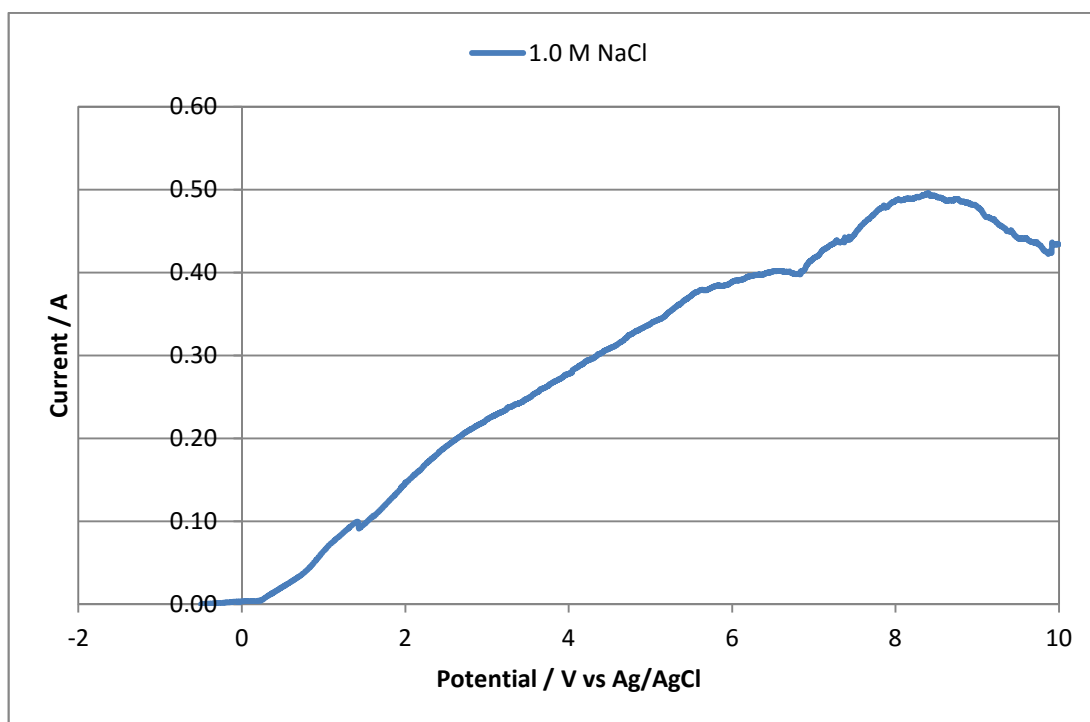
Figure 4-3 Polarisation curve of InSb in 1.0 M NaCl, scan rate 2 mV s^{-1}, working electrode area 2 x 2 x 2 mm, counter electrode area 8 x 10 x 0.25 mm, room temperature and natural oxygen levels

The black film can be seen in Figure 4-4a. This is likely to be a mixture of antimony and indium chlorides and oxides. Antimony can also be found in a non-metallic state which is black in colour. Indium oxide (In_2O) is a black crystalline solid also. (Panda 2013)

The sample was then washed with concentrated nitric acid which dissolved the black layer; see Figure 4-4b. Antimony compounds are soluble in nitric acid, as is antimony. (Budapest University of Technology and Economics - Department of Inorganic and Analytical Chemistry n.d.) Indium salts are also soluble in acids. (Panda 2013)

The surface under the salt layer was very rough although there were no deep pits evident on the surface so pitting corrosion was not prevalent in this instance.
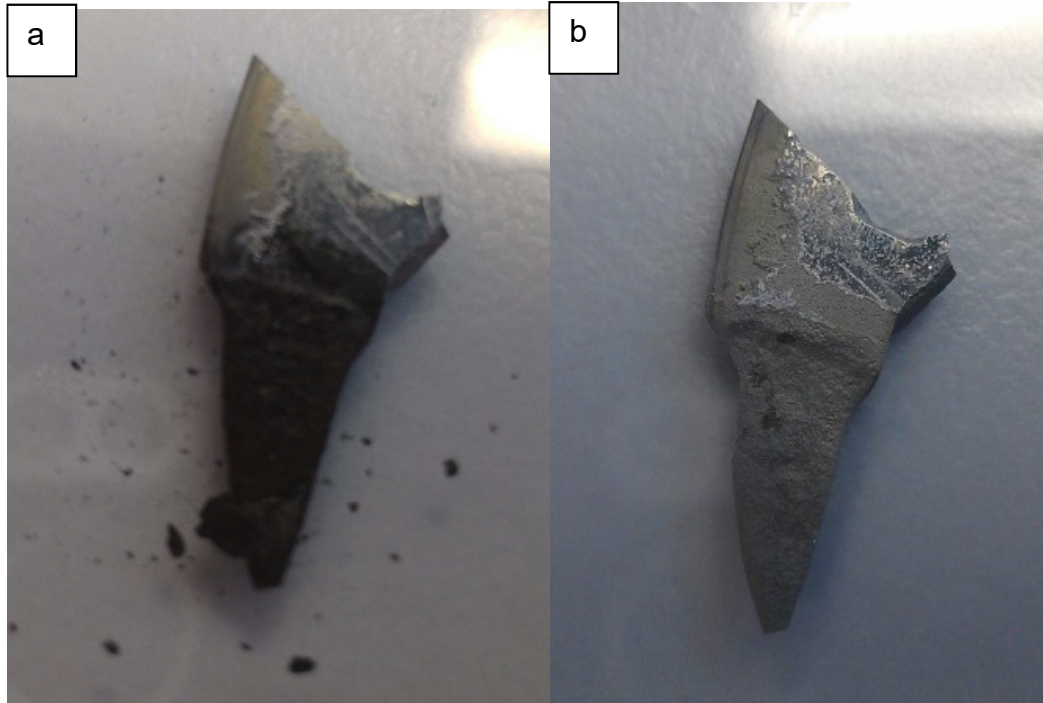
Figure 4-4 InSb sample a) after polarisation experiment in 1.00 M NaCl and b) and after subsequent washing in concentrated nitric acid

Polarisation experiments were also conducted in 1.00 M $NaNO_3$; see Figure 4-5. Sodium nitrate is known to be a passivating electrolyte which forms a protective film on the work piece surface. This behaviour is exploited to achieve higher resolution results in ECM but a higher machining voltage is generally needed to overcome the passivation. However, in this case, there is no evidence from the polarisation curve of passivation occurring as there is no drop in current; a characteristic feature of passive electrolyte polarisation curves. Current begins flowing at 0.4 V and rises linearly with the potential until 6.7 V at which point the current decreases. The current decreases due to a reduction in the surface area of the InSb sample as it is anodically dissolved. The sample submerged in the electrolyte is completely dissolved at 9.5 V which sees the current drop to zero.
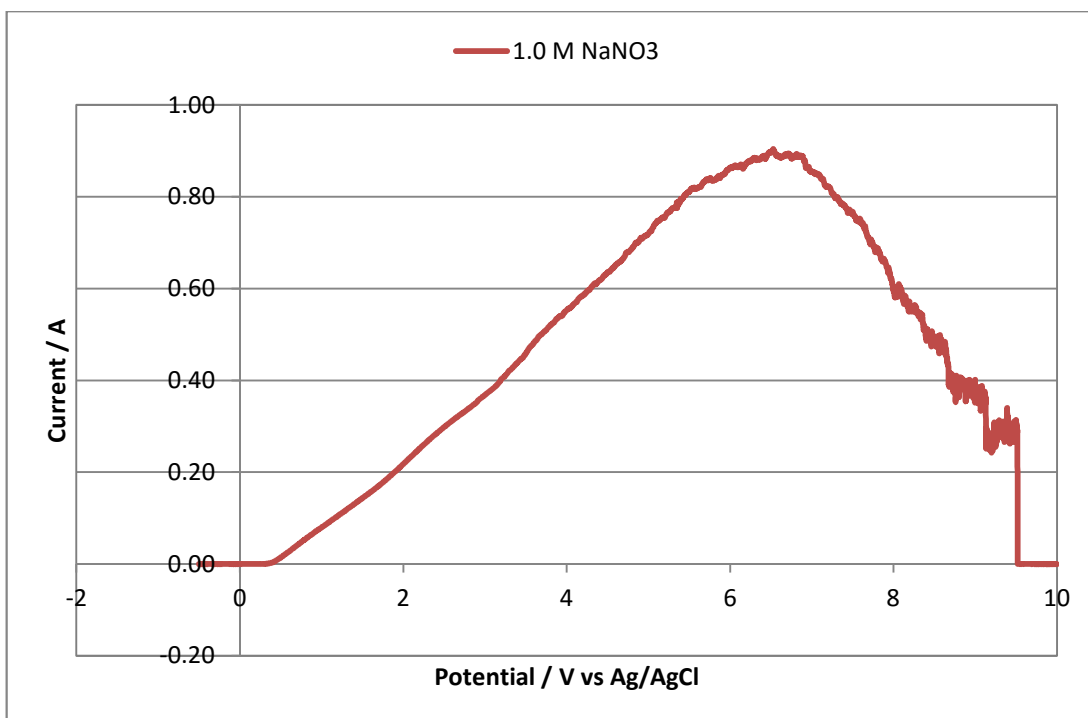
Figure 4-5 Polarisation curve of InSb in 1.0 M NaNO₃, scan rate 2 mV s⁻¹, working electrode area 2 x 2 x 2 mm, counter electrode area 8 x 10 x 0.25 mm, room temperature and natural oxygen levels

Whilst the polarisation experiment was taking place in NaNO$_3$, a black layer formed, as it did in NaCl, but this film grew in thickness as the experiment was continued. This black layer was electrically active as there is no evidence of passivation in the polarisation curve, as explained above. Eventually, the black layer began peeling away in layers. There was also a white precipitate formed on the sample near the electrolyte-air interface. This is most likely a mixture of indium and antimony oxides. The InSb samples submerged in the electrolyte were completely dissolved during the course of the polarisation experiment using 1.00 M NaNO$_3$, as can be seen in Figure 4-6.
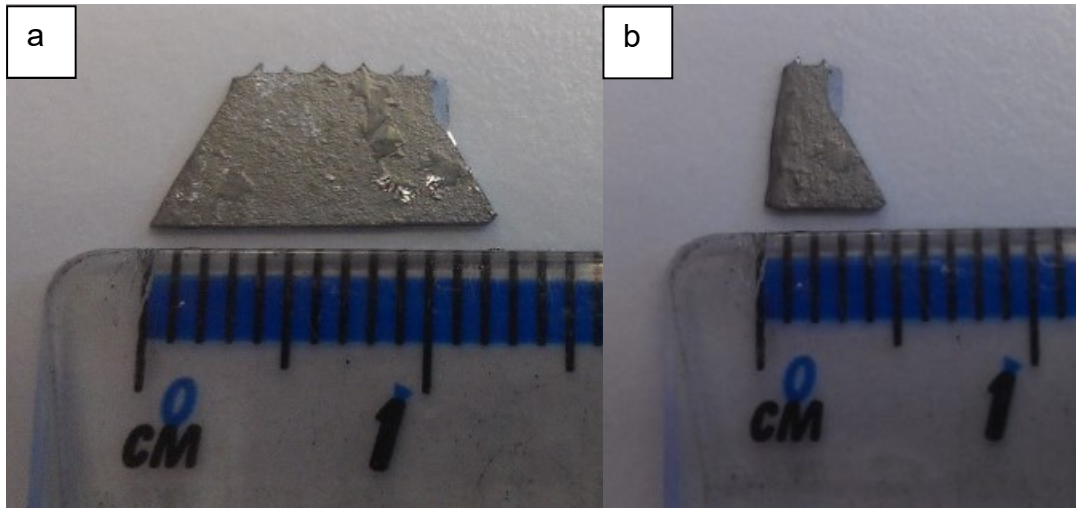
Figure 4-6 InSb sample a) before polarisation experiment and b) after polarisation experiment in 1.00 M NaNO$_3$ and washing in concentrated nitric acid

The surface finish cannot be easily assessed as the sample has been completely dissolved leaving very little of the anodically dissolved surface visible.

As sodium nitrate facilitated total dissolution of the sample during the polarisation experiment, this was chosen to perform tests on the ECM machine at pECM Systems Ltd, Barnsley.

4.3.2 Electrochemical Machining of Indium Antimonide

From polarisation experiments, it was determined that a machining voltage in excess of 7.5 V would facilitate machining at a reasonable rate. A 1.7 M NaNO$_3$ electrolyte was used to allow high dissolution rates.

The ideal feed rate and voltage were to be determined with these experiments. A pump frequency of 12 Hz was used for all the tests as a higher electrolyte delivery rate resulted in fracturing the brittle samples as the force of the electrolyte impacting on the sample was too great. An IEG of 0.1 mm was maintained for all tests. The voltages applied were applied as static voltage.

The aim of the testing was to create a hole through the InSb wafer, close in diameter to the tool used. High resolution machining, with non-tapered walls is imperative with semiconductors as semiconductor components' final dimensions are usually on the micrometre scale. The smallest dimension needed for the InSb bolometer is 200 μm, as can be seen in Figure 4-7. Due to limitations with the machine at pECM Systems Ltd, a tool of this size could not be held. As a result, a 1.0 mm diameter copper wire was used as the tool for the ECM experiments which was held in a V-block. The tip of the copper wire was coated with some insulating tape to prevent stray machining and the front edge of the z-axis was also coated with insulating tape to prevent machining of the stainless steel axis.
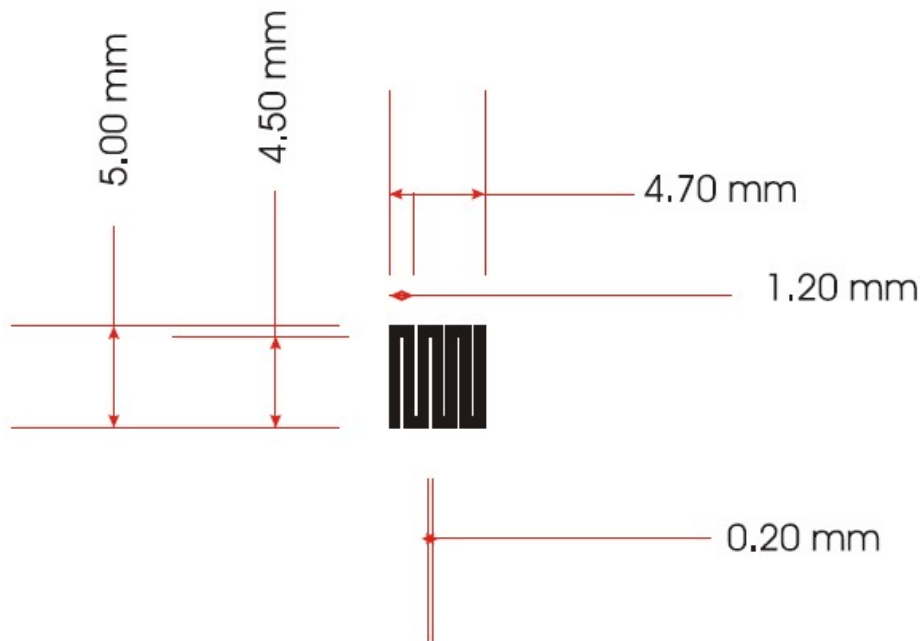
Figure 4-7 InSb element diagram and dimensions

Voltages ranging from 8.0 V to 12.0 V were tested with feed rates ranging between 0.5 mm min^{-1} and 1.0 mm min^{-1}, with an applied voltage of 8.0 V and a feed rate of 1.0 mm min^{-1}, resulted in varied machining success, sometimes the dissolution rate was not high enough to support the feed rate resulting in contact being made between the tool and the work piece,

snapping the InSb wafer; other times resulted in successful machining without snapping the sample. Increasing the voltage to 11.0 and 12.0 V allowed anodic dissolution with a feed rate of 1 mm min^{-1}. The resulting holes are very spherical in shape, as can be seen in Figure 4-8 even though the samples are broken.
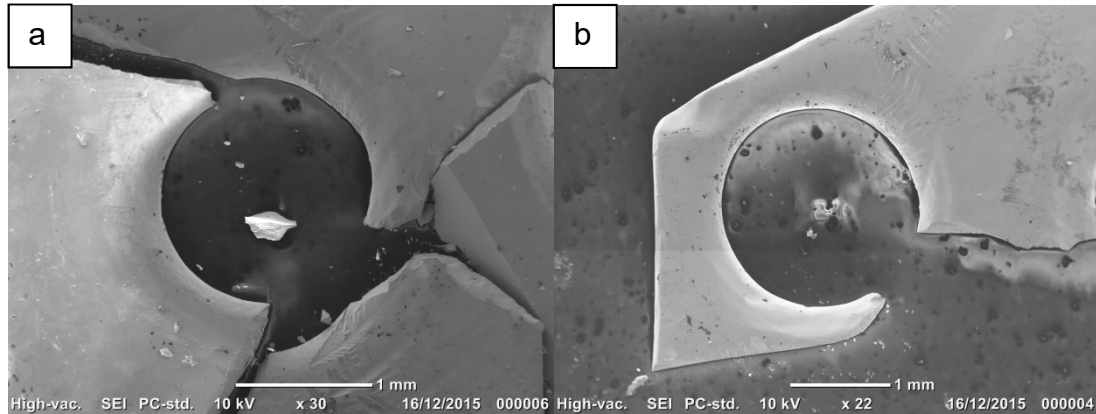
Figure 4-8 InSb samples after electrochemical machining at a feed rate of 1 mm min^{-1} at a) 11.0 V and b) 12.0 V

After machining, the samples were kept on double sided tape. When the samples were then lifted from the tape, cracks were formed. No cracks were formed during the ECM process. Whilst a combination of 11.0 V and a feed rate of 1 mm min^{-1} allowed penetration through the sample, there is evidence of tapering of the hole and the holes are much larger in diameter than the 1 mm tool used. The diameter of the hole in Figure 4-8b is 1.9 mm, almost double the diameter of the tool used. This is an unacceptable overcut.

It is known that using a lower voltage in ECM results in a smaller machining overcut. (Bhattacharyya & Munda 2003) Using a lower voltage would usually require a slower feed rate, which would mirror the dissolution rate more accurately. If the feed rate is not fast enough, the machining resolution will decrease due to the extended machining time and residence time of the tool electrode in the vicinity of the work piece. As the potential is applied constantly, the diffusion layer continually grows into the bulk electrolyte, only hindered by the electrolyte flow.

Figure 4-9 shows SEM images of the holes created using a constant voltage of 8.0 V with varying feed rates from 0.5 to 1.0 mm min^{-1}. As the feed rate is increased, the hole diameter decreases. This relationship is linear as shown in Figure 4-10.
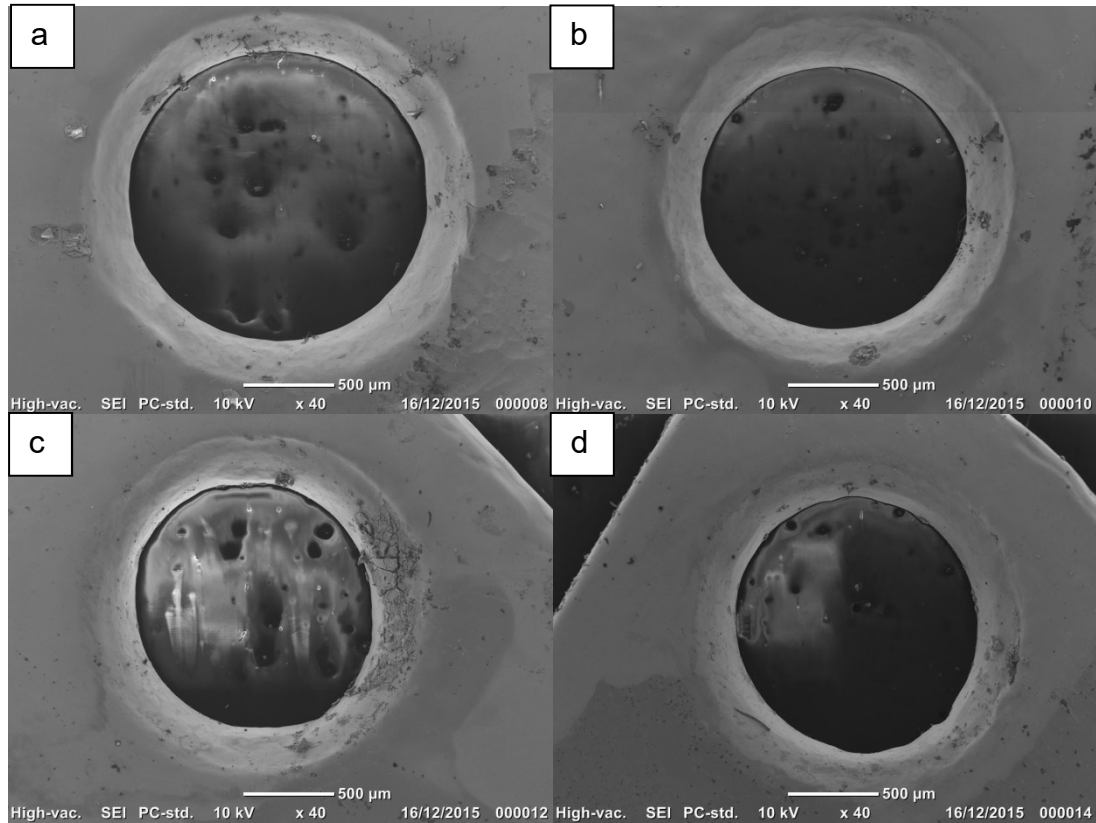
Figure 4-9 InSb samples after electrochemical machining at a voltage of 8.0 V at a feed rate of a) 0.5 mm min^{-1} b) 0.7 mm min^{-1} c) 0.9 mm min^{-1} and d) 1.0 mm min^{-1}

The holes still show evidence of tapering at all feed rates and despite the tool having been insulated with electrical tape at the end. This could be avoided with potential pulses; this would also improve the machining resolution. Despite the tapering, the surface finish of the machined surfaces is very good with a mirror like finish across all feed rates, although there are salt crystals on the surface of Figure 4-9c. The samples were washed with a gentle stream of deionised water.
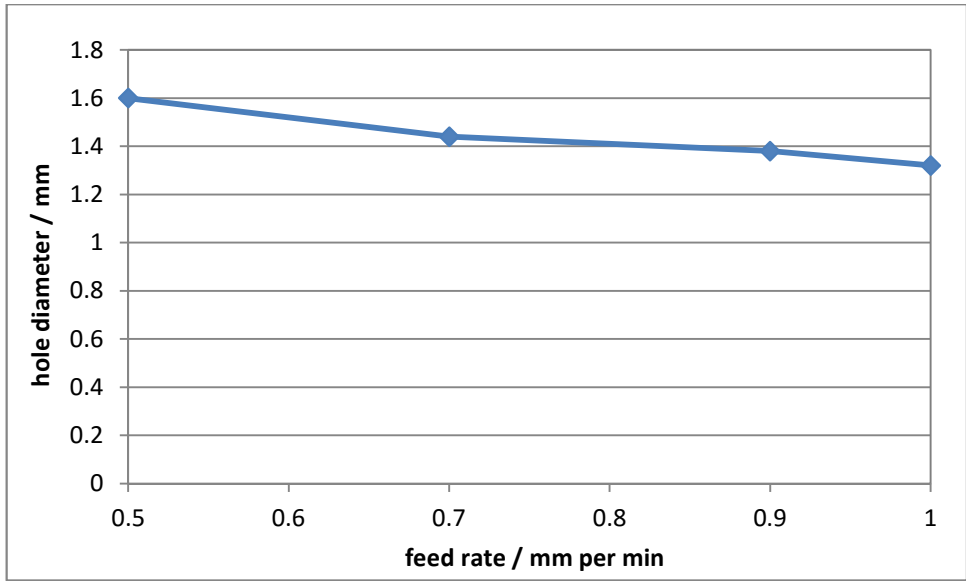
Figure 4-10 relationship between feed rate and hole diameter at 8.0 V for ECM of InSb samples in 1.7 M NaNO$_3$

As can be seen from the results above; a higher feed rate with a lower voltage results in the highest resolution machining. Due to the unpredictability of using a feed rate of 1 mm min^{-1} with a voltage of 8.0 V this combination was dismissed as a suitable machining condition for InSb due to a high proportion of sample which could snap. The next best option for machining with an IEG of 0.1 mm, an electrolyte pump frequency of 12 Hz in a 1.7 M NaNO$_3$ electrolyte was to apply a static potential of 8.0 V with a feed rate of 0.9 mm min^{-1} which produced a hole with a diameter of 1.38 mm.

4.4   Conclusion

Polarisation curves of InSb proved that both sodium chloride and sodium nitrate facilitates the anodic dissolution of indium antimonide. Anodic dissolution of InSb in both NaCl and NaNO$_3$ both commence via a salt film mechanism with a black film forming in both cases. The black film delaminates revealing the active surface underneath.

Sodium nitrate was chosen as the electrolyte in which to conduct electrochemical machining experiments. It was determined that a lower

potential resulted in a higher machining resolution than higher voltages and a faster tool feed rate also improved machining resolution due to a decrease in the electrode residence time at close proximity to the work piece. The conditions that provided the highest resolution hole used a static voltage of 8.0 V with a feed rate of 0.9 mm min^{-1}.

4.5   Further Work

Work needs to be conducted to improve the machining resolution and to develop a tool or a milling pathway to create the shape required for the bolometer.

Chapter 5 – Anodic Dissolution of Titanium with the Addition of Ultrasonic Vibrations

5.1 Introduction

5.1.1 Brief History of Titanium

Titanium was first discovered in 1791 but not identified until 1795. Titanium proved difficult to extract from its ores; the normal reduction method of heating the ore in the presence of coke produced titanium carbide rather than titanium. It was not until 1910 that pure titanium was produced by heating titanium tetrachloride ($TiCl_4$) with sodium at 700-800 °C. The current process for extracting titanium from its ore is called the Kroll process and is a variant of the latter process described, using magnesium instead of sodium. This is still an expensive process in comparison to other metal extraction techniques, and as such titanium is a costly metal. In the early 1950s, titanium became extensively used for military and aviation purposes after the United States of America (USA) Department of Defence determined titanium to be 'the metal of choice'.

5.1.2 Titanium Properties and Applications

Titanium is a transition metal which is commonly used across many disciplines as it is a lightweight yet strong material. It has a similar strength to low-grade steel alloys but titanium is less dense, reducing mass by up to 45 %. (Industrial Talks 2012) Titanium and its alloys find uses in aeronautical, medical, military, jewellery, sporting goods and high-end automobile industries. (Zhang et al. 2008)

Titanium products are popular as the material has remarkable properties such as high compressive and tensile strength, low density, high fatigue resistance in air and seawater, high strength to weight ratio and excellent corrosion resistance. Titanium has a low modulus of elasticity (Choragudi et al. 2010); this makes the material highly desirable for applications that require flexible materials which will not crack. (Pramanik 2014) This property,

however, also makes it difficult to cut to size as tools tend to push the material away rather than cut it. This strains the material which in turn causes it to harden further and wears the tool faster. (Benes 2007)

Titanium is corrosion resistant; it oxidises immediately on contact with air or water creating a protective, corrosion resistant titanium oxide layer, a couple of nanometres thick. This makes titanium ideal for naval vessels and aeronautical applications where the material comes in contact with salt water and moist conditions. It reacts similarly with nitrogen forming a protective nitride layer at the surface. (Manjaiah, S Narendranath, et al. 2014)

Titanium is also a biocompatible material; it is non-toxic and it is not rejected by the body so it is often used for medical implants, such as hip replacements. (Milacron Marketing Co. 2007) The high strength of the material is also beneficial here due to the pressure and stresses placed on joints within the body.

Titanium is used for large portions of both military and commercial aircraft due to its low density and high strength. It is used for *"aircraft structural parts, cold section components of jet engines and landing gear systems"*. (Asten & Nordberg 2013) The Blackbird SR-71 was made almost completely from titanium. (Merlin 2009) In 2014, in the USA, 75 % of titanium was used by the aerospace industry. (Bedinger 2015) It is also used in high-end automobile and sporting goods applications for this very reason, but it is an expensive material due to the methods required to extract the pure metal from its ores, explaining why titanium is not commonly used in commercial vehicles and less expensive sporting equipment.

Titanium is also used as an alloying element to decrease the grain size, as a deoxidiser and to remove carbon content from stainless steels. It is also added to increase an alloy's hardness.

Due to titanium's high chemical resistance and high corrosion resistance, it is used for nuclear waste storage. (Choragudi et al. 2010) Titanium oxide is a

bright white coloured powder which is used in many products from paint to paper to toothpaste. (Bedinger 2015)

Titanium is often found in architectural structures due to its high strength. Due to its high chemical resistance, titanium jewellery is often found as it is suitable for people with allergies. (Nourbakhsh 2012) It is also highly durable. Titanium can be oxidised to varying amounts which change the colour of the surface, dependent on the oxide thickness and the water content of the film. (Fushimi & Habazaki 2008)

However, titanium is considered a hard to machine material due to its high strength and other physical properties, such as its poor thermal conductivity. (Zhang et al. 2008)

5.1.3 Conventional Machining of Titanium

Conventionally machining titanium and its alloys with either milling or drilling is expensive; as with any other hard-to-machine material. With titanium, a small increase in cutting speed will lead to a large increase in tool edge wear. (Zhang et al. 2008) There is also a fire risk when drilling titanium due to the material's low thermal conductivity; this forces the cutting speed to be kept low. Titanium is a poor thermal conductor; during mechanical drilling of any metal, heat is generated due to the friction between the two materials. With titanium, this heat is concentrated around the cutting edge as the heat cannot be effectively dissipated throughout the material. As a result, heat builds in the tool, causing high tool wear. (Anonymous 2015) The heat can reach such high temperatures in the machining zone that the surface can be damaged. (Pramanik 2014)

Specialised tools are required to machine titanium and its alloys due to the high strength properties. (Machado & Wallbank 1990) These specialised tools come at a cost. High-speed steels or carbide drill pieces are needed to machine titanium; powder metallurgy tools have a more uniform structure with more highly controlled properties ensuring longer tool life and allowing

higher cutting speeds. (Choragudi et al. 2010) This, however, comes at a price as powder metallurgy tools are expensive in comparison to other high-speed steel drill bits. (Choragudi et al. 2010)

Carbide drill bits coated with titanium aluminium nitride (TiAlN) are preferred for machining titanium at high temperatures as the coating reduces the adhesion between the WC+Co powder sintered tool and the workpiece material. (Phantom Drills 2016) Aluminium within the coating forms aluminium oxide which decreases the chemical diffusion and thermal transfer into the tool. (Pramanik 2014) This improves the tool lifetime. Carbide tools are also preferred when smaller diameter cutters are necessary, as well as for complex geometries. (Asten & Nordberg 2013)

Titanium also has a strong tendency to alloy and chemically react with the cutting tool; this is detrimental to tool life. (Zhang et al. 2008; Pramanik 2014) As a result, titanium cannot be drilled using a diamond tool due to high corrosion rates of the diamond tool at high cutting speeds. (Cheng & Huo 2013; Pramanik 2014) As well as this, titanium chips tend to adhere to the tools. (Nouari & Makich 2014)

Titanium machining usually suffers from high tool wear, high machining cost and low productivity due to the reasons listed above. In the aero-industry, consistency in tool life is of paramount importance to ensure process control and the quality of the part produced takes precedent over the cost of production (Asten & Nordberg 2013). Titanium also suffers from strain hardening; this causes a thin layer of material to harden when pressure is applied. (Asten & Nordberg 2013) This makes the surface layer resistant to plastic deformation and reduces the ductility of the surface after machining but this increases the probability of crack propagation. This is undesirable in the aero-industry where monocrystalline materials are commonly used, undoing the work of creating the mono-crystal.

5.1.4 Non-Conventional Machining of Titanium

As mentioned above, conventional machining of titanium is expensive and slow due to the mechanical properties of the metal. As a result, non-conventional machining techniques were looked to in order to improve machining efficiency and quality, including high-speed machining (HSM), electric discharge machining (EDM), laser beam machining (LBM), ultrasonic machining (USM), water jet cutting (WJC), as well as ECM. (Manjaiah, S Narendranath, et al. 2014; Manjaiah, S. Narendranath, et al. 2014)

High-speed machining (HSM) is a technique used to increase productivity when machining hard-to-machine materials. It utilises a high spindle speed along with a high feed rate whilst making shallow cuts. The cutting speed is 5 to 10 times larger than those used in conventional machining. (Choragudi et al. 2010) The surface finish is usually improved by implementing HSM and less heat is generated. However, this technique is limited by the tools available. Advanced tools are required which are expensive; this increases the cost of the technique and the products machined this way. The tools still have limited lifetimes as with conventional machining. (Choragudi et al. 2010)

Electrical discharge machining (EDM) has been used to machine titanium, however, the sparks used to remove material create a heat-affected zone at the surface. This is detrimental to the quality of the finished product, especially in the production of turbine blades where single crystal of a finely tuned nickel metal alloy is commonly used. The introduction of a heat affected zone negates some of the benefits of employing the single crystal, adding weaknesses back into the material. This can affect the integrity of the material. EDM is dependent on the material's melting point rather than hardness. (Marinov 2008)

The melting point of titanium is very high; this means a high energy input is required for thermal removal methods, such as laser beam machining (LBM). The microstructure of the material is also affected by the application of

intense heat. Laser cutting also introduces a heat affected zone on the surface of the machined material. Whilst machining titanium this way is possible it is not practical for machining large areas and there are lots of safety precautions when using lasers. (Anonymous n.d.) Electron beam machining (EBM) is a similar method to LBM but uses a focused beam of electrons as opposed to light and must be conducted in a vacuum chamber to prevent the electrons colliding with gas particles. (Marinov 2008)

Ultrasonic machining (USM) is a machining method whereby a tool is vibrated at ultrasonic frequencies in close proximity to the workpiece whilst an abrasive slurry is passed through the small gap between the tool and the workpiece (Choragudi et al. 2010); material removal is facilitated by the use of an abrasive slurry which impacts the surface chipping material from the surface. The material is removed by micro-chipping. This process is advantageous as it is a heat-free process resulting in no heat affected layer on the workpiece. (Choragudi et al. 2010) Aspect ratios in USM are limited to around 3:1. (Zhang et al. 2008) However, ultrasonic machining suffers from high rates of tool wear which can affect machining precision as well as increase machining costs. The surface finish of this process is determined by the grain size of the abrasive particles but this is usually better than conventional twist-drilling. The material removal rate is also lower with USM than other methods. (Zhang et al. 2008; Choragudi et al. 2010; Marinov 2008)

Water jet cutting (WJC) uses high-pressure, high-velocity water jet to create slots in metals or ductile materials. Brittle materials will shatter under the force. The nozzle diameter ranges from 1.2 mm to 0.5 mm. The water can contain an abrasive particle which reduces cutting forces. (Marinov 2008)

Electrochemical machining (ECM) is another non-conventional machining technique which can successfully be applied to machining titanium. This technique is already employed in the shaping of turbine blades in the aero-industry as the process is a contact-free, heat-free and stress-free technique which maintains the properties imparted by creating a single crystal material

i.e. high strength and predictable, consistent behaviour. ECM is an attractive machining option as machining rates can be high; the machining is not dependent on the materials' mechanical properties and can be machined with a softer tool (e.g. a copper tool can be used to machine steel), and the workpiece microstructure is unaltered by ECM. (Anonymous n.d.)

Machining titanium with ECM is more difficult than it is for some other metals e.g. steel due to the chemically resistant oxide surface layer, this means a high potential is needed to break through passive layer. Voltages are usually in excess of 20 V. Highly aggressive electrolytes are also usually used to machine Ti, such as hydrofluoric acid, or expensive bromide salts, e.g. potassium bromide (KBr) (Bannard 1976) which are more capable of breaking through the passive layer than chlorine based electrolytes (Bannard 1976). Using aggressive, highly corrosive electrolytes brings its own difficulties with electrolyte handling and disposal. Care must also be taken to prevent corrosion or damage to the ECM system. Chloride salts are preferred by most ECM users as it is an inexpensive, easily available resource.

Many alterations have been made to the ECM set up, including the application of voltage pulses to improve machining resolution along with the reduction of the inter-electrode gap (IEG). Ultrasonic vibrations have also been applied to one of the electrodes (usually the tool) during machining. This has been used to improve material removal rates and the surface finish. There have also been examples where the electrolyte has been pulsed at low frequencies (1-40 Hz). (Qu et al. 2013) The authors reported an initial increase in machining rates and an initial decrease in surface roughness as the frequency of pulses was increased.

One could attempt to prevent the passive layer forming allowing active dissolution of the material through the employment of non-aqueous dry electrolytes. This requires strict preparations of the workpiece in an oxygen- and moisture-free environment before being transferred to a thoroughly dried non-aqueous electrolyte. A high potential can initially be applied to remove

the passive layer and the potential subsequently reduced to avoid the complex preparation of excluding oxygen and moisture from the environment. However, using non-aqueous electrolytes makes electrolyte disposal more difficult and costly. The process becomes less environmentally friendly too.

5.1.5 Motivation for the Work

As titanium is commonly used across a wide range of industries, machining is hugely important. The methods currently employed for titanium machining are expensive, time-consuming or detrimental to the metal's properties; excluding ECM and USM. As mentioned before USM suffers from low material removal rates and so is not suitable for mass production. Machining titanium with ECM uses high potentials which require a large amount of energy, although this has not deterred its use as a successful machining method where other processes have proved unsuitable.

It was stated by workers at pECM Systems Ltd, that titanium metal could be electrochemically machined at 8 V in a $NaNO_3$ electrolyte. Initial experiments conducted did not agree with this finding. However, it has been demonstrated with other materials how ultrasound can enhance electrochemical machining rates and reduce machining potentials required to initiate anodic dissolution. (Skoczypiec 2011) This is implemented usually by vibrating one of the electrodes at ultrasonic frequencies (> 20 KHz). When perturbations are applied to either electrode one can expect some form of lateral movement of the electrodes which could decrease machining precision. The idea here is to apply the ultrasonic vibrations directly to the electrolyte flowing between the tool and the workpiece, rather than to either of the electrodes, with the aim to reduce the machining potentials required to machine titanium thus reducing the energy consumption of the process as well as increasing machining rates. This would make ECM a more favourable process for titanium processing and reduce the cost of parts manufactured in this way. As ECM is already used for the machining of titanium and its alloys

in the aerospace industry there are potential energy and cost savings to be achieved.

5.2 Method

5.2.1 Preliminary Polarisation Curves in 'Silent' Electrolytes

5.2.1.1 Electrolyte Preparation

Polarisation experiments were first conducted in 'silent' solutions i.e. with no external convective forces applied to the cell in sodium chloride (NaCl), sodium nitrate ($NaNO_3$) and sodium chlorate ($NaClO_3$) at concentrations of 0.1, 0.5 and 1.0 M. All salts used for ACS Grade from Sigma Aldrich and 18.2 MΩ cm^{-1} water from an ELGA LabWater PURELAB Option-Q water purification system. The pH of the solution was adjusted with sodium hydroxide and hydrochloric acid or nitric acid depending on which salt was involved.

5.2.1.2 The Cell Set Up

A standard 3 electrode cell set up was used. The reference electrode was a double junction Ag/AgCl glass reference electrode from Sigma Aldrich, the counter electrode was a homemade platinum flag electrode and the working electrode was a 1 mm diameter titanium wire. The titanium wire was pre-treated by immersing the end in concentrated nitric acid for 10 seconds and rinsing with acetone before drying in a stream of argon gas. The electrolyte was heated to the correct temperature by immersing the electrochemical cell in a water bath set at the corresponding temperature.

5.2.1.3 The Polarisation Experiment

The potential was applied using an IviumStat potentiostat. The potential was scanned from -0.5 V to 10.0 V at a scan rate of 5 mV s^{-1}. The counter electrode and working electrode were held close together (approx. 5 mm) to replicate the ECM process as closely as possible. The electrodes were connected to the potentiostat via banana plugs for a good electrical connection. Polarisation curves allow the determination of the dissolution

106

potential that would be used on the electrochemical machine. For the experiments where the electrolyte was required to have the dissolved oxygen in the solution removed, nitrogen gas was bubbled through the electrolyte for 20 minutes to displace the oxygen.

5.2.1.4   Experimental Design

A Taguchi orthogonal array was chosen as the experimental design to reduce the number of experiments to be undertaken. An L_{18} design was used where there was 1 factor with 2 levels and 7 factors with 3 levels of which only 4 were used. This allowed just 18 polarisation curves to be conducted saving resources and time. See Table 5-1 for a detailed plan of experiments.

Table 5-1: Taguchi Design of Experiments for 'Silent' Electrolytes

Run	X_1	X_2	X_3	X_4	X_5
1	1	1	1	1	1
2	1	1	2	2	2
3	1	1	3	3	3
4	1	2	1	1	2
5	1	2	2	2	3
6	1	2	3	3	1
7	1	3	1	2	1
8	1	3	2	3	2
9	1	3	3	1	3
10	2	1	1	3	3
11	2	1	2	1	1
12	2	1	3	2	2
13	2	2	1	2	3
14	2	2	2	3	1
15	2	2	3	1	2
16	2	3	1	3	2
17	2	3	2	1	3
18	2	3	3	2	1

		Level		
		1	2	3
X1	Atmosphere	Inert	Oxygen	-
X2	Electrolyte	NaCl	$NaNO_3$	$NaClO_3$
X3	pH	3	7	12
X4	Temperature	20	40	60
X5	Concentration	0.1	0.5	1.0

5.2.2 Polarisation Curves with Ultrasonic Vibrations

5.2.2.1 Electrolyte Preparation

Having conducted polarisation curves in different electrolytes without the application of ultrasonic vibrations to the electrolyte, it was decided only experiments in NaCl should be conducted with insonation as $NaNO_3$ and $NaClO_3$ are passive electrolytes and titanium also has a strong chemically resistant oxide layer which requires an aggressive electrolyte to break through the layer. As the currents observed in the silent system were so low the concentrations investigated were increased to 1.0, 2.0 or 3.0 M at the natural pH of the solution (approximately neutral). All salts used were ACS Grade from Sigma Aldrich and made up with 18.2 MΩ cm water from an ELGA LabWater PURELAB Option-Q water purification system.

5.2.2.2 The Cell Setup

A standard 3 electrode cell set up was used. The reference electrode was a double junction Ag/AgCl glass reference electrode from Sigma Aldrich, the counter electrode was a homemade platinum flag electrode and the working electrode was a 1 mm diameter titanium wire. The titanium wire was pre-treated by immersing the end in concentrated nitric acid for 10 seconds and rinsing with acetone. The whole electrochemical cell was clamped in an ultrasonic bath (Skymen JP-031S) so the electrolyte was below the water level of the ultrasonic bath. An attempt was made to place the cell in the same position in the ultrasonic bath each time to try to reproduce the same ultrasonic profile through the electrolyte in each polarisation experiment.

5.2.2.3 The Polarisation Experiment

The potential was applied using an IviumStat potentiostat. The potential was scanned from +0.5 V to 10.0 V at a scan rate of 5 mV s^{-1}. The counter electrode and working electrode were held close together (approx. 5 mm) to replicate the ECM process as closely as possible. The electrodes were connected to the potentiostat via banana plugs for a good electrical

connection. The ultrasound bath was turned on before the potentiostat to ensure insonation was applied for the entirety of the experiment. Ultrasonic heating occurs within the bath so to keep the experimental temperature within ±5 °C of the experimental temperature ice was added to the ultrasonic bath water. Polarisation curves allow the determination of the dissolution potential that would be used on the electrochemical machine.

5.2.2.4 Experimental Design

Having done polarisation curves in a range of electrolytes without the application of ultrasonic vibrations a decision was made to only continue with NaCl as the other electrolytes were reported to be much more strongly passivating. Polarisation curves were conducted in 1.0, 2.0 and 3.0 M NaCl to enable higher currents to pass. The experimental design in shown in Table 5-2.

Table 5-2 Polarisation Experimental Design with USV applied to the NaCl electrolyte

Experiment No.	Concentration / M	Temperature / deg C
1	1.0	20.0
2	1.0	40.0
3	1.0	60.0
4	2.0	20.0
5	2.0	40.0
6	2.0	60.0
7	3.0	20.0
8	3.0	40.0
9	3.0	60.0

5.2.3 Chronoamperometry with Ultrasonic Vibrations
5.2.3.1 Electrolyte Preparation

1.0, 2.0 and 3.0 M NaCl electrolytes were used for the chronoamperometry experiments. All salts used were ACS Grade from Sigma Aldrich and made

up with 18.2 MΩ cm water from an ELGA LabWater PURELAB Option-Q water purification system.

5.2.3.2 The Cell Set Up

A standard 3 electrode cell set up was used. The reference electrode was a double junction Ag/AgCl glass reference electrode from Sigma Aldrich, the counter electrode was a homemade platinum flag electrode and the working electrode was a 1 mm diameter titanium wire. The titanium wire was pre-treated by immersing the end in concentrated nitric acid for 10 seconds and rinsing with acetone. The whole electrochemical cell was clamped in a Skymen ultrasonic bath (JP-031S) so the electrolyte was completely below the water level of the ultrasonic bath. An attempt was made to place the cell in the same position in the ultrasonic bath each time to try to reproduce the same ultrasonic profile through the electrolyte.

5.2.3.3 The Chronoamperometry Experiment

The constant potential was applied using an IviumStat potentiostat for 40 minutes. The counter electrode and working electrode were held close together (approx. 5 mm) to replicate the ECM process as closely as possible. The electrodes were connected to the potentiostat via banana plugs for a good electrical connection. The ultrasound bath was turned on before the potentiostat to ensure insonation was applied for the entirety of the experiment. Ultrasonic heating occurs within the bath so to keep the experimental temperature within ±5 °C of the experimental temperature ice was added to the ultrasonic bath water as the ultrasonic bath available did not have an inbuilt cooling system. The change in mass was recorded to be able to calculate the average material removal rate over the time of the experiment.

5.2.3.4 Experimental Design

A full factorial set of experiments was used for this as there were only 3 factors with 3 levels, totalling just 27 experiments. The temperature was

varied between 20, 40 and 60 °C; concentration varied between 1.0, 2.0 and 3.0 M and the potential was varied between 9.0, 9.5 and 10.0 V, see Table 5-3 below.

Table 5-3 Chronoamperometry experimental plan

Experiment No.	Temperature / deg C	Concentration / M	Potential / V
1	20.0	1.0	10.0
2	20.0	1.0	9.5
3	20.0	1.0	9.0
4	20.0	2.0	10.0
5	20.0	2.0	9.5
6	20.0	2.0	9.0
7	20.0	3.0	10.0
8	20.0	3.0	9.5
9	20.0	3.0	9.0
10	40.0	1.0	10.0
11	40.0	1.0	9.5
12	40.0	1.0	9.0
13	40.0	2.0	10.0
14	40.0	2.0	9.5
15	40.0	2.0	9.0
16	40.0	3.0	10.0
17	40.0	3.0	9.5
18	40.0	3.0	9.0
19	60.0	1.0	10.0
20	60.0	1.0	9.5
21	60.0	1.0	9.0
22	60.0	2.0	10.0
23	60.0	2.0	9.5
24	60.0	2.0	9.0
25	60.0	3.0	10.0
26	60.0	3.0	9.5
27	60.0	3.0	9.0

5.3 Results and Discussion

5.3.1 Polarisation Curves in 'Silent' Electrolytes

Expectations for titanium dissolution using the IviumStat potentiostat were low as the maximum applied voltage the potentiostat could reach was 10.0

V. This was considerably below all potentials reported for titanium machining with ECM. A high potential (usually > 20 V) is required to break down the strongly passivating oxide layer which protects titanium from corrosion and makes it such a popular material choice across many industries. Additionally, a quiescent electrolyte was used in these experiments. This means there was no external or applied convection to the solution meaning the reaction products could build up at the electrode surface limiting the current that can be passed.

Titanium forms a protective oxide surface layer upon contact with air or water, this in combination with a passive electrolyte such as sodium nitrate or sodium chlorate leads to a situation which requires high voltages to cause anodic dissolution (>> 10 V). Figure 5-1 and Figure 5-2 show polarisation curves conducted in $NaNO_3$ and $NaClO_3$ respectively. The current passed in all cases in very low, all below 3.5 mA but the majority of the experiments exhibited currents below 1.5 mA. The concentration, temperature, pH and the oxygen content was altered across these experiments; the dissolved oxygen content was altered by degassing the electrolyte before the commencement of the polarisation experiment which displaces the oxygen with nitrogen. There is an anomaly seen in Figure 5-1, experiment 4 where a peak is seen at approximately 6 V; experiment 4 was conducted in 0.5 M $NaNO_3$, pH 3 at 20 °C which had been degassed. There is no clear reason as to why this one experiment differed to the others which showed current profiles which rose linearly with the applied potential.

Although the current response was low, there was evidence of some reaction taking place. The titanium surface changed colour during the polarisation experiment. The natural Ti surface was a dull silver colour but at the end of the polarisation experiment for all salts, the surface became a pale purple colour. Fushimi et al (Fushimi & Habazaki 2008) observed the oxide layer changed colour in an ethylene glycol solution depending on the water content. With high water content, the passive film was violet in colour. This correlates well with the results observed here as the electrolyte is a purely
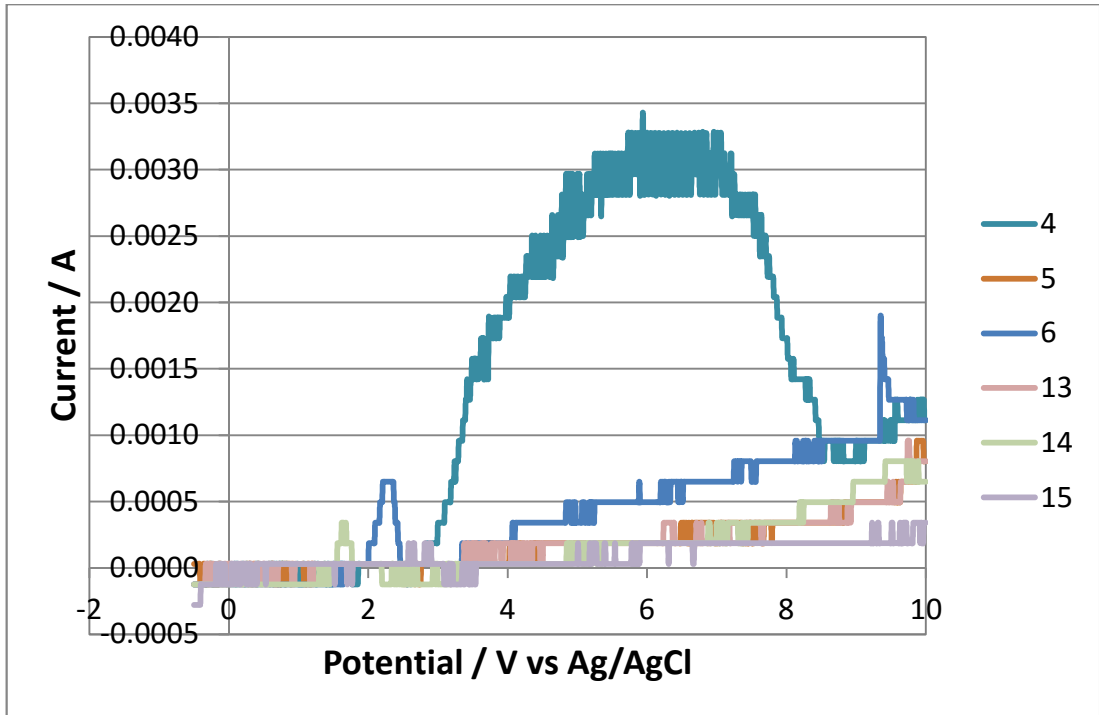
Figure 5-1 Polarisation Curves of titanium in NaNO₃, scan rate 5 mV s⁻¹, legend number relate to experiment number from Table 5-1
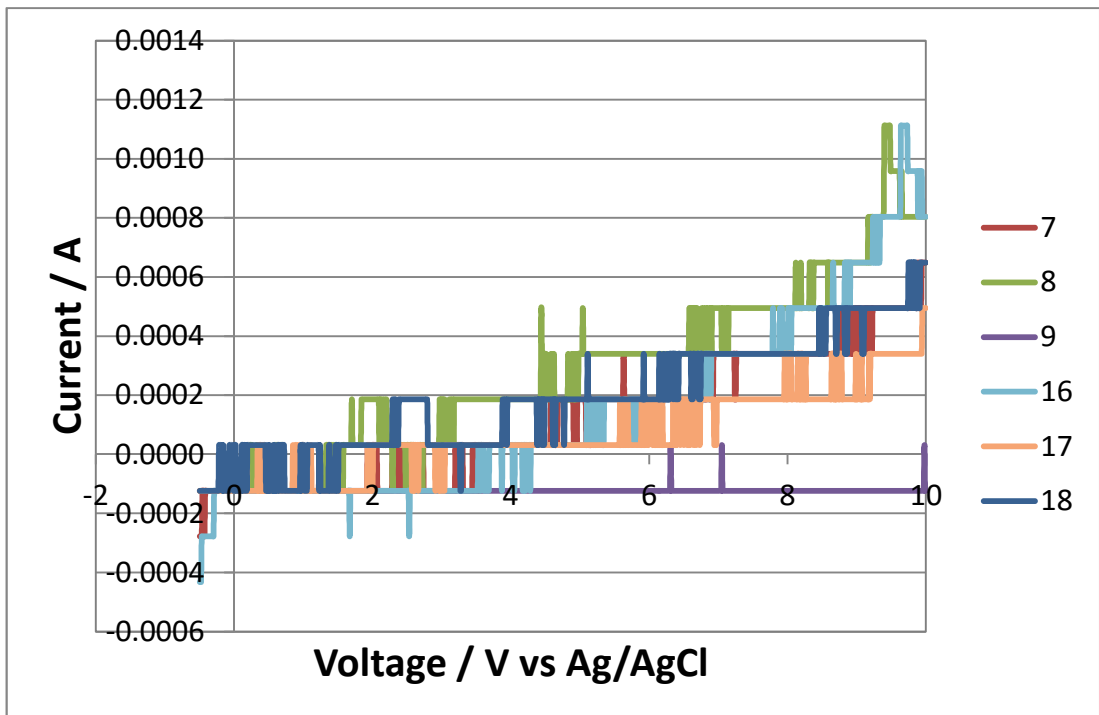
Figure 5-2 Polarisation Curves of Titanium in NaClO₃, scan rate 5 mV s⁻¹, legend number relate to experiment number from Table 5-1

113
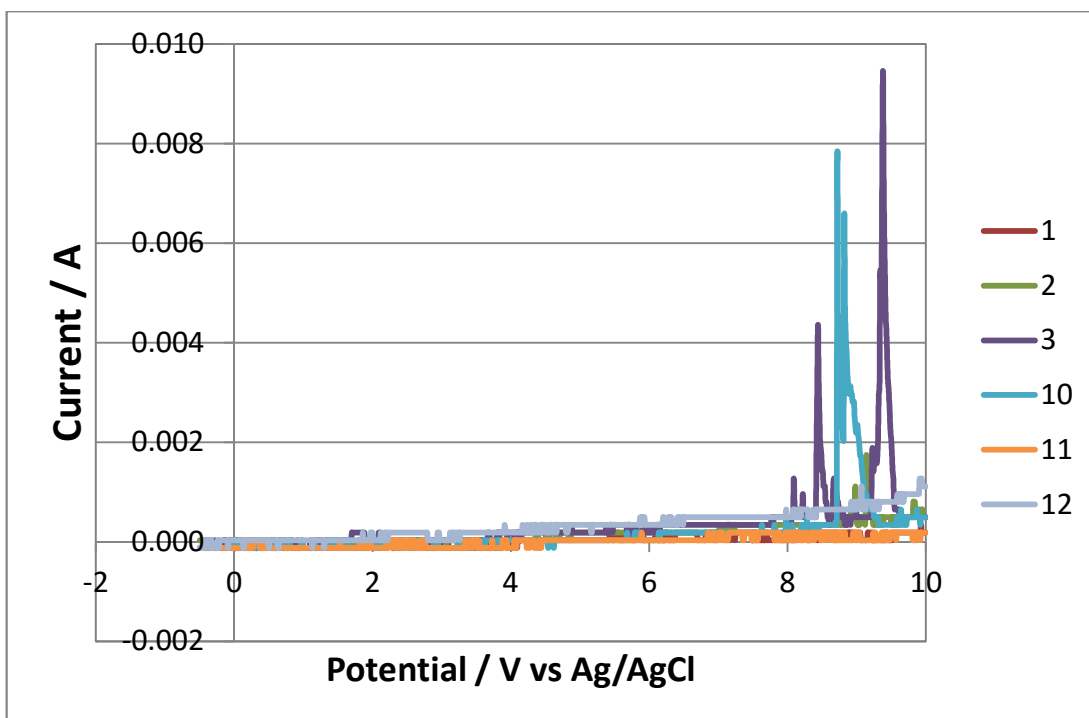
Figure 5-3 Polarisation Curves of Titanium in NaCl, scan rate 5 mV s^{-1}, legend number relate to experiment number from Table 5-1

aqueous solution. The violet colour relates to the formation of Ti^{3+} ions, which is the most stable ion of titanium.

The current response in NaCl is very similar to that of the passive electrolytes although there is a sharp peak between 8 and 10 V for the experiments conducted with 1.0 M NaCl at 60 °C which is shown in Figure 5-3. There was still no evidence of anodic dissolution when examining the sample after the experiment.

Changing the salt, the concentration, pH, temperature and oxygen content in the electrolyte did not affect the results. All tests resulted in a passive layer formation and did not facilitate anodic dissolution over the voltage range tested due to the resistant passive layer on the titanium surface.

5.3.2 Polarisation Curves with Ultrasonic Vibrations

As polarisation curves in a 'silent' electrolyte proved unsuccessful for the anodic dissolution of titanium, ultrasonic vibrations (USV) applied to the electrolyte were investigated.

The effect of the USVs is two-fold; firstly the vibrations increase the transport of ions to and from the electrode surface which in turn should increase the current which is passed. Secondly, USVs within a liquid cause cavitation bubbles (Walton 2002). These bubbles can "*form micro-jets that impinge towards the surface*" (Walton 2002), removing debris. Yeager (Yeager 1953) stated USVs could be used to strip "*irreversibly adsorbed materials on the electrode surface which would otherwise reduce the active surface area of the electrode*". (Yeager 1953) This effect is also utilised in ultrasonic cleaners commonly used to clean delicate pieces of jewellery.

It was hypothesised the USVs could remove the corrosion resistant oxide layer on the Ti surface, exposing the active metal underneath (Vian et al. 2010) in order to facilitate anodic dissolution at potentials obtainable with the equipment available at Brunel University, as well as reducing the energy consumption of the process. USV have been known to reduce the potentials needed for constant-current electrolysis cases. (Walton 2002)

A decision was made to use sodium chloride as the electrolyte after the polarisation curves in silent electrolytes, due to the presence of the aggressive chloride ion which would help break down or prevent the reformation of the passive oxide layer at such high rates. Sodium nitrate has a tendency to form passive layers on materials. This is good for resolution purposes but it is not ideal to use with materials which already have their own tendency to form passive, corrosion-resistant layers. The same can be said for sodium chlorate.

As the currents recorded in the silent polarisation experiments were so low, a decision was made to increase the concentrations of the NaCl electrolyte to

be studied. This would allow higher currents to be passed and, as a result, higher MRR would be achieved.

The polarisation curves were conducted to determine the activation potential for the anodic dissolution of Ti in the various concentrations of aqueous NaCl electrolytes. As such, only 9 experiments, repeated 3 times each, were conducted, as shown in Table 5-2.

The initial polarisation curves with the addition of USV to the electrolyte are very encouraging. Using a concentration of only 1.0 M NaCl, the current was seen to pass at potentials in excess of 8.0 V vs Ag/AgCl whereas no current was passed at this potential when USV were not applied, as can be seen in Figure 5-4. Comparing the two polarisation curves in 1.0 M NaCl in Figure 5-4, the current is higher in the range 3.0-7.0 V vs Ag/AgCl for the experiments where no USVs were applied. This is likely to be due to the formation of an oxide layer which is unable to form when ultrasound is applied to the electrolyte. When the USVs were applied, the concentrations of the active material in the electrolyte were not able to reach values high enough to cause considerable oxidation. This is because the USVs assist the transport of species in the electrolyte, both to and from the electrode surface. In this case, the oxidising species are carried away from the electrode surface with ultrasonic vibrations.

Beyond 7.0 V vs Ag/AgCl, active dissolution of titanium is seen in the experiment conducted with USVs, as can be seen by the passage of current in Figure 5-4. The addition of insonation prevents the protective oxide layer from forming on the titanium surface, exposing the active metal which facilitates anodic dissolution. The insonation also increases the transport of reaction products from the electrode surface into the bulk solution, as well as increasing the transport of material from the bulk to the electrode surface.

Increasing the concentration should allow a higher current to be facilitated at any given time, increasing the material removal rate. Figure 5-5 shows the polarisation curves of titanium with the addition of USV at 20 °C at various

concentrations. It is clear to see how the current, and therefore the charge passed during the course of the experiment increases with increasing electrolyte concentration. This behaviour was observed across all temperatures.
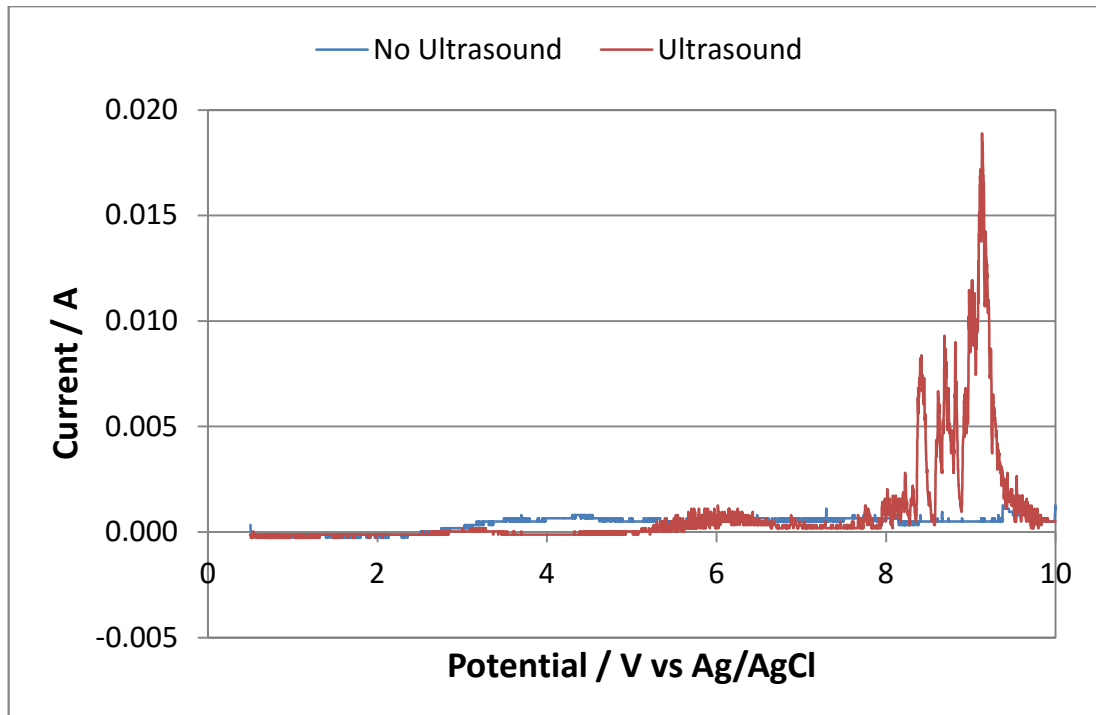
Figure 5-4 Polarisation Curves of Titanium in 1.0 M NaCl with (red) and without (blue) ultrasonic vibrations of the electrolyte at 60 °C at a scan rate of 5 mV s⁻¹. (Leese & Ivanov 2016a)

Increasing the temperature should also have the same overall effect as increasing the concentration would; the material removal can be expected to increase with an increase in temperature due to the improved diffusion rates. This can be seen in Figure 5-6, which shows the effect of temperature using 2.0 M NaCl as the electrolyte. Again this effect was seen across the other concentrations investigated.
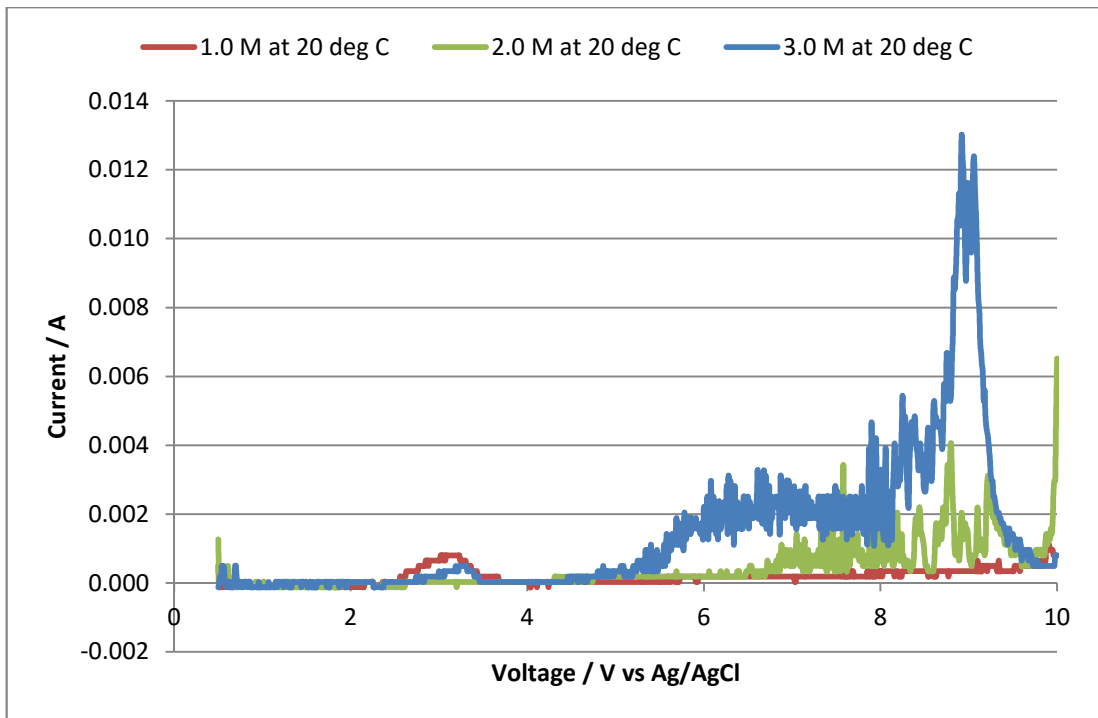
Figure 5-5 Polarisation Curves with USV of Titanium at 20 °C at various concentrations, scan rate 5 mV s^{-1} with natural oxygen levels
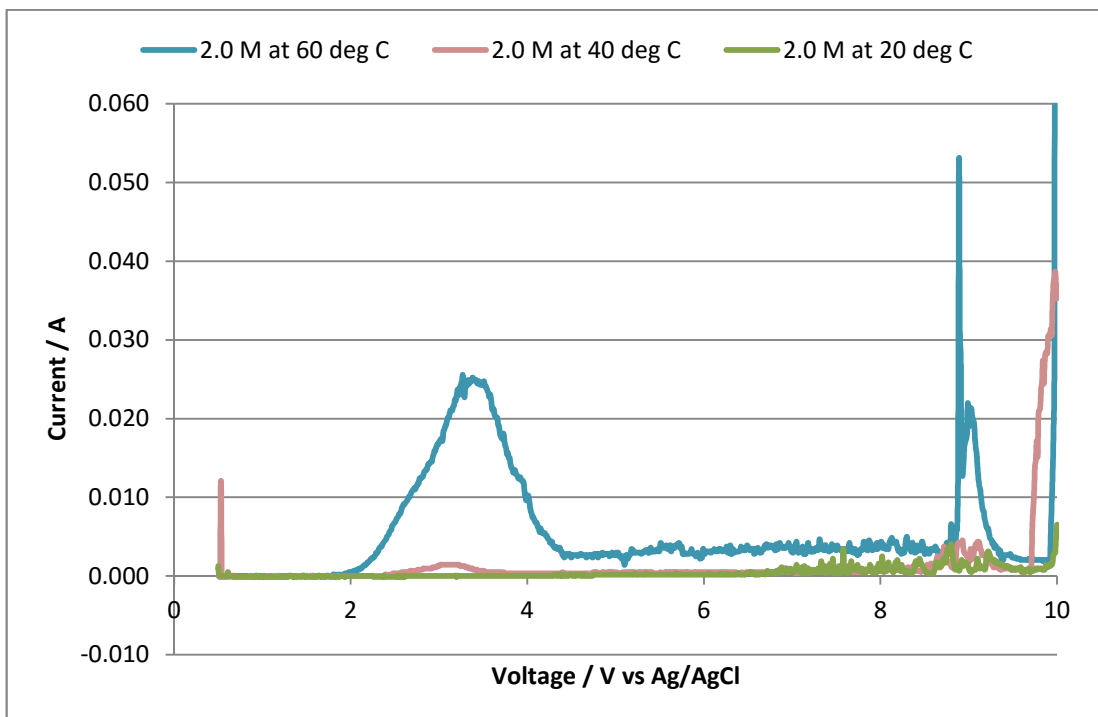
Figure 5-6 Polarisation curves with USV of titanium in 2.0 M NaCl at various temperatures, scan rate 5 mV s^{-1} with natural oxygen levels

Controlling the temperature of the electrolyte whilst USV are applied is difficult due to the natural heating phenomenon of cavitation and the turbulence and friction induced in the liquid by the mechanical oscillations. The heating was less obvious at higher temperatures, with temperatures increasing by ten degrees at the lowest temperature (20 °C) if no measures were taken to prevent this. The water in the ultrasound bath was refreshed periodically with cool water or ice to keep the temperature more stable.

Whilst the addition of USVs to the electrolyte has increased the current which passes during the experiment, the current observed is still low in comparison to those needed for macro-scale ECM. As such, this addition may be suitable for micro-ECM in its existing form.

5.3.3 Chronoamperometry with Ultrasonic Vibrations

Chronoamperometry experiments were conducted at several fixed potentials, determined by the polarisation experiments with USVs. The potentials studies were 9.0, 9.5 and 10.0 V. The potential was applied for 40 minutes (2400 s) which allowed some dissolution but not the total dissolution of the 1 mm diameter Ti wire. This permitted the MRR at each potential to be calculated.

Higher machining rates are preferable in manufacturing processes as the cost per part is reduced due to the decreased time required to produce each product. As such, the chosen voltage for the anodic dissolution of titanium should facilitate high MRRs. Alongside this, the potential should also enable high precision machining to take place. With ECM, a higher voltage usually results in a higher MRR up to a particular potential, dependent on workpiece and electrolyte choices; but a higher voltage also produces a larger overcut; so a compromise is usually made which balances an acceptable machining rate with an acceptable machining precision.

The first 100 s of the data should be dismissed as the electrodes were inserted into the electrolyte after the USVs and the potential had been

applied, as such there is a period of time where the electrodes are either not in the electrolyte or are being moved around making any current feedback unreliable during this period.

Very little mass change in the titanium samples was observed for any of the chronoamperometry tests conducted at 20 °C irrespective of the potential applied or the concentration used. This was expected as the current passed during the experiment was very low, as can be seen in Figure 5-7. The current remains below 0.2 A for the majority of the time period, apart from during experiment run 3 between 200 and 300 seconds which peaks at 0.90 A. This result is unexpected as the highest current is seen with the lowest concentration and potential used. However, this does not correspond with the change in mass observed with only a change of 0.0007 g recorded for this run. As the mass change is so low, the high current peak is likely to be caused by a pit formation and consequent oxidation of the surface. The surface after the chronoamperometry experiment is shown in Figure 5-8; it shows only minimal corrosion but there is evidence of pitting.

The highest mass change at 20 °C was seen using 3.0 M NaCl at 10.0 V which corresponds well with the chronoamperometry results shown in Figure 5-7; experiment number 7 has the highest overall current across the time period resulting in the largest amount of material removal. The titanium sample after this chronoamperometry experiment can be seen in Figure 5-9.
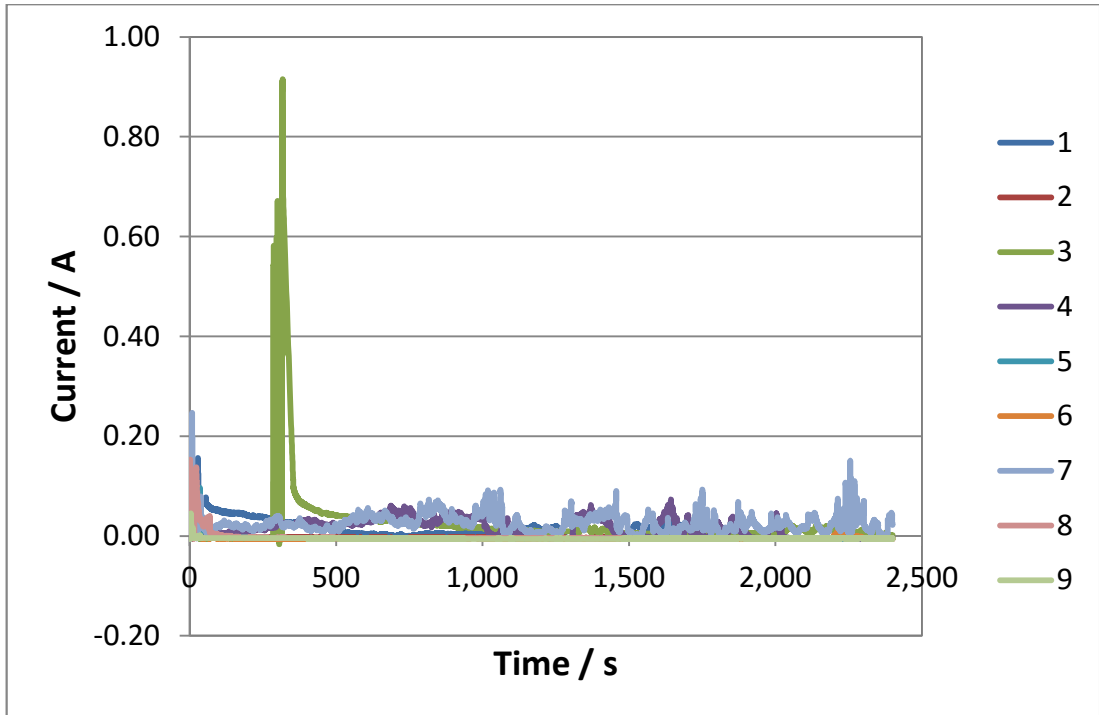
Figure 5-7 Chronoamperometry experiments of titanium in various concentration of NaCl at various applied potentials at 20 °C with USV (No. 1-3 1.0 M NaCl, No. 4-6 2.0 M NaCl, No. 7-9 3.0 M NaCl; No. 1, 4 and 7 at 10.0 V, No. 2, 5 and 8 at 9.5 V and No. 3, 6 and 9 at 9.0 V)
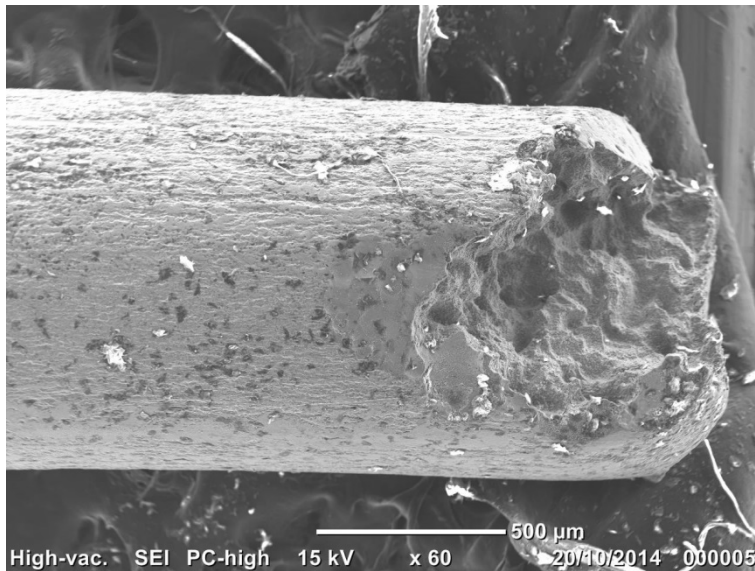
Figure 5-8 SEM image of titanium after chronoamperometry experiment in 1.0 M NaCl at 9.0 V
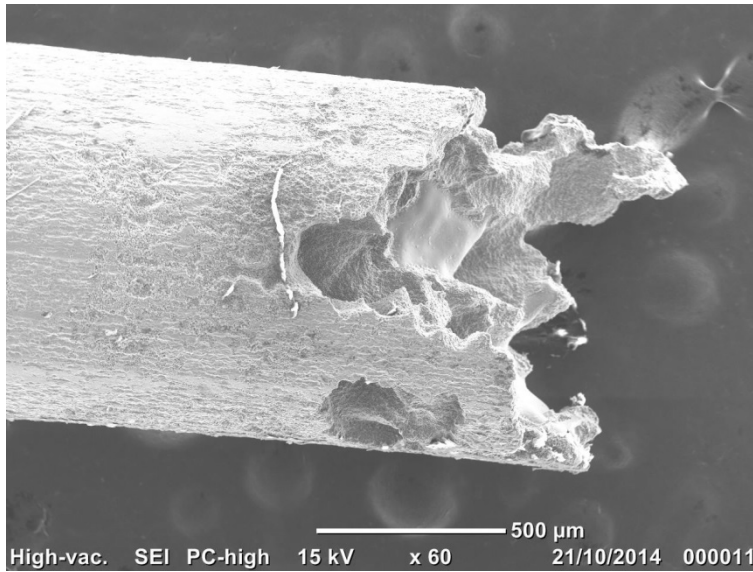
Figure 5-9 SEM image of titanium after chronoamperometry experiment in 3.0 M NaCl at 10.0 V
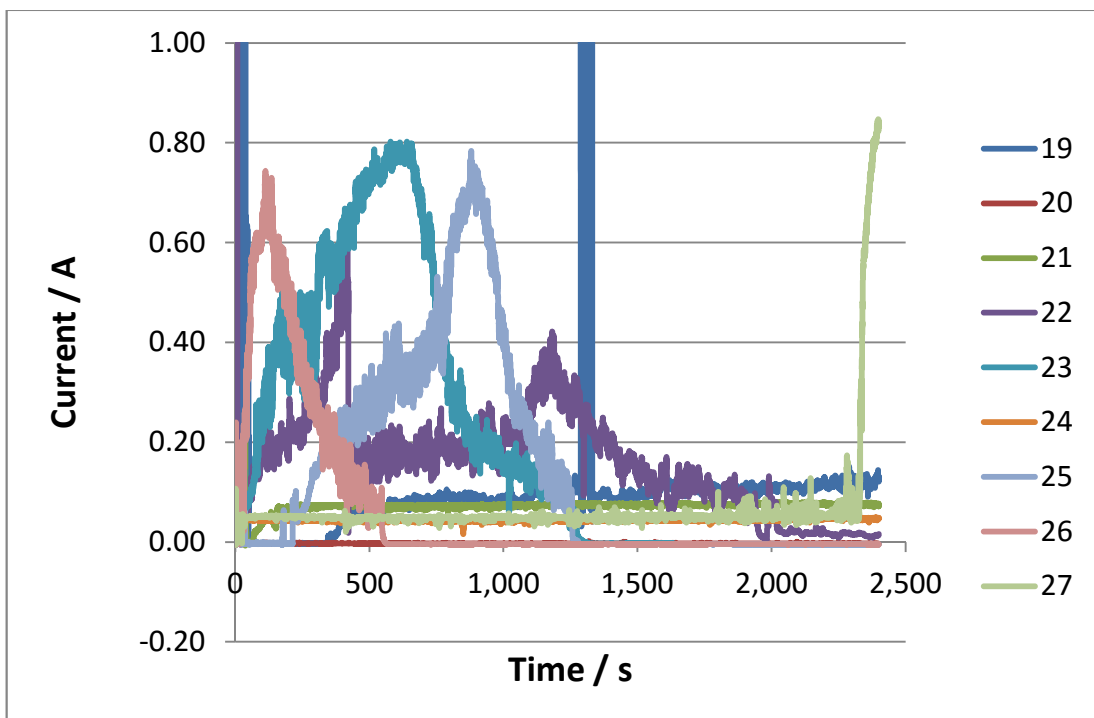
Figure 5-10 Chronoamperometry experiments of titanium in various concentrations of NaCl at various applied potentials at 60 °C with USV (No. 19-21 1.0 M NaCl, No. 22-24 2.0 M NaCl, No. 25-27 3.0 M NaCl; No. 19, 22 and 25 at 10.0 V, No. 20, 23 and 26 at 9.5 V and No. 21, 24 and 27 at 9.0 V)

As the temperature was increased the observed current also increased; the chronoamperometry results conducted at 60 °C are shown in Figure 5-10. This is expected as a higher temperature increases the ion mobility of species in the electrolyte which increases the conductivity of the electrolyte resulting in higher currents.

The highest mass change across the whole set of chronoamperometry experiments was observed using the highest concentration, temperature and potential as predicted. Increasing the electrolyte concentration increases the availability of active ions in the solution which facilitate the anodic dissolution of titanium. Increasing the temperature, as previously discussed, increases the mobility of the ionic species in solution. It also decreases the electrolyte viscosity which affects the mobility rate further. A higher potential facilitates a higher current when other variables remain the same to maintain the current-potential relationship $V = IR$.

If this were to be transferred to an ECM machine for testing, a 3.0 M NaCl electrolyte would be chosen at a potential of 10.0 V initially although this may be reduced to 9.0 V to improve resolution at the expense of MRR.

5.4   Conclusion

Titanium is an important manufacturing material due to its favourable properties. However, titanium is difficult to machine both conventionally and non-conventionally using ECM; due to its hardness and poor thermal conductivity and its chemical stability respectively.

It has been demonstrated in this thesis that the addition of USVs can reduce the dissolution potential of titanium in NaCl electrolytes at various temperatures and concentrations from over 10 V to 9.0 V. The USVs are thought to impinge on the metal surface, removing the passive oxide layer exposing the active metal surface to allow anodic dissolution at low applied potentials.

The highest removal rate was seen when using a concentration of 3.0 M NaCl with an applied potential of 10.0 V vs Ag/AgCl at 60 °C.

5.5   Further Work

The experimental set up of this work somewhat limited the results as to the applicability of the process to ECM as the IEG maintained in this work is much larger than those used in ECM. However, this work provides general conclusions to the electrochemical behaviour of titanium during anodic dissolution with insonation. As such, further work should be conducted on a real ECM set up with an ultrasonic nozzle delivering the electrolyte to the IEG.

Given more time and resources, it would also be favourable to model the process computationally to observe the effects of the USVs on the titanium surface during anodic dissolution to confirm whether the oxide layer is removed by cavitation.

Chapter 6 – Electrochemical Production of Hypodermic Needle Tips

6.1 Introduction

6.1.1 History of the Needle

The invention of the needle has been one of the most significant breakthroughs in medical science. The first documented use of a needle was during the 10th century by `Ammar ibn `Ali al-Mawsili, who is said to have removed a cataract from an eye via suction through a glass tube (Savage-Smith 2000). This technique was used until the 13th century to remove fluids from the body, but no evidence remains to suggest needles were used to inject anything into the body (Anonymous 2014b). Sir Christopher Wren created a crude 'needle'; he attached a pig's bladder to a goose feather quill which could be inserted into veins to administer drugs directly into the blood stream. He injected dogs with opium. (Anonymous 2014b)

In 1844 a needle close to the current understanding of a needle was created. Francis Rynd created a hollow steel needle which he used to inject drugs just under the skin. (Anonymous 2014b) However, Alexander Wood was recognised as the inventor of the hypodermic needle in 1953, although French scientist, Charles Pravaz, also reported a similar needle around the same time which was used to administer an anticoagulant into sheep to stem bleeding. Alexander Wood's needle was the first reported needle which included a syringe.

Needles were most commonly used to inject morphine as few other drugs were injectable at the time (less than 2% of drugs in 1905). However, the discovery of insulin in 1921 created a new market for hypodermic needles. In 1946 the Chance Brothers began mass producing a glass syringe with inter-changeable parts. (Anonymous 2014b) After issues with sterilisation, disposable plastic syringes were soon realised and a patent was filed by Colin Murdoch. The basic design of a needle has not changed too much

since. The syringe and injection needle manufacturing market is expected to grow 6.6 % between 2014 and 2018 (Anonymous 2014a).

6.1.2 Current Production Methods

The tubes for needles are predominantly made via a process known as tube drawing where a steel tube is drawn through increasingly smaller dies until the desired diameter is reached; the outer diameter is usually below 0.66 cm (0.259 in). (Vita Needle Company n.d.) Once the tubes are cut into the correct lengths, the tip is bevelled via precise mechanical grinding. This process is very quick (on the scale of seconds) but grinding needles creates burrs and small grooves on the surface as shown in Figure 6-1a. These are undesirable and add to the pain felt by the patient upon injection. The surface roughness is dictated by the grade of abrasive particle size on the sanding belt.
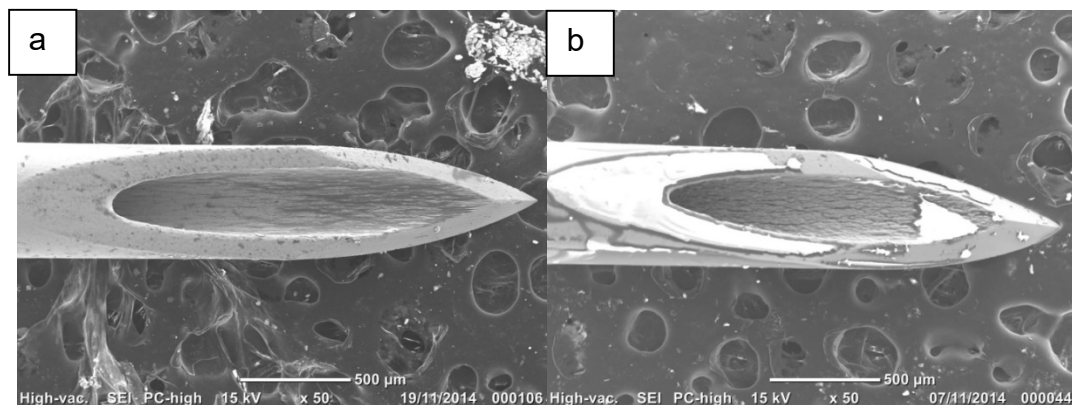
Figure 6-1 a) SEM image of a B. Braun 25G x 5/8" Long Bevel Sterican® Hypodermic Needle b) SEM image of a Becton Dickinson and Company 25G 1 1/2 PrecisionGlide Needle

The sharpness of the tip and the surface roughness are major factors in the pain felt by the patient. A sharper tip means less force is needed to penetrate the skin and a smoother surface finish decreases the friction between the needle and the skin. One method which needle manufacturers employ to the decrease the surface friction is through the application of a silicon based coating on the needle tip (B.Braun 2002) as can be seen in Figure 6-1b.

The design of the needle is important for reducing the insertion force required to penetrate the skin. A study has been conducted which examines the importance of the inclination and rake angles of the needle tip (Wang et al. 2013). This is beyond the scope of this study where the aim is to improve the surface finish of the initial cut of a needle tip of a given design in order to decrease the force needed to insert the needle through the skin. The initial cut is only investigated as the ECM machine at Brunel University was built in-house and does not have a controllable C-axis necessary for accurate replication between needles. This first cut is known as a 'bias bevel'. (Wang et al. 2013) Nor was there time to complete iterative tool designs to create a complete needle with just one step.

Current needle sharpening is limited to grinding, a process which only creates flat surfaces. ECM has the potential ability to create 3D sharpening which can be adjusted depending on the needle's application which could create a needle built to further reduce penetration forces depending on the biophysical requirements.

6.1.3 Motivation for the work

Brunel University was approached by Sarix SA to begin trials for ECM as a sharpening method for needles. The idea being that ECM could produce a high quality needle with a high surface finish with one step, as supposed to grinding where 4 steps are needed to form the correct tip geometry. (Wang et al. 2013) In some cases a fifth step is also included where the needle is coated with silicon to reduce the surface friction.

Electrochemical machining is a stress-free machining process which replicates the shape and surface finish of the tool being used. If the tool surface used to create the bevelled edge at the tip is mirror-finished then the bevelled edge would also be mirror-finished after machining. Not only that, there would only be the need for one manufacturing step once the tool design was complete.

As previously mentioned, this study will only focus on the bias bevel due to time restrictions preventing iterative tool design. The aim is to create a high quality machined surface which would be an improvement on the surface finish created by grinding.

6.2   Method

Nickel chromium steel tubes were sent from Sarix SA. The tubes' external diameter was 400 µm. The machining time and finished product quality were crucial outputs in the manufacturing process which had to be competitive with current processing times. Due to the limited number of 400 µm diameter tubes sent the number of tests carried out on these was restricted. Instead the majority of experiments were conducted with 600 µm tubes of the same material. Since the initial tests were observing how the material reacted with different electrolytes this variance in diameter was not a crucial factor as one would expect the material to react in the same way, regardless of dimension.

6.2.1 Polarisation Curves

Firstly, polarisation curves were conducted on the NiCr steel tubes which would be used for the needles. This would determine a suitable electrolyte and concentration to be used for machining NiCr steel.

6.2.1.1   Attaching Steel Tubes to Copper Wire

The steel tubes were attached to copper wire via silver loaded epoxy (Circuit Works) and cured in an oven at 55 °C for ten minutes. The insulated copper wire attached to the NiCr steel tube provided an easy electrical connection to the potentiostat.

6.2.1.2   Cell Set Up

A three electrode cell was used containing a homemade platinum flag counter electrode, a Sigma Aldrich double junction silver/silver chloride reference electrode and the NiCr tube connected to an insulated copper wire

with silver loaded epoxy was used as the working electrode. Care was taken when inserting the working electrode into the electrolyte to ensure the silver epoxy remained above the electrolyte level. This was to avoid mixed potentials and prevent the needle becoming prematurely unattached. The needle was inserted approximately 1 cm into the electrolyte solution. This was to ensure the current recorded could be compared from one run to another. The solution was not subjected to any external convection forces.

The working electrode was kept in close proximity to the counter electrode (approx. 2 mm) in an attempt to emulate a set up typically used in ECM.

6.2.1.3   The Polarisation Experiment

The polarisation experiment allows the machining potential and a suitable electrolyte to be determined for the NiCr steel used. Polarisation curves were conducted by scanning the potential between -0.5 V and 10.0 V at a scan rate of 50 mV s^{-1}. Five different electrolytes were used; these were sodium chloride (NaCl), sodium bromide (NaBr), sodium nitrate (NaNO$_3$), sodium chlorate (NaClO$_4$) and sodium hydroxide (NaOH). A polarisation curve was conducted with each different electrolyte at 5 different concentrations (0.5, 1.1, 1.7, 2.3 and 3.0 M). The surface finish was compared using an SEM microscope (JOEL 6000), although the surface finish would likely be different under real ECM applications due to the reduced inter-electrode gap in ECM compared with the electrode separation achieved in the polarisation experiments.

6.2.2 Chronoamperometry

After analysis of the polarisation curves chronoamperometry experiments were conducted. Chronoamperometry examines how the current response changes over time with an applied potential.

6.2.2.1　The Cell Set Up

The cell set up for the chronoamperometry experiments was the same three electrode set up as used for the polarisation experiments.

6.2.2.2　The Chronoamperometry experiment

Three potentials for each electrolyte (excluding NaOH) were examined. Significant potentials were observed from the polarisation curve for the lowest concentration of each electrolyte. The first potential was the potential during the polarisation curve where current first began to flow. The second potential was taken from the linear region between the first defined potential and the current plateau region. The third potential was taken from the onset of the current plateau. If the needle had begun to dissolve before the plateau could be reached the potential at the peak was taken as the highest third potential. See Table 6-1 for the potentials used for each electrolyte.

The length of time the potential was applied for varied between 30 s to 600 s (30, 240, 420 and 600 s).

Table 6-1 Potentials investigated during chronoamperometry experiments for each electrolyte

	V_{min}	V_{mid}	V_{max}
NaCl	0.50	4.00	8.00
$NaNO_3$	1.20	4.50	8.50
$NaClO_3$	1.25	5.00	7.25
NaBr	0.40	4.00	7.50

Images were again taken with the SEM to observe the surface finish. This allowed a direct comparison of the surface quality produced at different potentials over the same time period and between electrolytes. It also allowed the study of the change of surface quality over time as different time periods were used for each electrolyte and concentration.

Using the results from the polarisation and chronoamperometry experiments, an electrolyte and suitable machining potential was defined which could be used on the electrochemical machine at Brunel University.

6.2.3 Tool Design

The required angle of the bevel cut was 15 ° from the z-axis, see Figure 6-2 for a visual representation.
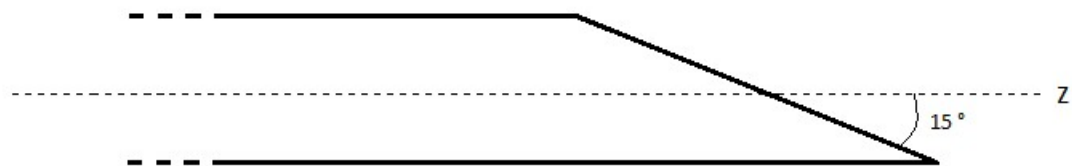
Figure 6-2 Angle of the Bias Bevel Cut

The ECM machine only has a controllable z-axis during machining which limited the tool design; the angle had to be incorporated into the tool design. If other axes had been controllable during machining, one could have utilised this by moving along a vector in the yz-plane of the machine to create the desired angle.

The first design was very simple; a copper rod (1 cm diameter) was mechanically ground and polished to a 15 ° angle from the z-axis, see Figure 6-3, to create a highly polished flat surface that could replicate the surface finish and angle onto the NiCr steel tube to create the bias cut.
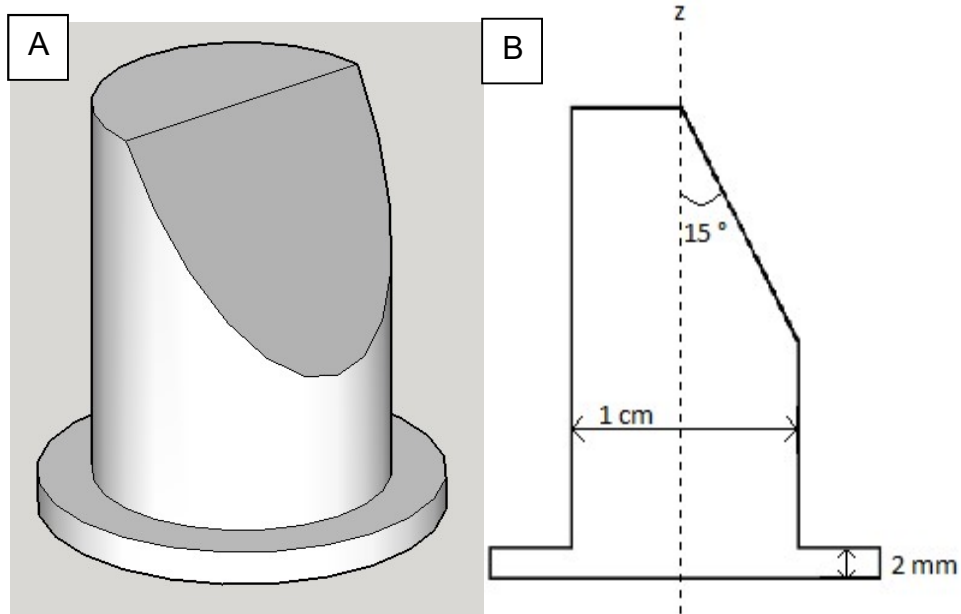
Figure 6-3 A) Initial 3D Tool Design B) Initial Tool Design Outline with Dimensions (not to scale)

As testing commenced, issues were highlighted with the design. The large flat area created an overcut on the needles causing poor shape replication regardless of applied potential, pulse width or electrolyte concentration. It became clear that to continue the study successfully an alternate tool design needed to be used.

The solution had to be something which could easily be transferred from a research environment to industry. Insulating the needle did not seem practical if the process were to be scaled to industrial sizes so to reduce overcut, a tool was designed which would decrease the area of the tool which would be in close proximity to the work piece (the NiCr steel tube) during machining, see Figure 6-4. The angle remained the same as the initial design (15°) with the addition of thin struts protruding from the flat angled surface. Five struts were placed across the surface, 2 struts each 200 µm in width, 2 struts each 300 µm in width and 1 strut 400 µm in width. Each strut was separated by a distance of 1.35 mm which allowed them to be spaced evenly across the whole structure whilst being a large enough distance to prevent interaction with the adjacent strut during machining.
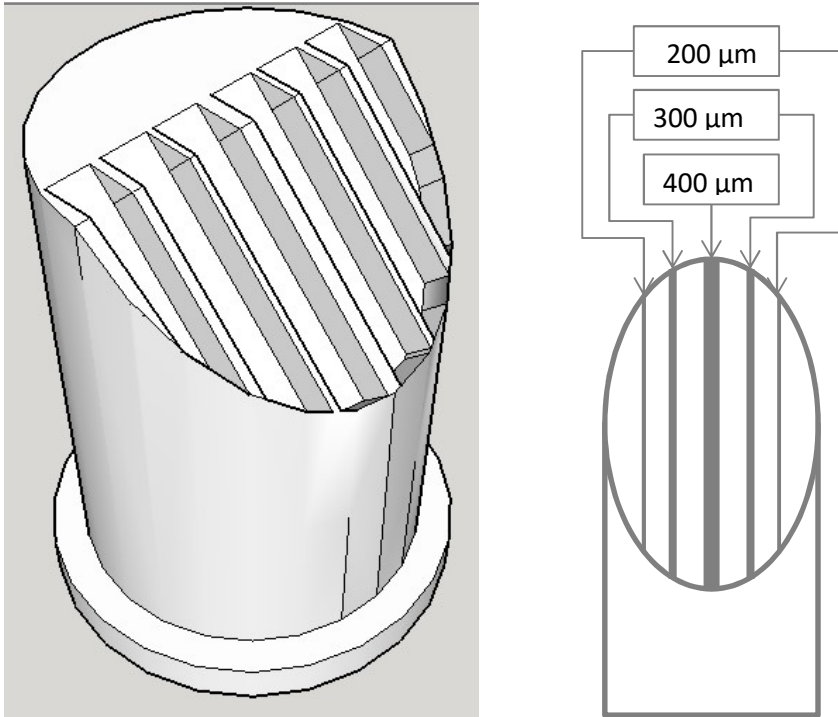
Figure 6-4 Modified & Final Tool Design

6.2.4 Electrochemical Machining Experiments

6.2.4.1 Design of Experiments

Four machining parameters were to be investigated; the electrolyte pump frequency (i.e. electrolyte flow rate), the IEG, the feed rate in the z-axis and the voltage will be optimised. Although the polarisation and chronoamperometry experiments have investigated the voltage, the IEG in a real machining situation is much smaller than can be achieved in the initial testing in an electrochemical cell. As such the voltage determined will be used as a guide.

For the electrochemical machining experiments, an ECM machine at pECM Systems Ltd was used. The machine was an 'Impulse ECM' machine manufactured at pECM Systems Ltd. The machine is more powerful and reliable than the machine built in-house at Brunel University with the ability to apply a constant feed rate as supposed to one based on the current feedback during machining, such as adaptive feed rate, where the feed rate

is constantly changed throughout machining based on the number of time the 'over-current protection' system is triggered. For example, if the initial feed rate, set by the machine, triggers the over-current protection system several times in quick succession the feed rate will be reduced gradually until the protection system is no longer triggered. Whilst this protects the tool and the work piece from damage caused by sparks, reproducibility cannot be achieved from one run to the next.

6.2.4.2 Electrochemical Machine Set Up

The steel tube work piece was held in a V-block with a plastic block, connected to the positive terminal of the ECM machine. The tool was held on the z-axis connected to the negative terminal. The tool was positioned so one of the struts was central to the work piece in the x-axis but behind the work piece in the y-axis as seen in both Figure 6-5 and Figure 6-6. The alignment of the tool with the steel tube was done by eye so some misalignment is inevitable although the x-axis was not moved between each run so as to maintain some reproducibility in the experiments.
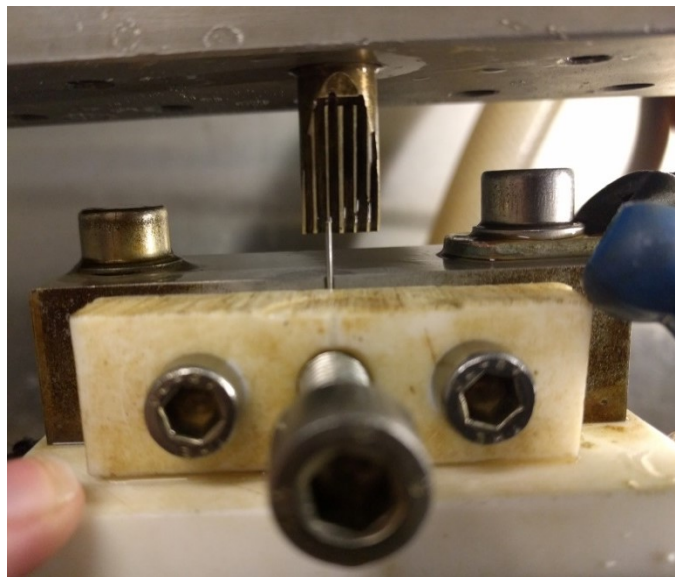
Figure 6-5 Electrode set up for needle machining
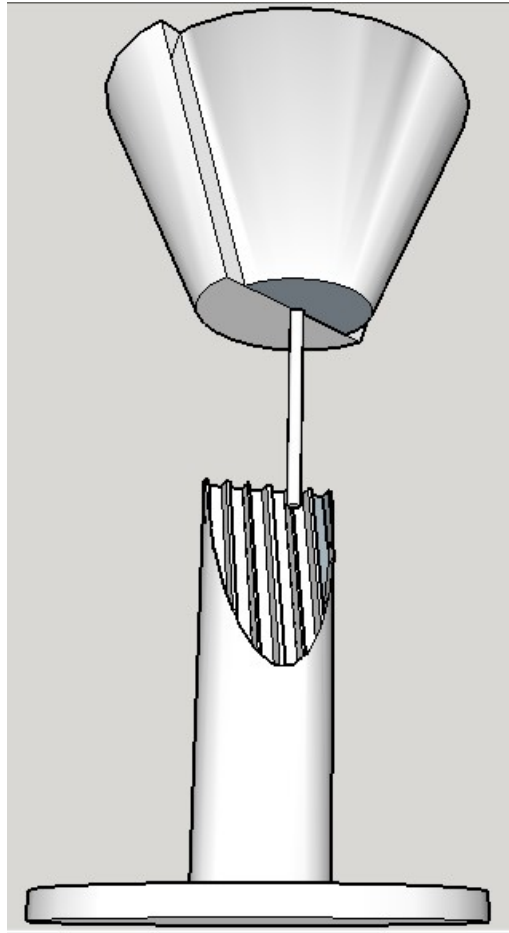
Figure 6-6 3D Model of the Electrode Set Up During Electrochemical Machining Needles

A multi-meter was used to determine when contact had been made between the electrodes, the tool was then moved a set distance away from the work piece in the z-axis to set the IEG. This position was defined as the starting position. With the start position defined, machining could commence. The bevel length is an important factor when forming the needle. The bevel must pass through the cylinder completely, leaving a level surface. To ensure the bevel length is correct, the z-axis must move a minimum distance. For a 600 µm tube, the z-axis must descend a minimum of 2.24 mm; see Equation 18 or Figure 6-7 for a visual representation.

$$z = \frac{0.6\ mm}{\tan 15} = 2.24\ mm \tag{18}$$
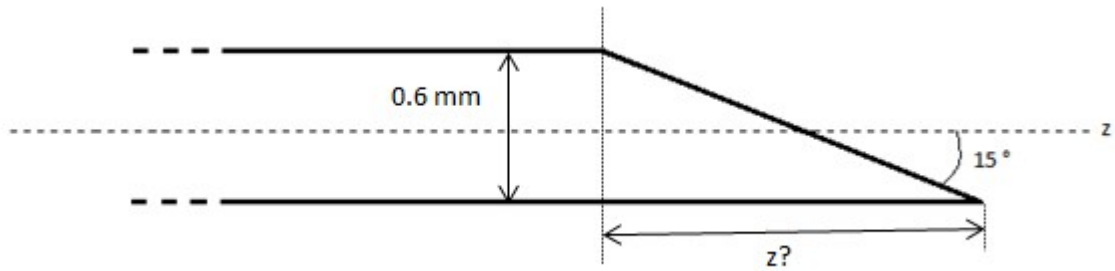
Figure 6-7 Calculation for Minimum z-axis Machining Length

After the newly formed needle was removed from the ECM, the needles were washed in an ultrasonic bath (Skymen JP-030S) for 10 seconds filled with purified water to remove any salt residue from the surface. The needles were then rinsed with acetone and dried in a stream of nitrogen gas.

6.2.4.3 Analysis of Results

There are several important factors to consider when machining a needle; the surface roughness of the machined surface, the machining precision and accuracy and the machining time per needle.

The aim was to produce a high quality machined needle surface within a time competitive to the current grinding methods. It was crucial the machined surface produced was planar with no rounded edges. The surface also has to be of lower surface roughness than produced through grinding. This is of paramount importance; if ECM does not improve the quality of the final product there is little incentive for the process to be changed from its current methods. Equally, if the time taken to machine a single needle is not competitive with grinding times the cost per needle would increase, which would be a disincentive for switching production methods.

The surface roughness was visually observed with high-magnification scanning electron microscopy (SEM) images. The shape of the bias bevel was also observed visually with SEM images and optical microscope images. The machining time of each needle was recorded. The machining was defined as finished when the z-axis had moved 1.5 mm.

6.3   Results and Discussion

6.3.1   Polarisation Curves

A total of 25 polarisation experiments were conducted; 5 electrolytes at 5 different concentrations which were repeated twice. Only 2 repetitions were conducted due to the limited materials available but more repetitions would have been more favourable. An attempt was made to insert the work piece to the same depth for each run but this was done by eye so some discrepancies are unavoidable.

As expected, for each electrolyte, as the concentration increased the maximum current observed also increased, unless the surface area of the needle decreased due to dissolution; in which case a drop in current was observed, as seen with sodium chloride in Figure 6-8. This is because there are more ions available in the solution to carry the charge. An increase in concentration reduces the electrical resistance of the electrolyte, allowing a
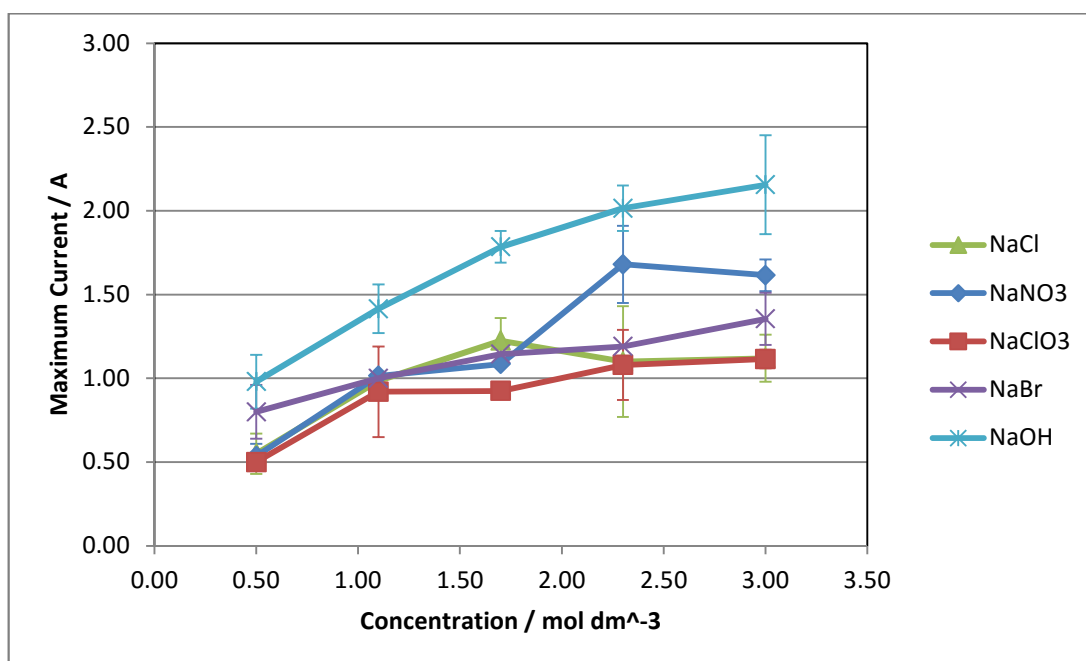
Figure 6-8 Graph Showing the Effect Concentration has on Maximum Current Passed During a Polarisation Experiment

higher current to be passed. See Figure 6-8 for a graphical representation of how concentration affected the maximum observed current for the electrolytes investigated.

Sodium hydroxide shows the highest current across the selection of electrolytes investigated. With the maximum current being the highest for sodium hydroxide, one would expect the removal rate to be highest. However, when the tubes were examined with a scanning electron microscope (SEM) no anodic dissolution had occurred, see Figure 6-9. One can assign the current to the evolution of oxygen at the work piece surface rather than anodic dissolution. This observation allowed sodium hydroxide to be excluded as a suitable electrolyte for anodic dissolution of nickel chromium steel used for the metal shaft of hypodermic needles. It may be possible to anodically dissolve the NiCr steel with NaOH but at a much higher potential than is achievable with the IviumStat potentiostat.
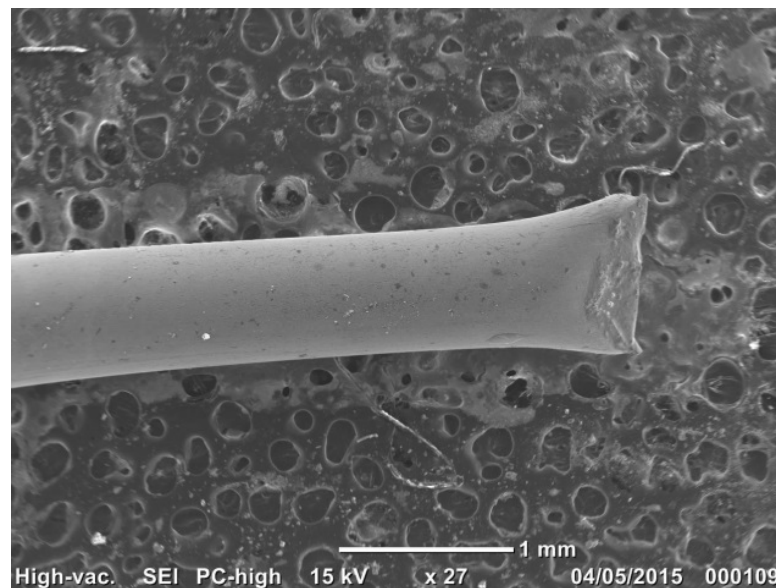
Figure 6-9 SEM image (27x Magnification) of NiCr Steel Tube after Polarisation Experiment in 3.0 M Sodium Hydroxide

The 4 other salt electrolytes successfully facilitated the anodic dissolution of the nickel chromium steel, albeit at different rates.

Polarisation curves in sodium chlorate produced the lowest current over the range of concentrations studied. This resulted in low material removal compared to the other electrolytes. SEM images confirm this and appear to show inter-granular attack, see Figure 6-10. The white material on the right hand side of the image in Figure 6-10 is salt. As $NaClO_3$ is known to be a passive electrolyte, it is possible to assume the salt was electrochemically formed. These salt films are formed because the rate of transport of dissolving metal ions into the bulk electrolyte is rate limiting. (Lohrengel et al. 2003) Whilst salt films can reduce machining overcut the films significantly reduce the machining rates and increase the machining potential.
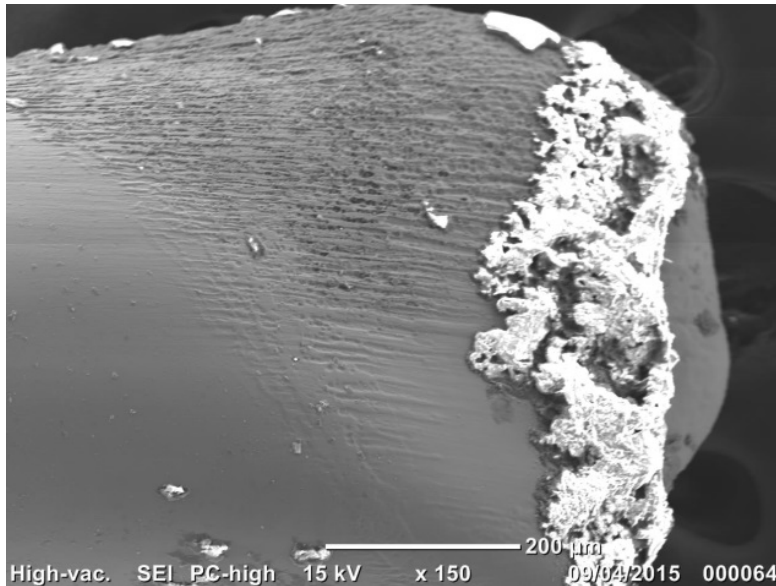
Figure 6-10 SEM Image (150x Magnification) of NiCr Steel Tube after Polarisation Experiment in 1.1 M NaClO$_3$

Polarisation Curves in sodium bromide show a linear increase in maximum current over the concentration range. This is the expected trend. Sodium bromide is an electrolyte which facilitates active dissolution due to the presence of the aggressive anion bromide. (Bhattacharyya et al. 2004) One problem with aggressive anions is that they can cause pitting rather than even dissolution across the work piece. Chloride ions can penetrate the protective oxide film present on stainless steels which can initiate pitting. Pitting can also occur due to selective dissolution of one component. At low

concentrations, pitting did occur on the NiCr steel tubes, as seen in Figure 6-11. The surface is not evenly machined; there has been selective attack which has resulted in a rough surface finish. As the concentration of NaBr was increased, the surface finish improved, see Figure 6-12. This is because the dissolution is more complete with a higher concentration due to the higher current which can be passed through the cell.

Sodium chloride is one of the most commonly used salts for electrochemical machining as it is inexpensive and safe to use. Sodium chloride is a non-passive electrolyte, like sodium bromide, so one would expect to see active dissolution. The maximum current initially increased as concentration was increased but beyond 1.7 M the maximum current began to decrease. One would suggest that there is selective dissolution at the region where the needle crosses the air-electrolyte interface; this caused a small amount of material to be removed without undergoing anodic dissolution itself. This has been observed before by several authors (Wu et al. 2013; Lim & Kim 2001; Lim et al. 2003). This was explained by reaction products building at the electrode surface, these particles at the electrode are 'dragged down' by gravity causing a thickening of the surface layer at the electrode tip. This thinning of the surface layer at the electrolyte-air interface in comparison to the tip allows higher dissolution rates in comparison to the rest of the electrode, which causes the lower electrode portion to fall away before being electrochemically removed. Also, the electrode near the air-electrolyte interface is less likely to experience bubble formation as the oxygen can diffuse to the electrolyte surface and into the atmosphere easily. This means there are no bubbles which block the electrode surface.

Figure 6-13 shows an SEM image of the steel tube after polarisation in 3.0 M NaCl, it shows the typical taper shape associated with enhanced dissolution at the electrolyte-air interface. The surface is also highly polished towards the tip but shows some pitting corrosion to the left of the image.

Another commonly used electrolyte in ECM is sodium nitrate. Sodium nitrate, like sodium chlorate, is a passive electrolyte so one would expect a

protective layer to form on the work piece surface; this is evident in Figure 6-14. It also demonstrates how a passive electrolyte can enhance machining precision, as seen by the flat, taper-less cut, with no stray machining.
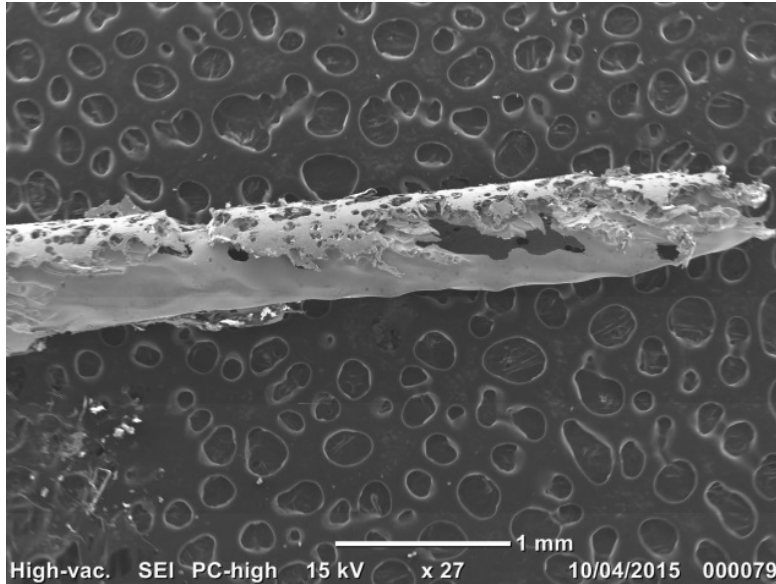
Figure 6-11 SEM (27x Magnification) of NiCr Steel Tube after Polarisation Experiment in 0.5 M NaBr
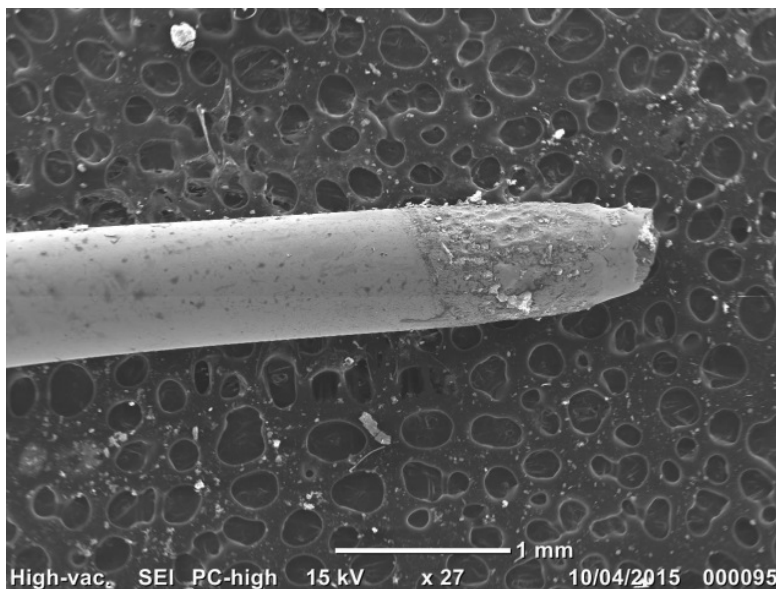
Figure 6-12 SEM (27x Magnification) of NiCr Steel Tube after Polarisation Experiment in 3.0 M NaBr
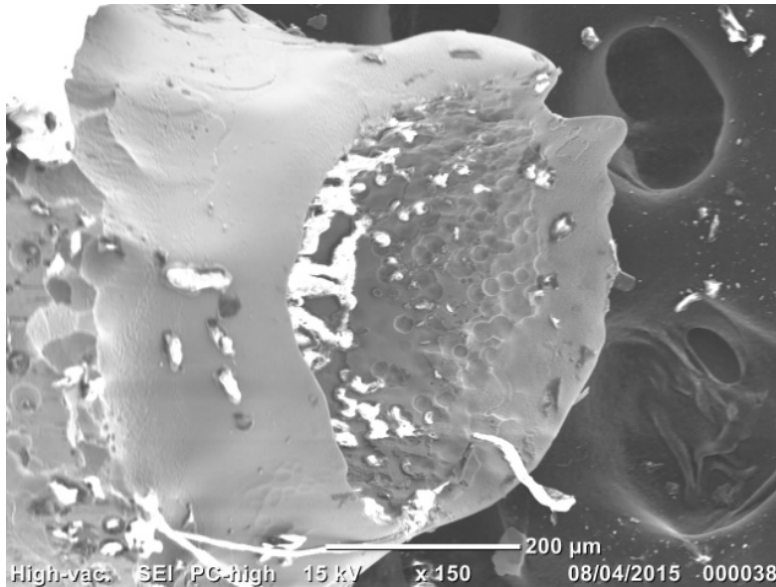
Figure 6-13 SEM (150x Magnification) of NiCr Steel Tube after Polarisation Experiment in 3.0 M NaCl
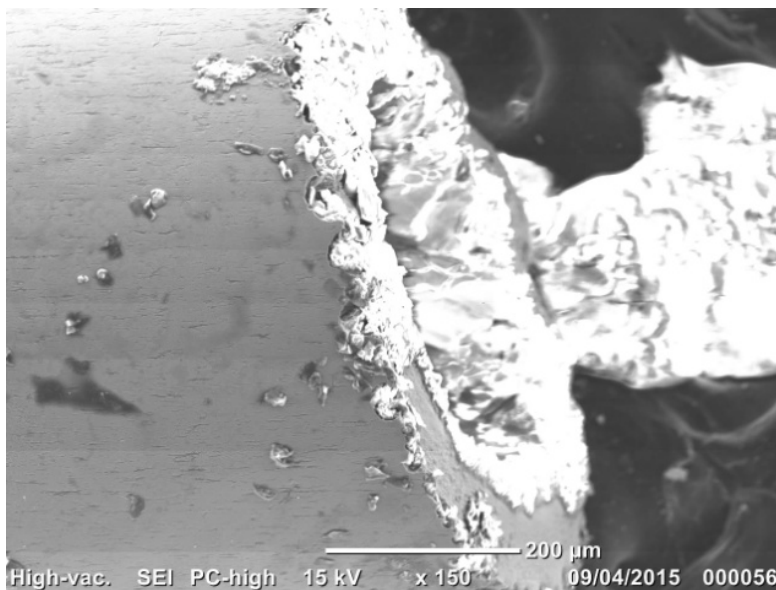
Figure 6-14 SEM (150x Magnification) of NiCr Steel Tube after Polarisation Experiment in 3.0 M NaNO$_3$

From the polarisation curves one can determine the potential at which anodic dissolution begins. For sodium nitrate and sodium chlorate, a distinctive shape characteristic for passive electrolytes is presented, see Figure 6-15. As the protective layer forms the current drops to near zero until a potential is

reached which provides enough energy to break down the passive layer; dissolution in this region is known as transpassive dissolution. Both are passive electrolytes which form protective salt films on the work piece surface. The potential stated as the initial potential at which anodic dissolution begins is the beginning of the transpassive region; this is because the region of active dissolution shows only low currents, approximately 3 mA, which is unsuitable if machining is to be competitive with current grinding methods.
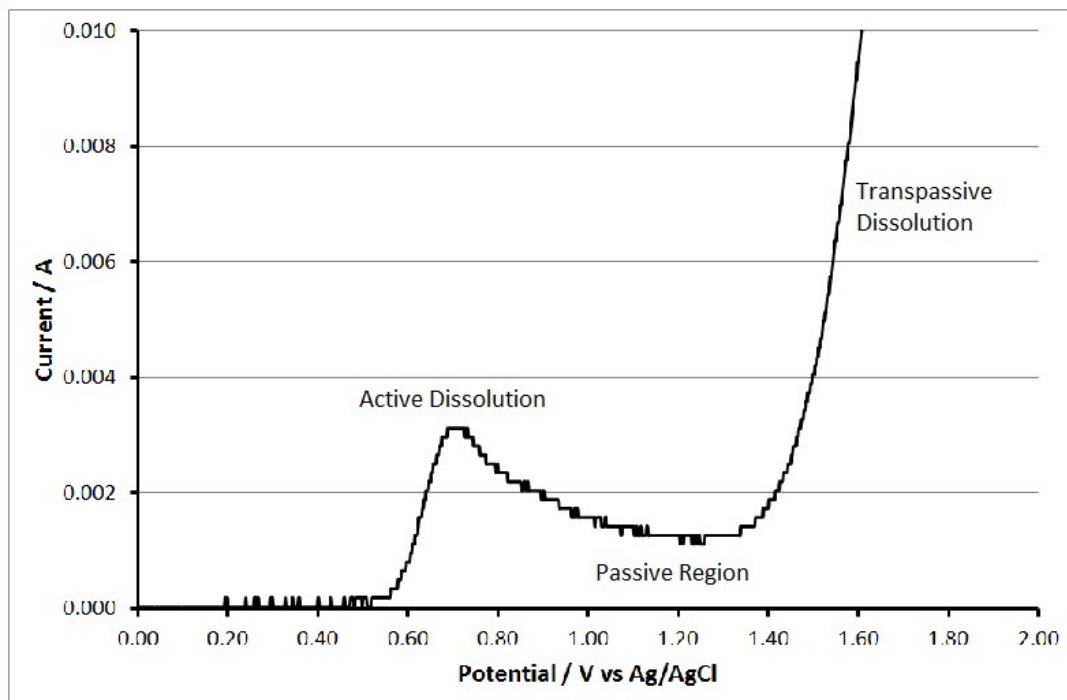
Figure 6-15 2 V Section of a Polarisation Curve for NiCr steel in 2.3 mol dm^{-3} Sodium Nitrate (scan rate = 2 mV s^{-1})

Sodium chloride and sodium bromide are both non-passive electrolytes which facilitate active dissolution. The potentials listed as the onset of current is truly when the current begins to flow and as such, show the lowest onset potential, see Figure 6-16, bar sodium hydroxide; but, as already discussed NaOH has been discounted as a suitable electrolyte for this purpose. This suggests that NaBr and NaCl would provide the lowest energy machining

options for needle manufacturing, with $NaNO_3$ and $NaClO_3$ providing higher energy but potentially more precise results.

From the results of the polarisation experiments one can only conclude that NaOH is an unsuitable electrolyte from machining NiCr needles, as all the other electrolytes successfully anodically dissolved the material.
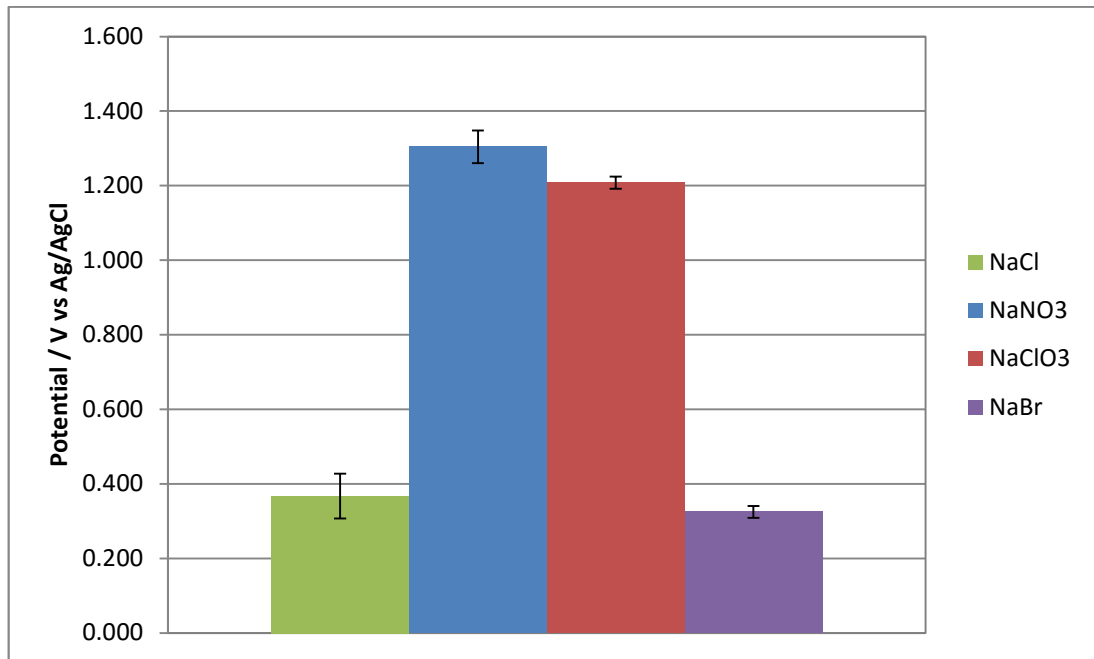
Figure 6-16 Average Onset Potential for All Concentrations for Each Electrolyte Excluding NaOH

6.3.2 Chronoamperometry

Chronoamperometry studies the current response over time with respect to a constant applied potential. It was used to observe how the needle surface changed with time with a small IEG, approximately 2 mm. This was done for 3 potentials, for 4 different time periods, across the 4 electrolytes which successfully dissolved the NiCr steel in the polarisation experiments (NaCl, NaBr, $NaNO_3$, and $NaClO_3$) at 5 different concentrations. A total of 240 experiments were conducted here to give a thorough picture of the machining evolution.

As expected, for all electrolytes, using the lowest potential, see Table 6-1, there was little to no machining. The potential was the point when current had begun to flow; as such the currents passed were small; too small to remove significant amounts of material over the length of the experiment across all concentrations. Figure 6-17 shows the low currents passed during a 600 s chronoamperometry experiment in 0.5-3.0 M NaCl with the minimum potential of 0.5 V vs Ag/AgCl applied. The currents for all other electrolytes are comparable to those seen in Figure 6-17.
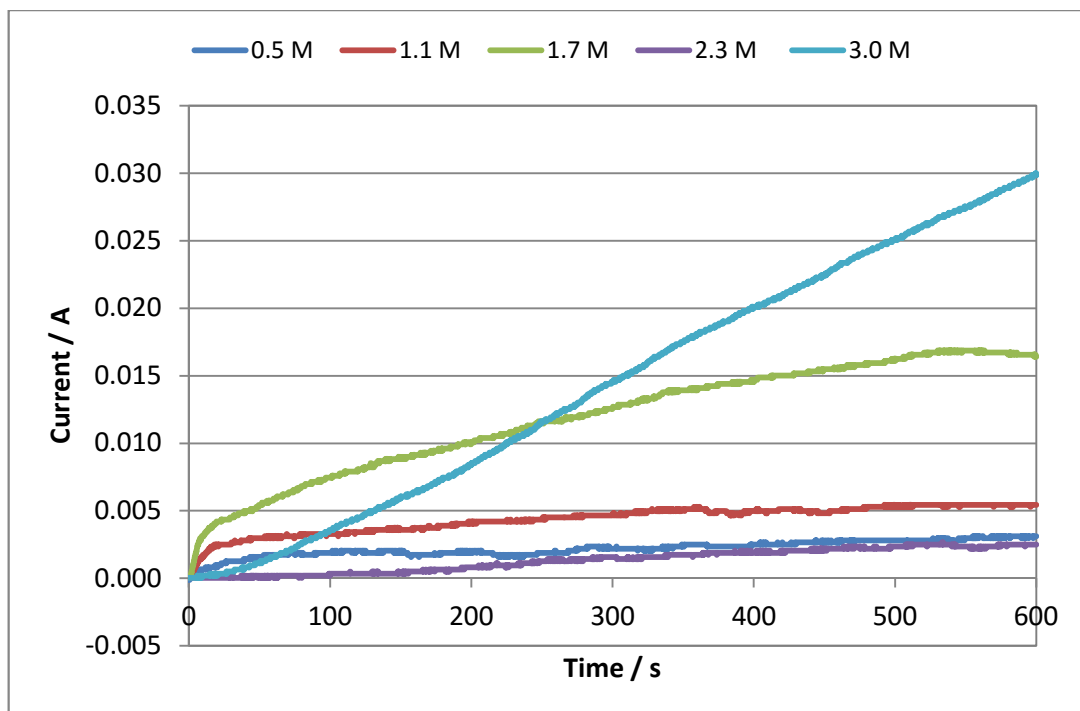
Figure 6-17 Chronoamperometry results in 0.5-3.0 M NaCl at 0.5 V vs Ag/AgCl for 600 s

Since one of the critical parameters of the final needle is the surface finish the SEM images will first be analysed to determine which electrolyte results in the best surface roughness visually. A high quality surface finish is of utmost importance in the needle manufacture, so an electrolyte which causes irregularities in the surface profile is unsuitable.

As mentioned previously, sodium chloride is a non-passive electrolyte, containing aggressive chloride ions. Consequently, passivation is not

expected to occur at the work piece surface. However, chloride ions are associated with corrosion, particularly pitting corrosion. There is evidence of pitting in Figure 6-18, although it appears as though the pitting is reduced as the applied potential is increased. At lower potentials, close to the pitting potential, there is selective pitting, potentially at grain boundaries. However, at higher potentials, the potential is so high it does not discriminate certain areas of the needle and so 'pits' across the whole surface equally, appearing as though the amount of pitting has reduced.
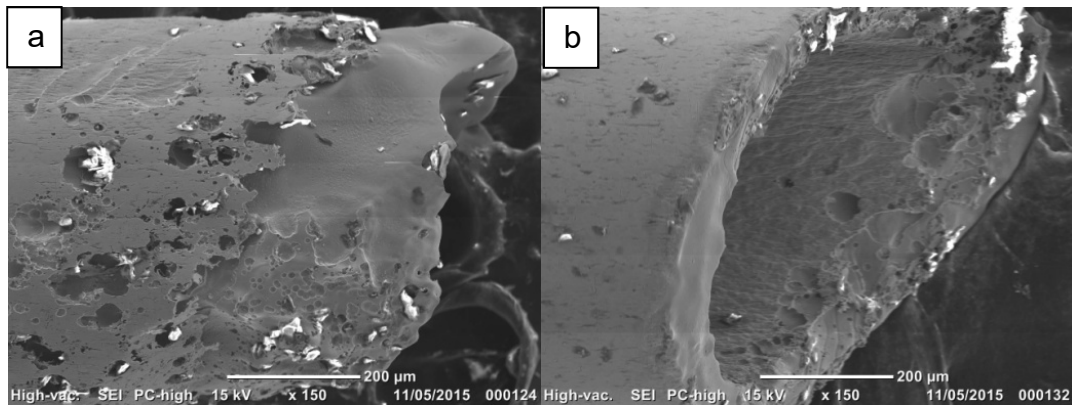
Figure 6-18a) SEM image of NiCr Steel Tube after 240 s at 4.0 V in 0.5 M NaCl b) SEM image of NiCr Steel Tube after 240 s at 8.0 V in 0.5 M NaCl

No improvement was seen in the surface finish across the cut face as the concentration was increased after chronoamperometry at the same potential, for the same period of time. The highest quality surface finish achieved in NaCl at 8.0 V vs Ag/AgCl was with 1.1 M after 240 s as seen in Figure 6-19. Wika (Wika 2012) observed that as the chloride concentration increased, the pitting potential decreased. This results in an increased susceptibility to pitting occurring at higher chloride concentrations. There appears to be an increase in pitting corrosion at the point where the steel tube met the electrolyte as the concentration was increased. In Figure 6-19a there is a smooth transition between machined to non-machined areas whereas in Figure 6-19d there is extensive pitting on the far left where the steel tube was inserted into the electrolyte in line with Wika's observations.
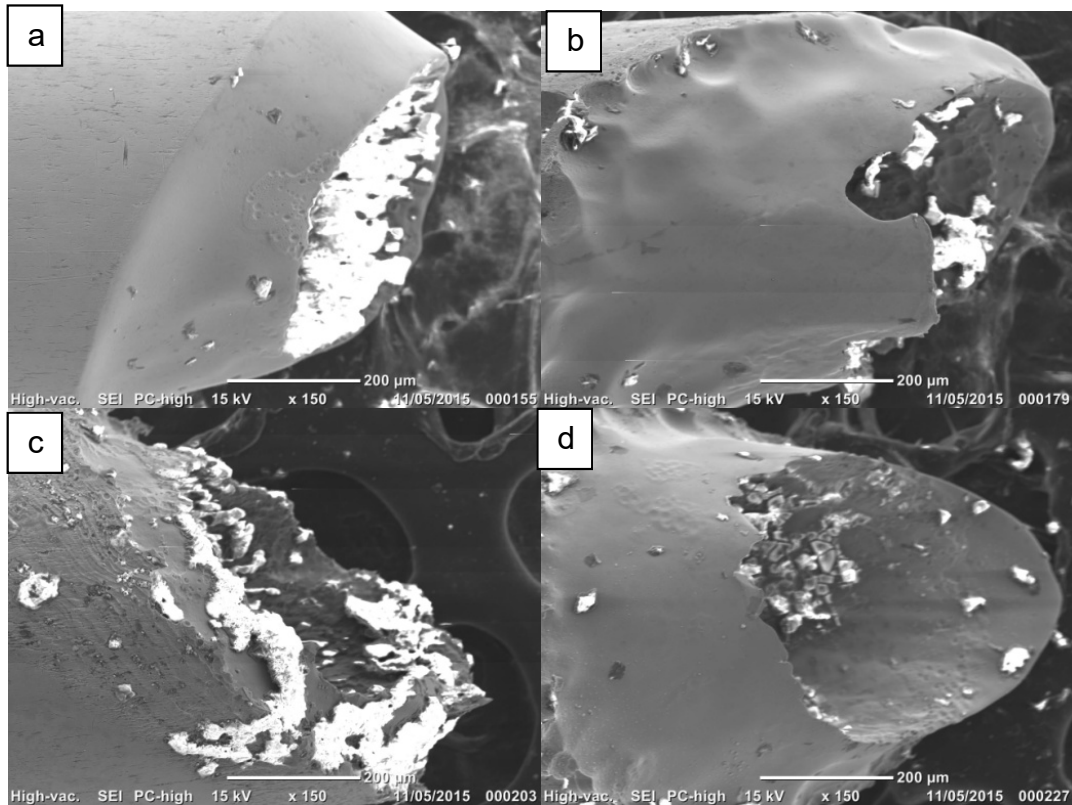
Figure 6-19a) SEM image of NiCr Steel Tube after 240 s at 8.0 V in 1.1 M NaCl b) SEM image of NiCr Steel Tube after 240 s at 8.0 V in 1.7 M NaCl c) SEM image of NiCr Steel Tube after 240 s at 8.0 V in 2.3 M NaCl d) SEM image of NiCr Steel Tube after 240 s at 8.0 V in 3.0 M NaCl

Overall, sodium chloride would not likely produce a product with a surface finish competitive with those currently achieved through grinding with the necessary accuracy.

The other active electrolyte studied for needle manufacture was sodium bromide. As with sodium chloride, pitting was observed on the steel surface, see Figure 6-20a. Again, as the higher potential is used a decrease in pitting was observed, as can be seen in Figure 6-20.

Figure 6-20a SEM image of NiCr Steel Tube after 240 s at 4.0 V in 0.5 M NaBr b) SEM image of NiCr Steel Tube after 240 s at 7.5 V in 0.5 M NaBr

The ionic radius of bromide is slightly larger than the chloride ionic radius so diffusion through the passive oxide layer, formed on stainless steel in an oxidising atmosphere e.g. water, will be slower in comparison to that seen in NaCl. As a result, pitting caused by aggressive anion diffusion through the oxide film would be less prominent in NaBr. More likely, the pitting is driven by the applied potential. From the polarisation curve experiments it was seen that dissolution began at the lowest potential in NaBr, see Figure 6-16. As such, it can be expected that the pitting potential will be lower in NaBr that in NaCl. With a lower pitting potential, it would be expected to see a higher proportion of pitting on the surface, and indeed Figure 6-21 shows this. The pits formed in NaBr are mostly complete, penetrating the full depth of the tube wall, whereas the pits in NaCl do not fully penetrate the tube wall and are much smaller in diameter.

As was observed with NaCl, pitting was increased as the aggressive anion concentration was increased in NaBr. This can be seen in Figure 6-22 with a highly pitted surface observed in Figure 6-22c. Bromide and chloride chemistry is very similar as the two elements are from the same group on the periodic table. Consequently, it can be assumed there will also be an increased susceptibility to pitting as the NaBr concentration is increased.
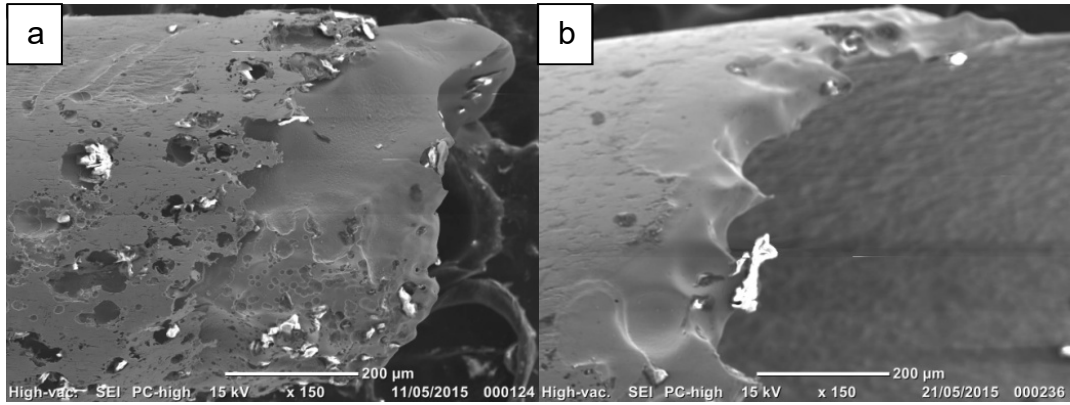
Figure 6-21a) SEM image of NiCr Steel Tube after 240 s at 4.0 V in 0.5 M NaCl b) SEM image of NiCr Steel Tube after 240 s at 4.0 V in 0.5 M NaBr
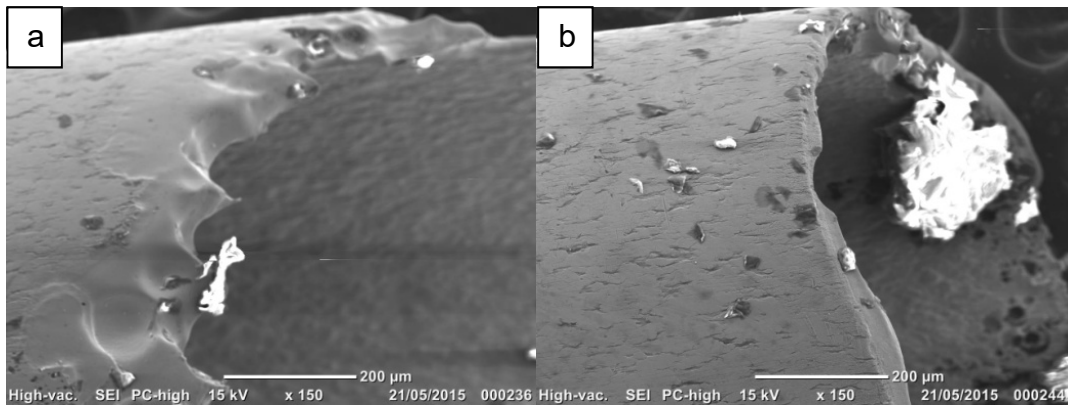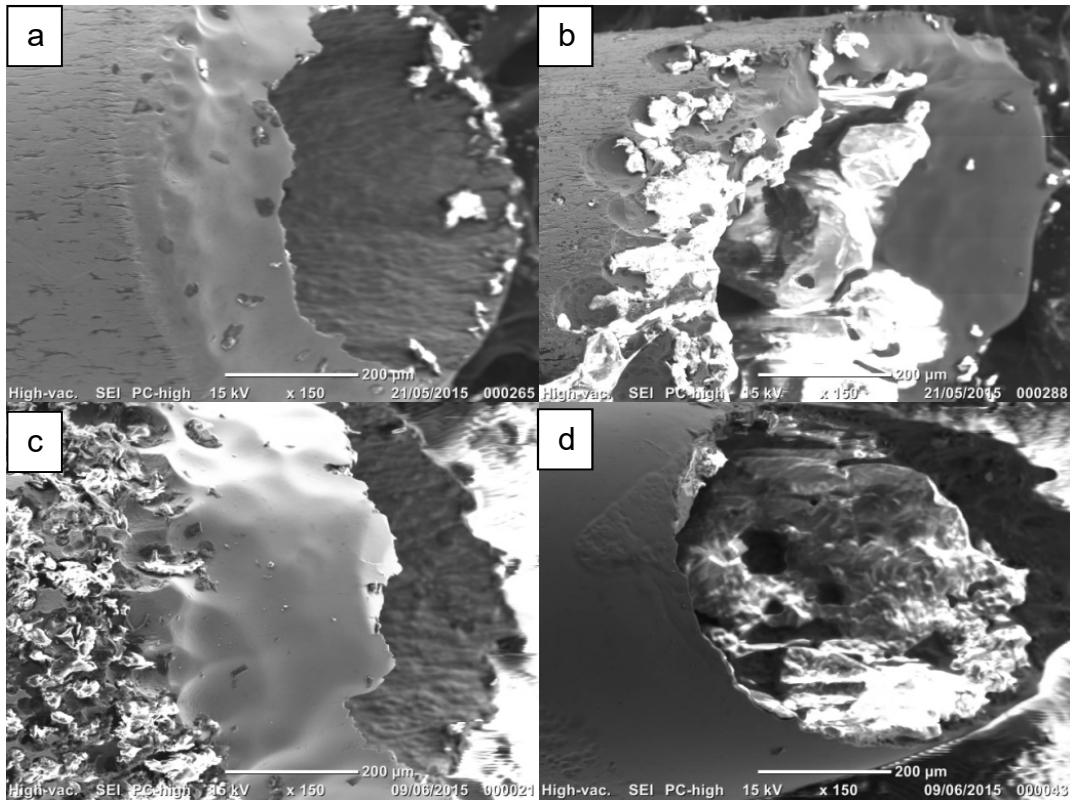

Figure 6-22 SEM image of NiCr Steel Tube after 240 s at a) 7.5 V in 1.1 M NaBr b) 7.5 V in 1.7 M NaBr c) 7.5 V in 2.3 M NaBr d) 7.5 V in 3.0 M NaBr

From the chronoamperometry results in NaBr, it can be said that it is not a suitable electrolyte for the manufacture of needles due to excessive pitting corrosion which causes a poor surface finish. This would not be competitive with the surface finish achieved with current production methods for needles.

Sodium nitrate and sodium chlorate are both passive electrolytes. Passive electrolytes facilitate precise machining due to the formation of resistive oxide layers at areas with lower current density. Current density is a function of the current path length. Shorter current path lengths encounter lower electrolyte resistance so higher current densities are achieved. With larger electrode distances the electrolyte resistance is increased, resulting in lower current densities. This prevents stray machining, leading to more precise results.

With sodium nitrate, a low concentration (0.5 M) prevented the higher current densities required to favour the dissolution reaction. Thus, a passive film was preferentially formed at all potentials with 0.5 M $NaNO_3$. Even after treatment in the ultrasonic bath, the salt layer remains on the steel surface, see Figure 6-23.

As the $NaNO_3$ concentration is increased, higher current densities can be achieved due to the increase in electrical conductivity of the electrolyte. As previously mentioned higher current densities facilitate anodic dissolution, rather than passivation in $NaNO_3$. As the concentration is increased, it is expected to observe an increase in material removal and a decrease in oxide formation on the steel surface. Figure 6-24 does indeed show an increase in material removal, with complete dissolution of the material submerged in the electrolyte. There is also minimal decrease in the oxide layer present on the steel surface as the concentration is increased.

Figure 6-23 SEM image of NiCr Steel Tube after 240 s at 8.5 V in 0.5 M NaNO₃
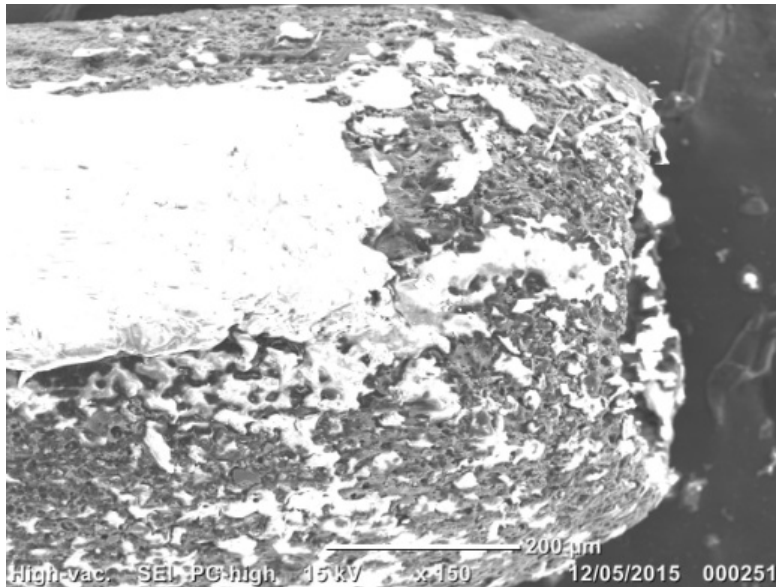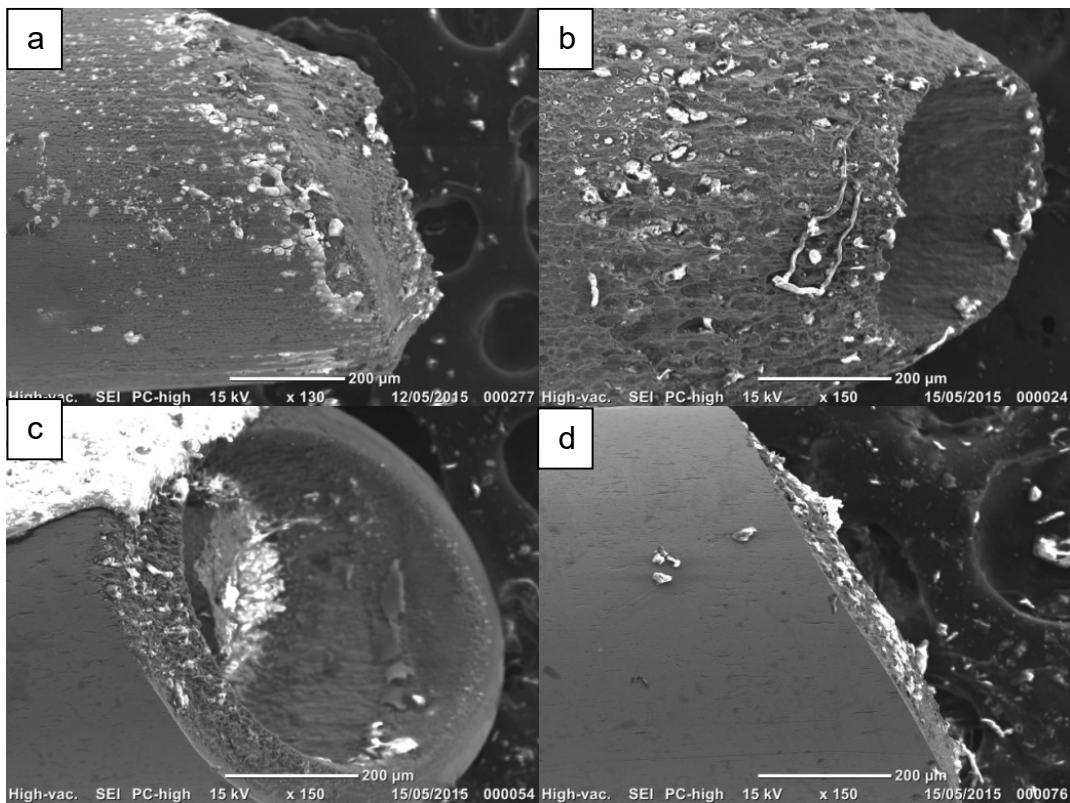

Figure 6-24 SEM image of NiCr Steel Tube after 420 s at a) 8.5 V in 1.1 M NaNO₃ b) 8.5 V in 1.7 M NaNO₃ c) 8.5 V in 2.3 M NaNO₃ d) 8.5 V in 3.0 M NaNO₃

The quality of the cut improves as the concentration increases as well. The aim is to create a distinct cut which is not rounded or thinned at any point. The sharpest cut is seen with the highest concentration 3.0 M NaNO$_3$ as shown in Figure 6-24d at 8.0 V vs Ag/AgCl. The surface is also much smoother than at any other concentration at 8.0 V.

Figure 6-25 compares SEM images of the machined tip at varying concentrations at 4.5 V and 8.0 V. At 1.1 M NaNO$_3$ the surface finish at 4.5 V is more rutted than at 8.5 V. This is in part due to the current densities reached at 4.5 V are less than at 8.5 V because of the relationship shown in Equation 19.

$$V = IR \tag{19}$$

As the concentration is increased the surface finish appears to be improved at the lower potential of 4.5 V. In previous research, authors have observed brighter surfaces at high concentrations as the saturation limit for metal dissolution products at the electrode surface is reached. The salt film mechanism is commonly exploited for surface brightening. The diffusion of dissolution products to the bulk electrolyte becomes the rate determining step and reduces the dissolution rate. (Landolt et al. 2003) The dissolution rate difference is particularly clear in 1.7 M NaNO$_3$ where the steel tube is completely dissolved at 4.5 V but remains partially intact at 8.5 V. Machining precision also decreases as the concentration is increased. This cannot be observed in these chronoamperometry experiments however as there is total dissolution of the samples at higher concentrations so when choosing an appropriate potential to begin testing with the electrochemical machine only the surface finish can be taken into full consideration keeping in mind the known effect concentration has on precision.

Observing the SEM images in Figure 6-25, a good surface finish is achieved at all potentials for 2.3 and 3.0 M NaNO$_3$ and at 4.5 V in 1.7 M NaNO$_3$. Knowing that higher potentials and higher concentrations can lead to poorer

machining precision, 1.7 M NaNO3 at 4.5 V seems to be the ideal machining voltage and electrolyte concentration to still achieve a good surface finish.

Sodium chlorate is also a passive electrolyte and the same behaviours as observed with sodium nitrate are to be expected. With 0.5 M $NaClO_3$ there was no machining at any applied potential as the current densities are too low to facilitate anodic dissolution but sufficient enough to cause passivation. There is evidence of this passive layer at the tip of the tube which has not been removed by insonation in deionised water after the chronoamperometry experiment, see Figure 6-26.

As the concentration of $NaClO_3$ is increased, initially the salt layer increased in thickness until 2.3 M. With 2.3 and 3.0 M, anodic dissolution is present with a better surface finish at the higher concentration, as shown in Figure 6-27. The chlorate ion is larger than the chloride ion so diffusion through the electrolyte to the steel surface would be slower. This meant the chlorate ions which form complexes with the metal dissolution ions are less readily available resulting in the saturation limit of the dissolution products being reached forming a salt layer. A higher concentration of $NaClO_3$ was required to have the same effect as $NaNO_3$.

Figure 6-28 compares the effect of applied potential at $NaClO_3$ concentrations between 1.7 M and 3.0 M. There was no machining at 0.5 M or 1.1 M so these have not been compared. At 1.7 M there is little oxide formation or dissolution at 5.0 V but a large salt layer is present at 7.25 V. Figure 6-29 shows the current response for the 2 experiments discussed. At 7.25 V there is an initial peak current of around 1.1 A which can be associated with oxide formation. This peak is less obvious at 5.0 V which corresponds to the reduced oxide film observed at this potential.
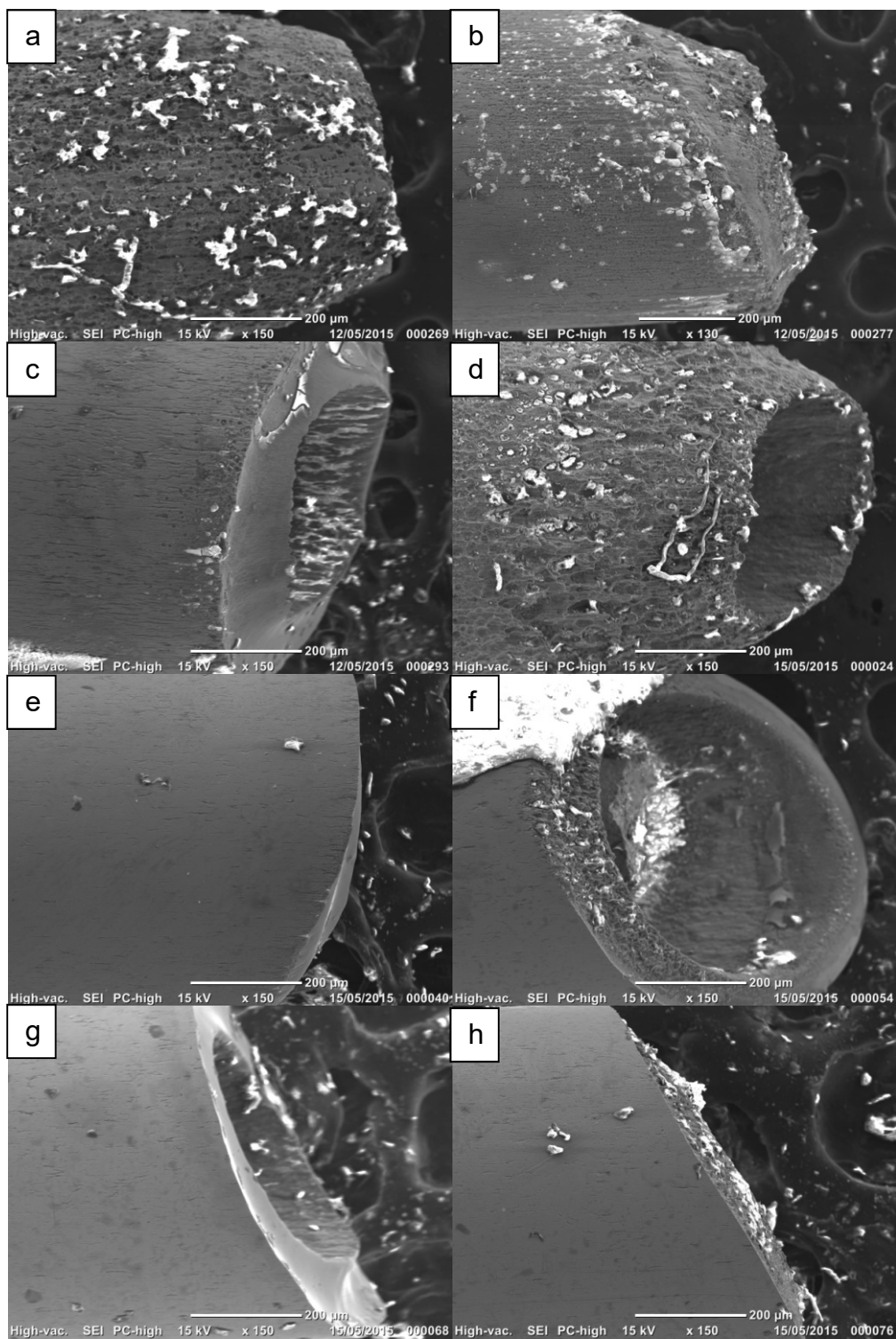
Figure 6-25 SEM image of NiCr Steel Tube after 420 s at a) 4.5 V in 1.1 M NaNO$_3$ b) 8.5 V in 1.1 M NaNO$_3$ c) 4.5 V in 1.7 M NaNO$_3$ d) 8.5 V in 1.7 M NaNO$_3$ e) 4.5 V in 2.3 M NaNO$_3$ f) 8.5 V in 2.3 M NaNO$_3$ g) 4.5 V in 3.0 M NaNO$_3$ h) 8.5 V in 3.0 M NaNO$_3$

154
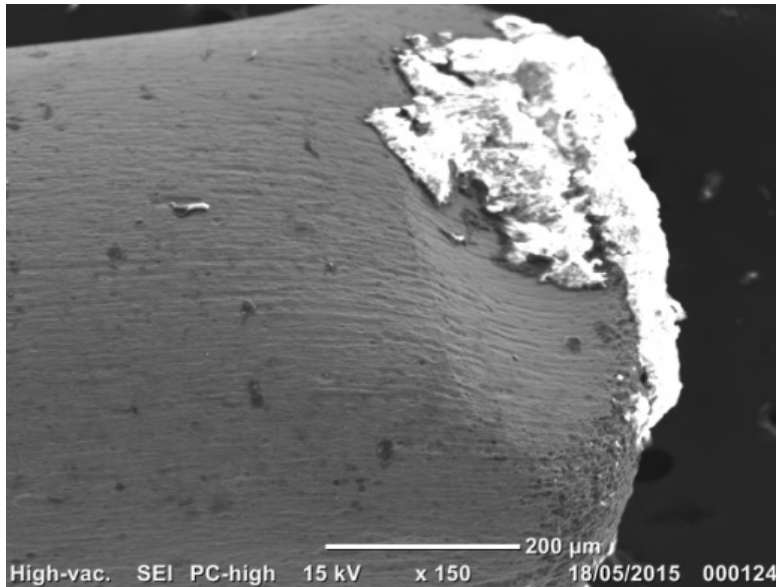
Figure 6-26 SEM image of NiCr Steel Tube after 600 s at 7.25 V in 0.5 M NaClO$_3$
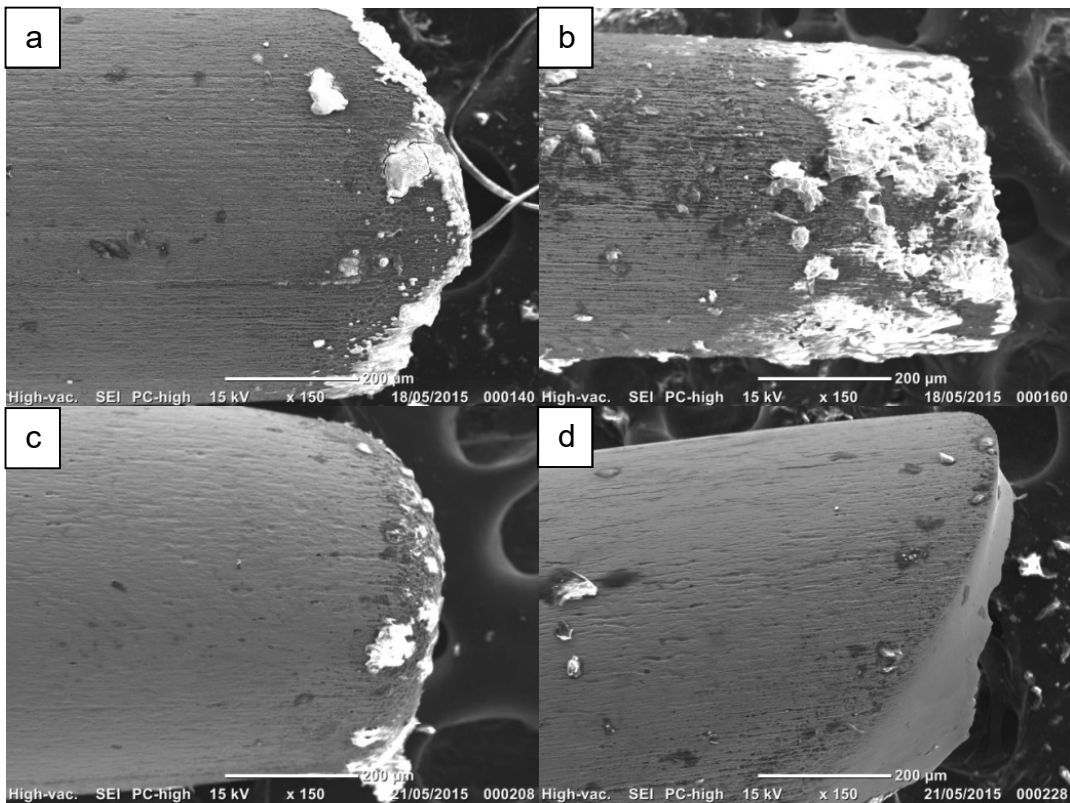
Figure 6-27 SEM image of NiCr Steel Tube after 600 s at a) 7.25 V in 1.1 M NaClO$_3$ b) 7.25 V in 1.7 M NaClO$_3$ c) 7.25 V in 2.3 M NaClO$_3$ d) 7.25 V in 3.0 M NaClO$_3$

155

At 2.3 M there is a similar amount of salt formation at both potentials. This suggests the rate of anodic dissolution has a similar rate to the salt formation at this concentration and at both potentials. Initially the reactions seem to be dominated by oxide formation as the current drops quickly from the onset suggesting the surface is becoming blocked. The current response can be seen in Figure 6-30. However, after approximately 70 s at 7.25 V and 180 s at 5.00 V the current begins to drop less rapidly and forms almost a plateau, this suggests the rates of dissolution and oxide formation are beginning to converge.

At 3.0 M there is a clear distinction between the 5.0 V and 7.25 V chronoamperometry results. At 5.0 V there is a heavy salt/oxide layer which is not present at 7.25 V. The current density at 5.0 V is not high enough to only facilitate anodic dissolution so an oxide layer forms. At 7.25 V in 3.0 M $NaClO_3$ the current begins high and rapidly decreases due to the high dissolution rate. By 300 s the current has dropped to zero after complete dissolution of the steel in the electrolyte, see Figure 6-31. The machined surface also appears very smooth in comparison to any of the surfaces in Figure 6-28.
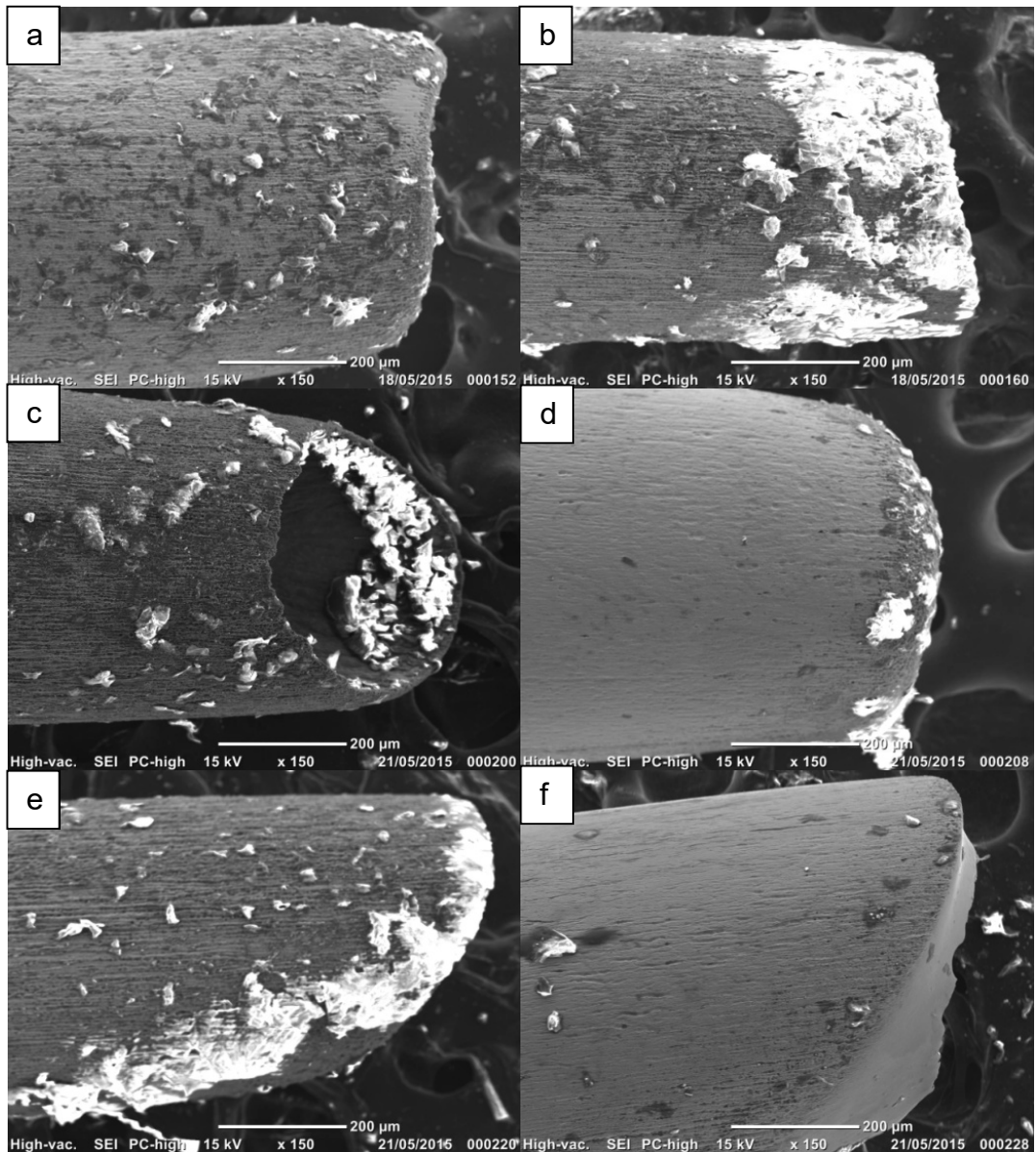
Figure 6-28 SEM image of NiCr Steel Tube after 600 s at a) 5.0 V in 1.7 M NaClO₃ b) 7.25 V in 1.7 M NaClO₃ c) 5.0 V in 2.3 M NaClO₃ d) 7.25 V in 2.3 M NaClO₃ e) 5.0 V in 3.0 M NaClO₃ f) 7.25 V in 3.0 M NaClO₃
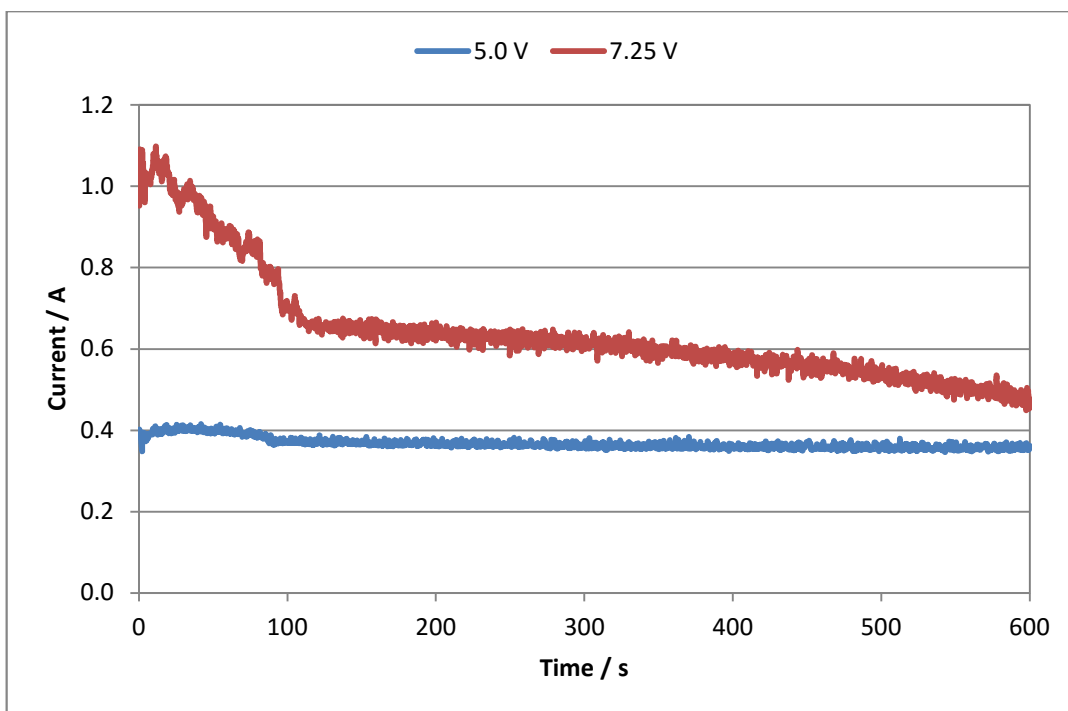
Figure 6-29 Chronoamperometry results of NiCr steel in 1.7 M NaClO$_3$ at 5.0 V and 7.25 V vs Ag/AgCl
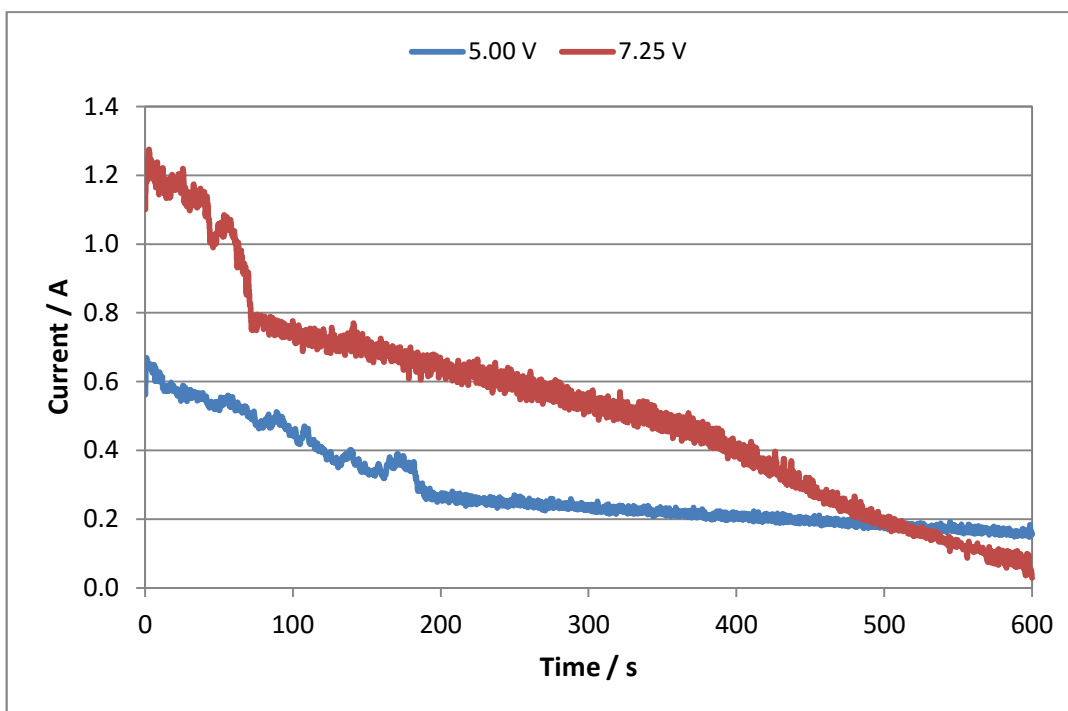
Figure 6-30 Chronoamperometry results of NiCr steel in 2.3 M NaClO$_3$ at 5.0 V and 7.25 V vs Ag/AgCl
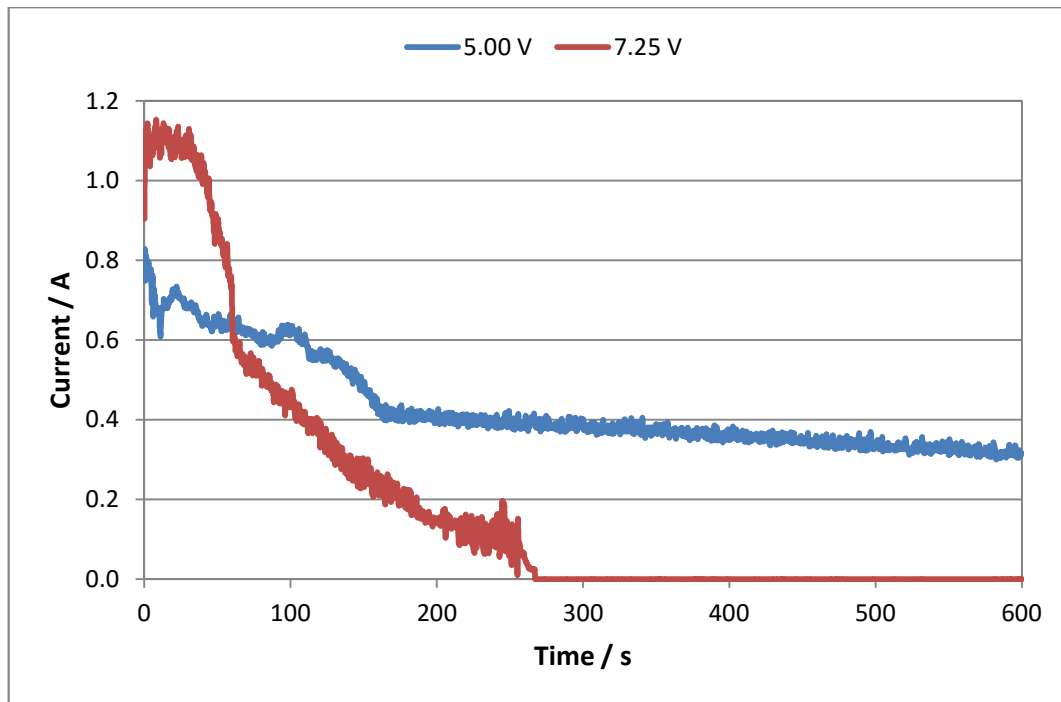
Figure 6-31 Chronoamperometry results of NiCr steel in 3.0 M NaClO$_3$ at 5.0 V and 7.25 V vs Ag/AgCl

If NaClO$_3$ were to be used in the electrochemical machining experiments the best concentration and potential to use would be 3.0 M at 7.25 V. However, as mentioned before high concentrations and voltages lead to poorer machining precision. As a result, it was decided to continue the electrochemical machining experiments with 1.7 M NaNO$_3$ at 4.5 V.

6.3.3 Electrochemical Machining Experiments

Having considered the results from the polarisation experiments and the chronoamperometry experiments, electrochemical machining was carried out with sodium nitrate at 1.7 M which equates to a specific gravity of 1.09. The voltage of 4.5 V, determined from the chronoamperometry experiments, was used as a guide with voltages in excess of this being used for machining. The IEG was varied between 0.05 mm and 0.20 mm, the feed rate was varied between 1 mm/min and 3 mm/min and the frequency of the electrolyte pump was varied between 7.1 Hz and 20 Hz. The maximum voltage used was 16.0 V.

A feed rate in excess of 1 mm/min induced sparking regardless of the IEG, electrolyte pump frequency or voltage applied. As such, all experiments were conducted using a feed rate of 1 mm/min resulting in a machining time of 90 s per needle. Whilst this is not competitive with grinding methods it may eliminate the need to coat the needles with silicon to decrease the surface friction which may in turn reduce the processing costs by removing one of the processing steps.

An IEG of 0.05 mm in the z-direction resulted in the best replication of the machining angle. A larger gap resulted in higher machining rates at the tube tip creating a highly angled tip which did not replicate the angle of the tool. Decreasing the IEG to 0.05 mm improved the machining precision with regards to replicating the angle from the tool in the work piece as can be seen in Figure 6-32.
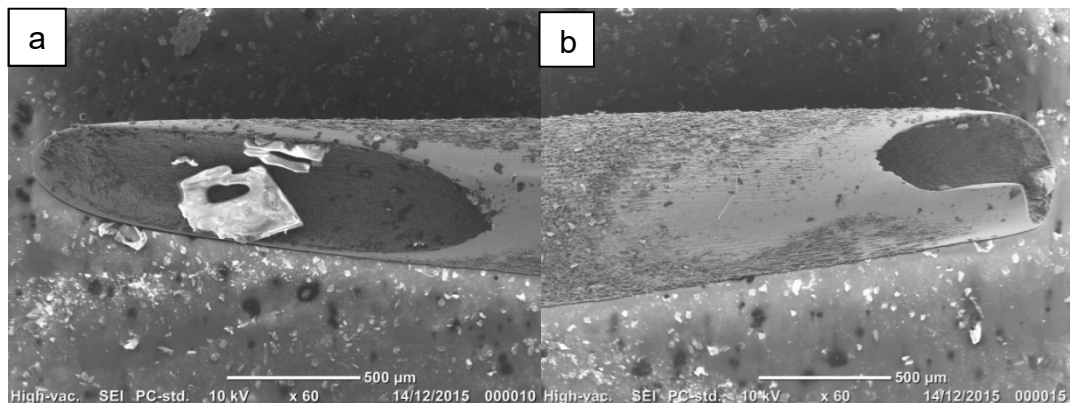
Figure 6-32 SEM image of needle manufacture using 7.0 V, 12.00 Hz flow with a 1 mm/min feed rate at a) 0.05 mm IEG and b) 0.10 mm IEG

Reducing the IEG has been proven to improve machining resolution so it is no surprise that this has been observed here also but the ideal IEG has to be determined in each individual case. Here 0.05 mm was determined as the ideal IEG.

The electrolyte flow in the IEG is very important to ensure the complete removal of reaction products, including heat and gases produced by the reactions at either electrode. A compromise has to be made when selecting

the correct flow rate, a high flow rate ensures the IEG is kept free of reaction products but a flow rate too high will cause turbulent flow which can cause over-machining and under-machining in areas of stagnant electrolyte or eddies creating discrepancies between the desired shape and the outcome. A flow rate too low will not maintain a consistent electrolyte concentration profile in the IEG with a build-up of reaction products being present towards the electrolyte exit. An excessive build-up of reaction products can lead to sparking, damaging either the tool or the work piece.

Figure 6-33 shows the results of changing the frequency of the electrolyte pump; a higher frequency relates to a higher flow rate. As the pump frequency is increased the surface finish appears visually improved and the length of the bevel is increased, highlighting that the machining is constant across the gap.
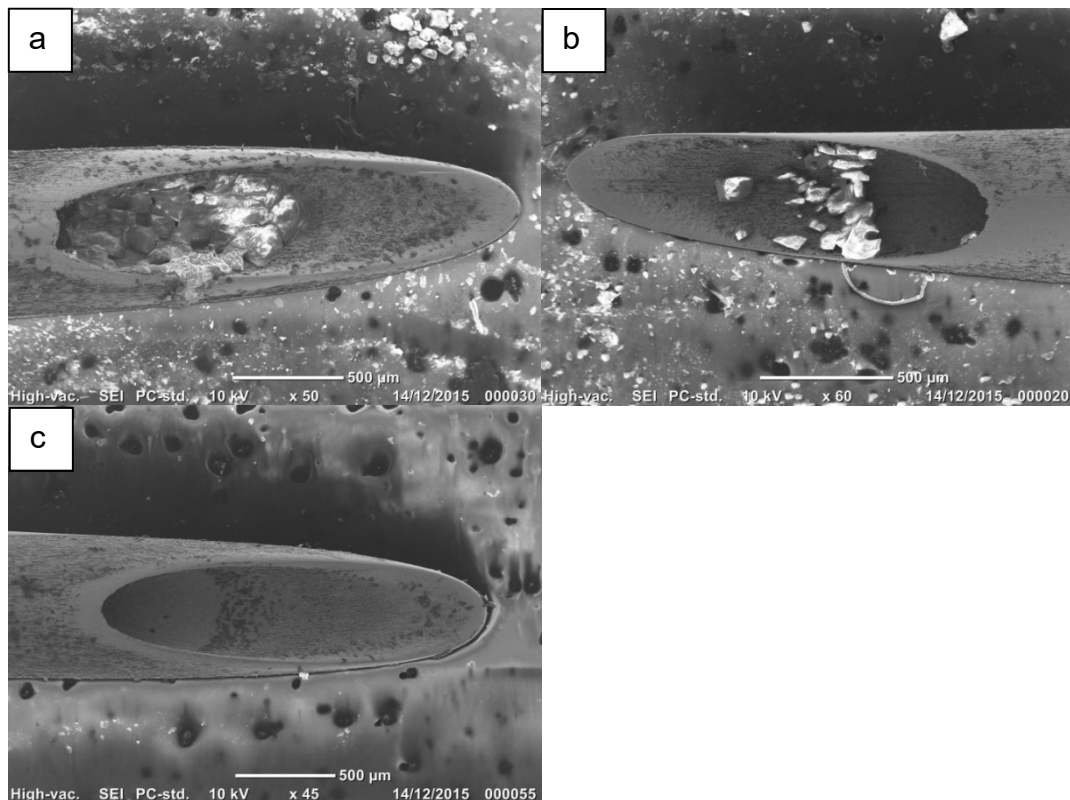
Figure 6-33 SEM images showing needles using 8.0 V with 1 mm/min feed rate and 0.05 mm gap at a) 7.1 Hz b) 12 Hz and c) 15 Hz on the electrolyte pump

The ideal bevel length, as previously mentioned is 2.24 mm for a 600 μm diameter tube; Figure 6-33c shows the closest match to this length with a bevel length of 1.88 mm. Pump frequencies above 15 Hz visibly deflected the work piece, as such rendering higher pump frequencies unsuitable.

The final parameter which was investigated was the voltage. A voltage of 4.5 V did not facilitate machining. This is because the cables used from the power supply to the electrodes were 1.5 cm in diameter and would have drawn a large inductance reducing the voltage that was actually applied between the electrodes. As such voltages as high as 8.5 V were used at a feed rate of 1mm/min. In past research, higher voltages have been used to obtain a mirror like finish but lower voltages have been utilised to maintain machining resolution. The surface finish is important to reduce the friction of the surface allowing less force to be used to insert the needle into the skin.

Figure 6-34 shows the SEM images of needles manufactured using differing voltages.

The bevel length increases as the potential is increased from 7.0 V to 8.5 V leading more towards the desired length, this is likely because the machining rate is well matched to the feed rate at the higher voltages. However, there is still some stray machining which is most obvious at 8.5 V with deep pits on the tube shaft.

The best combination of parameters tested in this study was using a feed rate of 1 mm/min, 15 Hz frequency on the pump, a 0.05 mm gap and a voltage of 8.0 V, shown in Figure 6-34c.
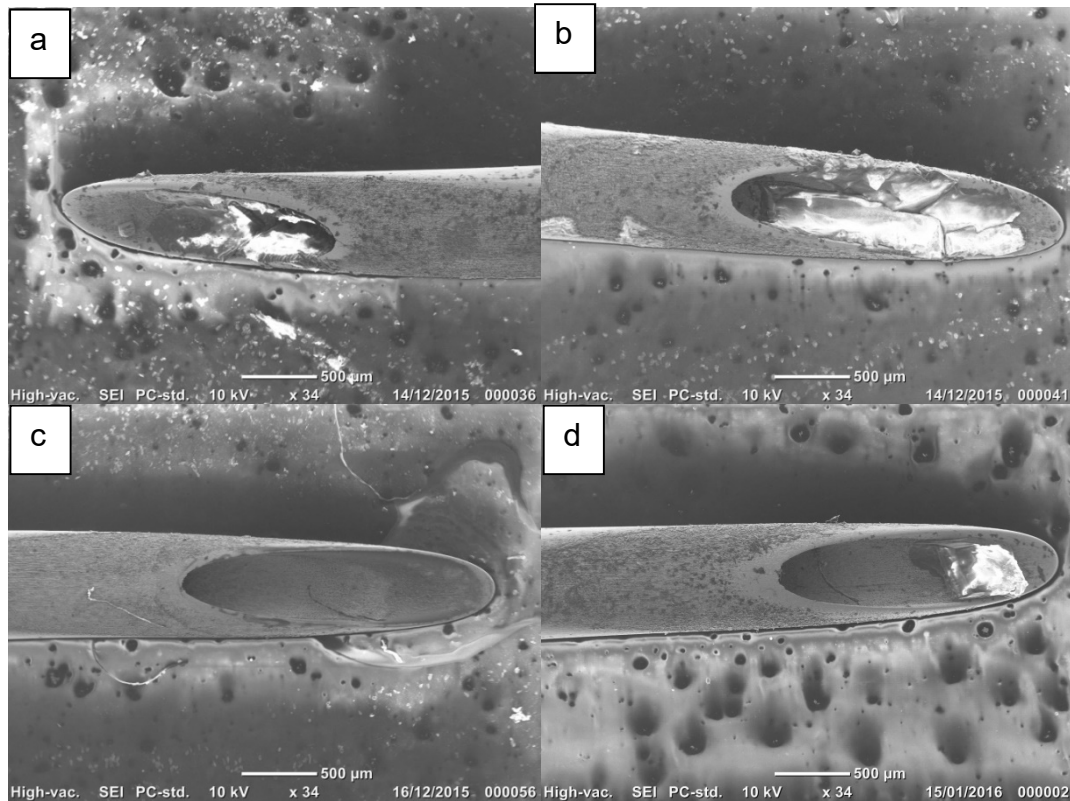
Figure 6-34 SEM images showing needles using 1 mm/min feed rate, 0.05 mm gap and 15 Hz on the electrolyte pump at a) 7.0 V b) 7.5 V c) 8.0 V and d) 8.5 V

Pulsating the voltage would minimise the stray machining by increasing the machining resolution by one of two mechanisms depending on the pulse length; either the distance into the solution the diffusion layer reaches will be reduced preventing the stray machining or the time constant for the pulse length and IEG width will not facilitate complete double layer charging of the work piece at greater distances from the tool, restricting the machining to areas of the work piece in close proximity to the tool. Electrochemical machining can only occur when the electrochemical double layer is fully charged. Adding pulses to the voltage profile increases the total machining time as the length of time where active dissolution is occurring is decreased. This is not favourable when trying to deliver a product in a competitive time frame to the methods already available.

Another solution, and perhaps a more suitable alternative, to prevent stray machining would be to mask areas of the work piece to prevent anodic dissolution. This could be done by creating a shroud for the work piece to slot into which left only the areas of the work piece to be machined exposed. Figure 6-35 shows the proposed design for such a shroud.
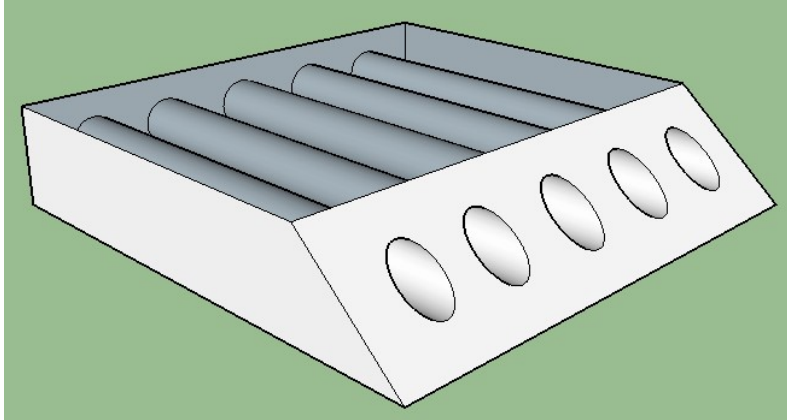
Figure 6-35 Model of proposed shroud to eliminate stray machining on needle shaft. The top surface has been removed to show the proposed internal design

6.4   Conclusion

Having conducted preliminary polarisation and chronoamperometry experiments, it was determined that sodium nitrate at a concentration of 1.7 M was the optimum electrolyte for needle production at a voltage of 4.5 V after having shown that this combination provides the best surface finish with little stray machining.
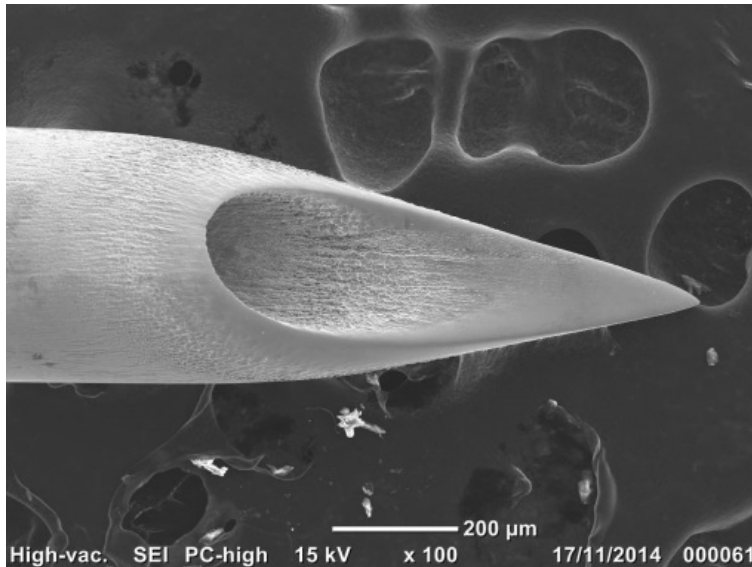
Figure 6-36 3D needle shape made with the in-house ECM machine at Brunel, applied potential of 8 V 100 % duty cycle using adaptive feed rate. Initial IEG of 5 μm.

Figure 6-36 shows a 3D shape which has no flat edges, this demonstrates the ECM process is not limited to producing flat cuts as grinding is. This 3D shape may provide additional benefits, including reducing the penetration force necessary to pierce the skin making an injection less painful for the patient.

Electrochemical machining experiments were conducted at pECM Systems Ltd. It was observed that the cables on the ECM machine had high inductance so a higher voltage had to be applied to achieve anodic dissolution. The ideal parameters for replicating the tool angle on the work piece was found to be a voltage of 8.0 V with a feed rate of 1mm/min after establishing a gap of 0.05 mm and a frequency of 15 Hz on the pump for the electrolyte delivery.

There was still evidence of stray machining, however, which may be resolved by the application of pulses to the voltage or using a shroud to protect areas of the work piece where machining is undesirable.

6.5   Further Work

Given more time, a more suitable tool would be designed which would be capable of producing the final needle tip shape in one process. A shroud may also need to be developed to prevent stray machining, along with the application of voltage pulses to further reduce stray machining.

7   Conclusions and Further Work

7.1   Conclusions

The following conclusions can be drawn from the research conducted in this body of work:

7.1.1 Conclusions regarding the literature Review

An extensive literature review was conducted which provided insights into the electrochemical machining process.

It highlighted that little work had been conducted on workpieces outside of stainless steels and brass alloys. It also highlighted that anodically dissolving titanium metal, an important engineering material, required high voltages to facilitate machining.

7.1.2 Conclusions regarding Anodic Dissolution of Superconductors

Ceramic cuprate superconductors are an important group of materials due to the high temperatures at which the material becomes superconductive. These materials are very brittle though and conventional machining techniques cause internal cracks within the material, reducing or destroying the superconductive properties of the material. An alternative method was needed to be able to process the materials without affecting the superconductive properties.

It was demonstrated that electrochemical machining is a suitable method for machining ceramic cuprate superconductors, namely gadolinium barium copper oxide with a silver inclusion (GdBCO-Ag). This, however, requires a non-aqueous electrolyte due to the water-sensitivity of the material.

7.1.3 Conclusions regarding Anodic Dissolution of Semiconductors

Semiconductors are used widely across the electronics sector. After being approached by QMC Instruments Ltd, work began on the anodic dissolution

of indium antimonide (InSb) with the final aim of achieving a desired shape for a bolometer.

Whilst the final shape was not achieved, this work demonstrated the electrochemical machining is a suitable method to machine InSb at potentials below 10 V using an aqueous electrolyte. A surface mirror finish was achieved.

7.1.4 Conclusions regarding Anodic Dissolution of Titanium with the Addition of Ultrasonic Vibrations

Titanium is an important manufacturing material due to its favourable properties. It is strong, yet half the weight of steel and it is chemically resistant, making it an ideal material choice for tough environments e.g. sea water or within the human body.

Titanium is difficult to machine conventionally due to its hardness and its poor thermal conductivity. Electrochemical machining is not dependent on a material's hardness so is an attractive alternative manufacturing method. However, high potentials are required to overcome the passive oxide layer which protects titanium making it such an attractive material choice. This work illustrated that the addition of ultrasonic vibrations to the electrolyte facilitated the anodic dissolution of titanium in sodium chloride electrolytes at voltages below 10 V.

7.1.5 Conclusions regarding the Electrochemical Production of Hypodermic Needle Tips

Hypodermic needles are currently manufactured using mechanical grinding. This leaves a poor surface finish on the needle tip so they are subsequently coated in silicon to reduce the friction and therefore the force needed to pierce the skin. A hypodermic needle is created by three separate cuts.

In theory, ECM should provide a production method capable of achieving the desired shape and surface finish with only one step. This work showed that

168

electrochemical machining is capable of producing the initial cut, as is currently made via mechanical grinding, with high precision and with a good quality surface finish.

7.1.6 Contributions to Knowledge

The research contained within this thesis contributes the following knowledge:

- The demonstration of the suitability of ECM for the anodic dissolution of GdBCO-Ag.
- The demonstration of the suitability of ECM for the anodic dissolution of InSb.
- The addition of ultrasonic vibrations to the electrolyte which reduces the required machining potential significantly.
- The first demonstration of the suitability of ECM for the electrochemical production of hypodermic needles.

7.2 Future Work

The author proposes the following future work to be undertaken:

- The application of pulsed potential in order to improve machining resolution of superconductor dissolution.
- Design of a tool suitable for forming shells of superconductive material which can withstand the pressures of the electrolyte flow without flexing.
- Improving the machining resolution for semiconductor dissolution along with a pathway design in order to create the desired shape of the bolometer.
- Ultrasonic vibrations of the electrolyte need to be applied in a real ECM situation when machining titanium.
- Modelling the effects of the ultrasonic vibrations on the machining mechanism of titanium.

- A tool needs to be designed which will facilitate the production of hypodermic needles in one step.

- A shroud also needs to be made to prevent stray machining on the shaft of the hypodermic needle during machining.

7.3 Publications

- **Chapter 6 – Micro-electrochemical Machining**
  Atanas Ivanov, Rebecca Leese, Alexandre Spieser
  Micromanufacturing Engineering and Technology (Second Edition), 2015, 121-145
  DOI:10.1016/B978-0-323-31149-6.00006-2

- **The Potential to Machine Superconductors with Electrochemical Machining**
  Rebecca J. Leese, *Atanas Ivanov*, *Hari Babu-Nadendla*
  Journal of Multiscale Modelling, 2016
  DOI: 10.1142/S1756973716400011

- **Electrochemical micromachining: An introduction**
  Rebecca J. Leese, Atanas Ivanov
  Advances in Mechanical Engineering, 2016, Vol. 8(1) 1–13
  DOI: 10.1177/1687814015626860

- **Comparison of polarisation curves and chronoamperometry experiments of titanium with and without ultrasonic vibrations of the electrolyte**
  Rebecca J Leese, Atanas Ivanov
  Advances in Mechanical Engineering, 2016, Vol. 8(3)
  DOI: 10.1177/1687814016637984

- **Electrochemical Machining – Review of Factors Affecting the Process Applicability in Micro-Manufacturing**
  Rebecca J Leese, Atanas Ivanov
  Proceedings of the Institution of Mechanical Engineers, Part B: Journal of Engineering Manufacture, 2016, Vol(

References

Acharya, B.G., Jain, V.K. & Batra, J.L., 1986. Multi-objective optimization of the ecm process. *Precision Engineering*, 8(2), pp.88–96.

Anon, The History of Superconductors. Available at: www.superconductors.org/History.htm [Accessed January 19, 2015].

Anonymous, 2015. A New Approach to Titanium Machining. *Radical Departures*. Available at: http://www.radical-departures.net/articles/a-new-approach-to-titanium-machining/ [Accessed May 13, 2015].

Anonymous, *Conventional Machining VS Non-Conventional Machining*, Available at: http://ncm.ic.polyu.edu.hk/online/document/notes/Conventional VS Non conventional.pdf.

Anonymous, 2014a. Global Hypodermic Needles Market 2014-2018. *Research and Markets - the world's largest market research store*. Available at: http://www.researchandmarkets.com/research/nk3vws/global_hypoderm ic [Accessed July 31, 2015].

Anonymous, 2014b. The history of the hyodermic needle. Available at: http://www.medibank.com.au/bemagazine/post/wellbeing/the-history-of-the-hypodermic-needle/ [Accessed July 31, 2015].

Arteche, I.R., Superconductors: obtaining higher critical currents (Jc) and critical temperatures (Tc). Could the "nano-world" play a role?

Asten, T. V. & Nordberg, P., 2013. Milling and Drilling Tough Materials. *Modern Manufacturing India*, (July), pp.52–54.

Ayyappan, S. & Sivakumar, K., 2014a. Experimental investigation on the performance improvement of electrochemical machining process using

oxygen-enriched electrolyte. *The International Journal of Advanced Manufacturing Technology*, 75(1-4), pp.479–487. Available at: http://link.springer.com/10.1007/s00170-014-6096-9.

Ayyappan, S. & Sivakumar, K., 2014b. Investigation of electrochemical machining characteristics of 20MnCr5 alloy steel using potassium dichromate mixed aqueous NaCl electrolyte and optimization of process parameters. *Proceedings of the Institution of Mechanical Engineers, Part B: Journal of Engineering Manufacture*, pp.1–13. Available at: http://pib.sagepub.com/lookup/doi/10.1177/0954405414542136.

B.Braun, 2002. Sterican. , pp.1–4.

Bannard, J., 1977. Electrochemical machining. *Journal of Applied Electrochemistry*, 7(1), pp.1–29.

Bannard, J., 1976. On the electrochemical machining of some titanium alloys in bromide electrolytes. *Journal of Applied Electrochemistry*, 6(6), pp.477–483.

Bedinger, G.M., 2015. Titanium and titanium dioxide 1. *US Geological Survey*, Mineral Co, pp.170–171.

Bednorz, J.G. & Müller, K. a, 1986. Possible High-Tc Superconductivity in the Ba-La-Cu-O System. *Zeitschrift für Physik B Condensed Matter*, 64, pp.189–193.

Benes, J., 2007. Cool Tips for Cutting Titanium. *American Machinist*, pp.1–3. Available at: http://americanmachinist.com/features/cool-tips-cutting-titanium?page=1 [Accessed November 12, 2015].

Bhattacharyya, B., Mitra, S. & Boro, A.K., 2002. Electrochemical machining: New possibilities for micromachining. *Robotics and Computer-Integrated Manufacturing*, 18(3-4), pp.283–289.

Bhattacharyya, B. & Munda, J., 2003. Experimental investigation on the

influence of electrochemical machining parameters on machining rate and accuracy in micromachining domain. *International Journal of Machine Tools and Manufacture*, 43(13), pp.1301–1310.

Bhattacharyya, B., Munda, J. & Malapati, M., 2004. Advancement in electrochemical micro-machining. *International Journal of Machine Tools and Manufacture*, 44(15), pp.1577–1589.

Bilgi, D.S. et al., 2004. Electrochemical deep hole drilling in super alloy for turbine application. *Journal of Materials Processing Technology*, 149(1-3), pp.445–452.

Bilgi, D.S. et al., 2007. Hole quality and interelectrode gap dynamics during pulse current electrochemical deep hole drilling. *International Journal of Advanced Manufacturing Technology*, 34(1-2), pp.79–95.

Bilgi, D.S. et al., 2008. Predicting radial overcut in deep holes drilled by shaped tube electrochemical machining. *International Journal of Advanced Manufacturing Technology*, 39(1-2), pp.47–54.

Bobroff, J. & Bouquet, F., 2010. File:Stable Levitation of a magnet on a superconductor.jpg. Available at: https://commons.wikimedia.org/wiki/File:Stable_Levitation_of_a_magnet _on_a_superconductor.jpg [Accessed September 25, 2015].

Bristol, U. of, BSC Superconductivity Theory. Available at: http://www.chm.bris.ac.uk/webprojects2000/igrant/bcstheory.html [Accessed January 19, 2015].

Budapest University of Technology and Economics - Department of Inorganic and Analytical Chemistry, The Group Va Elements (N, P, As, Sb, Bi) and Their Principal Anions and Cations. , pp.36–77. Available at: http://www.inc.bme.hu/en/subjects/inchem/sillabus/36-77.pdf.

Cagnon, L. et al., 2003. Electrochemical Micromachining of Stainless Steel

by Ultrashort Voltage Pulses. *Zeitschrift für Physikalische Chemie*, 217(4), pp.299–313.

CERN, The Higgs Boson. *Accelerating Science*. Available at: http://home.web.cern.ch/topics/higgs-boson [Accessed January 20, 2015].

Cheng, K. & Huo, D., 2013. *Micro Cutting: Fundamentals and Applications* John Wiley & Sons Ltd, ed., Chichester.

Choi, S.H. et al., 2013. Analysis of the electrochemical behaviors of WC-Co alloy for micro ECM. *Journal of Materials Processing Technology*, 213(4), pp.621–630.

Choragudi, A. et al., 2010. Investigation of the Machining of Titanium Components for Lightweight Vehicles. In *SAE technical paper*.

Clark, J., Atomic and Ionic Radius. *UC Davis ChemWiki*. Available at: http://chemwiki.ucdavis.edu/Physical_Chemistry/Physical_Properties_of _Matter/Atomic_and_Molecular_Properties/Atomic_and_Ionic_Radius [Accessed October 23, 2015].

Clifton, D. et al., 2003. Characterization and representation of non-ideal effects in electrochemical machining. *Proceedings of the Institute of Mechanical Engineers, Journal of Engineering Manufacture*, 217(Article), pp.373–385.

Cook, N.H., Loutrel, S.P. & Meslink, M.C., 1967. *Increasing Electrochemical Machining Rates*. Cambridge: Massachusetts Institute of Technology.

Van Damme, S. et al., 2006. Numerical model for predicting the efficiency behaviour during pulsed electrochemical machining of steel in NaNO3. *Journal of Applied Electrochemistry*, 36(1), pp.1–10.

Das, A.K. & Saha, P., 2014. Fabrication of cylindrical micro tools by micro electrochemical form turning operation. *Proceedings of the Institution of*

Mechanical Engineers, Part B: Journal of Engineering Manufacture, 228(1), pp.74–81.

Datta, M., 1993. Anodic dissolution of metals at high rates. *IBM Journal of Research and Development*, 37(2), pp.207–226.

Datta, M. & Landolt, D., 1983. Electrochemical saw using pulsating voltage. *Journal of Applied Electrochemistry*, 13(6), pp.795–802.

Datta, M. & Landolt, D., 2000. Fundamental aspects and applications of electrochemical microfabrication. *Electrochimica Acta*, 45(15-16), pp.2535–2558.

Diko, P., Pelerin, N. & Odier, P., 1995. Microstructure analysis of melt-textured YBa2Cu3O7-x ceramics by polarized light microscopy. *Physica C*, 247, pp.169–182.

Eck, J., Uses for Superconductors. *Superconductors*. Available at: www.superconductors.org/uses.htm [Accessed January 20, 2015].

Engineer on a Disk, Electrochemical Machining (ECM). Available at: http://engineeronadisk.com/V2/notes_manufacturing/engineeronadisk-142.html [Accessed January 24, 2014].

Engineering and Technology Wiki, 2015. Semiconductors. Available at: http://ethw.org/Semiconductors [Accessed January 20, 2016].

Fan, Z.W., Hourng, L.W. & Lin, M.Y., 2012. Experimental investigation on the influence of electrochemical micro-drilling by short pulsed voltage. *International Journal of Advanced Manufacturing Technology*, 61(9-12), pp.957–966.

Fang, X. et al., 2014. Improvement of hole exit accuracy in electrochemical drilling by applying a potential difference between an auxiliary electrode and the anode. *Journal of Materials Processing Technology*, 214(3), pp.556–564.

Fushimi, K. & Habazaki, H., 2008. Anodic dissolution of titanium in NaCl-containing ethylene glycol. *Electrochimica Acta*, 53(8), pp.3371–3376.

Fushimi, K., Kondo, H. & Konno, H., 2009. Anodic dissolution of titanium in chloride-containing ethylene glycol solution. *Electrochimica Acta*, 55(1), pp.258–264.

Ghoshal, B. & Bhattacharyya, B., 2013. Micro electrochemical sinking and milling method for generation of micro features. *Proceedings of the Institution of Mechanical Engineers, Part B: Journal of Engineering Manufacture*, 227(11), pp.1651–1663.

Gombos, M. et al., 2012. Reduced twinning efficiency and tri-dimensional crack structure in melt-textured NdBa2Cu3O7−δ bulk samples fragmentation process. *Superconductor Science and Technology*, 25(12), p.125017.

Graser, S. et al., 2010. How grain boundaries limit supercurrents in high-temperature superconductors. *Nature Physics*, 6(8), pp.609–614.

Günther, W. et al., 1996. Topotactic reactions of superconducting YBa2Cu3O7 thin films with water vapour. *Solid State Ionics*, 84(1-2), pp.23–32.

Habisreuther, T. et al., 2001. Requirements on Melt-textured Y-Ba-Cu-0 for the Use in Magnetic Bearings or Electric Motors. *IEEE Transactions on Applied Superconductivity*, 11(1), pp.3501–3504.

Haj33, 2009. File:Ybco.jpg. Available at: https://commons.wikimedia.org/wiki/File:Ybco.jpg.

Hilgenkamp, H. & Mannhart, J., 2002. Grain boundaries in high-Tc superconductors. *Reviews of Modern Physics*, 74(2l), pp.485–549.

Huaiqian, B., Jiawen, X. & Ying, L., 2008. Aviation-oriented Micromachining Technology—Micro-ECM in Pure Water. *Chinese Journal of*

Aeronautics, 21(5), pp.455–461.

Hurley, D.T., 1997. High speedd diamond-based machining of silicon semiconductor die in wafer and packaged form for backside emission microscope detection. , pp.1–6.

Hyperphysics, Superconductivity. Available at: http://hyperphysics.phy-astr.gsu.edu/hbase/solids/scond.html. [Accessed January 19, 2015].

Industrial Talks, 2012. Why Titanium Is Used in the Aircraft Industry. *Industrial Talks*. Available at: https://industrialtalks.wordpress.com/2012/12/12/why-titanium-is-used-in-the-aircraft-industry/ [Accessed May 18, 2015].

Inman, M. et al., 2011. Electrochemical System and Method for Machining Strongly Passivating Metals. , 1, pp.1–18.

Isfort, D. et al., 2003. Cracking and oxygenation of YBaCuO bulk superconductors: Application to c -axis elements for current limitation. *Physica C*, 390(4), pp.341–355.

Jain, N.K. & Jain, V.K., 2007. Optimization of Electro-Chemical Machining Process Parameters Using Genetic Algorithms. *Machining Science and Technology: An International Journal*, 11(2), pp.235–258.

Jain, N.K., Jain, V.K. & Jha, S., 2007. Parametric optimization of advanced fine-finishing processes. *International Journal of Advanced Manufacturing Technology*, 34(11-12), pp.1191–1213.

Jain, V.K. et al., 2012. Fabrication of micro-features and micro-tools using electrochemical micromachining. *International Journal of Advanced Manufacturing Technology*, 61(9-12), pp.1175–1183.

Jain, V.K. & Gehlot, D., 2015. Anode Shape Prediction in Through-Mask-Ecmm using Fem. *Machining Science and Technology: An International Journal*, 19(2), pp.286–312.

Jain, V.K. & Pandey, P.C., 1979. Design and analysis of ECM toolings. *Precision Engineering*, 1(4), pp.199–206.

Jain, V.K. & Pandey, P.C., 1982. Investigations into the use of bits as a cathode in ECM. *International Journal of Machine Tools and Manufacture*, 22(4), pp.341–352.

Jain, V.K. & Pandey, P.C., 1980. Tooling Design for Ecm. *Precision Engineering*, 2(4), pp.195–206.

Jain, V.K. & Rajurkar, K.P., 1991. An integrated approach for tool design in ECM. *Precision Engineering*, 13(2), pp.111–124.

Jo, C.H., Kim, B.H. & Chu, C.N., 2009. Micro electrochemical machining for complex internal micro features. *CIRP Annals - Manufacturing Technology*, 58(1), pp.181–184.

Kock, M., Kirchner, V. & Schuster, R., 2003. Electrochemical micromachining with ultrashort voltage pulses-a versatile method with lithographical precision. *Electrochimica Acta*, 48(20-22), pp.3213–3219.

Konstantopoulou, K. et al., 2014. Mechanical characterization of GdBCO/Ag and YBCO single grains fabricated by top-seeded melt growth at 77 and 300 K. *Supercond. Sci. Technol*, 27, pp.1–11.

Kósa, J. & Vajda, I., 2007. Environmentally friendly machining of ceramic based YBCO bulk superconductor. *Journal of Materials Processing Technology*, 181(1-3 SPEC. ISS.), pp.48–51.

Kozak, J., Budzynski, A.F. & Domanowski, P., 1998. Computer simulation electrochemical shaping (ECM-CNC) using a universal tool electrode. *Journal of Materials Processing Technology*, 76(1-3), pp.161–164.

Kozak, J., Gulbinowicz, D. & Gulbinowicz, Z., 2008. The Mathematical Modeling and Computer Simulation of Pulse Electrochemical Micromachining. *IAENG TRANSACTIONS ON ENGINEERING*

TECHNOLOGIES VOLUME 2: Special Edition of the World Congress on Engineering and Computer Science, (November), pp.174–185.

Kozak, J., Rajurkar, K.P. & Makkar, Y., 2004. Study of Pulse Electrochemical Micromachining. *Journal of Manufacturing Processes*, 6(1), pp.7–14.

Labib, A.W. et al., 2011. Towards next generation electrochemical machining controllers: A fuzzy logic control approach to ECM. *Expert Systems with Applications*, 38(6), pp.7486–7493.

Landolt, D., Chauvy, P.F. & Zinger, O., 2003. Electrochemical micromachining, polishing and surface structuring of metals: Fundamental aspects and new developments. *Electrochimica Acta*, 48(20-22), pp.3185–3201.

Lee, E.S. et al., 2010. Investigation of short pulse electrochemical machining for groove process on Ni-Ti shape memory alloy. *International Journal of Precision Engineering and Manufacturing*, 11(1), pp.113–118.

Leese, R.J. & Ivanov, A., 2016a. Comparison of polarisation curves and chronoamperometry experiments of titanium with and without ultrasonic vibrations of the electrolyte. *Advances in Mechanical Engineering*, 8(3).

Leese, R.J. & Ivanov, A., 2016b. Electrochemical machining - review of factors affecting the process applicability in micro-manufacturing. *Proceedings of the Institution of Mechanical Engineers, Part B: Journal of Engineering Manufacture*.

Leese, R.J. & Ivanov, A., 2016c. Electrochemical micromachining: An introduction. *Advances in Mechanical Engineering*, 8(1), pp.1–13. Available at: http://ade.sagepub.com/lookup/doi/10.1177/1687814015626860.

Leese, R.J., Ivanov, A. & Babu-Nadendla, H., 2016. The Potential to Machine Superconductors with Electrochemical Machining. *J. Multiscale*

Modelling, pp.1–14.

Lim, Y.M. et al., 2003. Fabrication of cylindrical micropins with various diameters using DC current density control. *Journal of Materials Processing Technology*, 141(2), pp.251–255.

Lim, Y.M. & Kim, S.H., 2001. An electrochemical fabrication method for extremely thin cylindrical micropin. *International Journal of Machine Tools and Manufacture*, 41(15), pp.2287–2296.

Lohrengel, M.M. et al., 2003. Microscopic investigations of electrochemical machining of Fe in NaNO3. *Electrochimica Acta*, 48(20-22), pp.3203–3211.

Machado, A.R. & Wallbank, J., 1990. Machining of Titanium and Its Alloys - a Review. *Proceedings of the Institution of Mechanical Engineers, Part B: Journal of Engineering Manufacture*, 204(6), pp.53–60.

Mack, C.A., Semiconductor Lithography (Photolithography) - The Basic Process. *Lithography*. Available at: http://www.lithoguru.com/scientist/lithobasics.html [Accessed January 21, 2016].

Manjaiah, M., Narendranath, S. & Basavarajappa, S., 2014. A Review on Machining of Titanium Based Alloys. *Reviews on Advanced Materials Science*, 36, pp.89–111.

Manjaiah, M., Narendranath, S. & Basavarajappa, S., 2014. Review on non-conventional machining of shape memory alloys. *Transactions of Nonferrous Metals Society of China (English Edition)*, 24(1), pp.12–21.

Marinov, V., 2008. Non-Traditional Processes. In *Manufacturing Processes for Metal Products*. Kendall Hunt Publishing Company, pp. 141–148.

Mathew, R. & Sundaram, M.M., 2012. Modeling and fabrication of micro tools by pulsed electrochemical machining. *Journal of Materials Processing*

Technology, 212(7), pp.1567–1572.

McGeough, J.A., 1988. Electrochemical Machining. In *Advanced Methods of Machining*. London: Chapman and Hall, pp. 55–88.

Meijer, J. & Veringa, J.C.M., 1984. Characteristic numbers to describe the detail transfer quality of electro-chemical machining. *Precision Engineering*, 6(2), pp.79–82.

Merlin, P.W., 2009. Design and development of the Blackbird: Challenges and lessons learned. In *47th AIAA Aerospace Sciences Meeting Including The New Horizons Forum and Aerospace Expostition*. pp. 1–38.

Milacron Marketing Co., 2007. *Machining Titanium*, Cincinnati.

Muir, R.N. et al., 2007. Real-time parameterization of electrochemical machining by ultrasound measurement of the interelectrode gap. *Proceedings of the Institution of Mechanical Engineers, Part B: Journal of Engineering Manufacture*, 221(4), pp.551–558.

Nelson, C.W., 1953. *Metals as anodes in Non-aqueous media*,

Nouari, M. & Makich, H., 2014. On the Physics of Machining Titanium Alloys: Interactions between Cutting Parameters, Microstructure and Tool Wear. *Metals*, 4(3), pp.335–358.

Nourbakhsh, F., 2012. *Machining Stability of Wire EDM of Titanium*. University of Nebraska.

Panda, H., 2013. *The complete book on electroplating and allied chemicals*, Asia Pacific Business Press.

Parmeter, J.E., Schwalke, U. & Weinberg, W.H., 1988. Formamide with the Ru(001) Surface. *Journal of the American Chemical Society*, 110, pp.53–62.

Phantom Drills, 2016. TiAlN Coated Drill Bits. Available at: http://www.phantomdrills.co.uk/shop/product/tialn_coated_drill_bits [Accessed January 18, 2016].

Pletcher, D., 2009. *A First Course in Electrode Processes* 2nd ed., The Royal Society of Chemistry.

Powell, W.J.A., 1967. Spark-machining of photoconductive indium antimonide. *Journal of Scientific Instruments*, 44, pp.973–975.

Pramanik, A., 2014. Problems and solutions in machining of titanium alloys. *International Journal of Advanced Manufacturing Technology*, 70(5-8), pp.919–928.

Qu, N.S. et al., 2013. Enhancement of surface roughness in electrochemical machining of Ti6Al4V by pulsating electrolyte. *International Journal of Advanced Manufacturing Technology*, 69(9-12), pp.2703–2709.

Rajurkar, K.P. et al., 2006. Micro and nano machining by electro-physical and chemical processes. *CIRP Annals - Manufacturing Technology*, 55(2), pp.643–666.

Rajurkar, K.P. et al., 1995. Modelling and Monitoring Interelectrode Gap in Pulse Electrochemical Machining. *Annals of the CIRP*, 44(I), pp.177–180.

Rajurkar, K.P. et al., 1993. Study of Pulse Electrochemical Machining Characteristics. *CIRP Annals - Manufacturing Technology*, 42(1), pp.231–234.

Rajurkar, K.P., Zhu, D. & Wei, B., 1998. Minimization of Machining Allowance in Electrochemical Machining. *Annals of the CIRP*, 47(1), pp.165–168.

Rao, R. V, Pawar, P.J. & Shankar, R., 2008. Multi-objective optimization of electrochemical machining process parameters using a particle swarm

optimization algorithm. *Proceedings of the Institution of Mechanical Engineers, Part B: Journal of Engineering Manufacture*, 222(8), pp.949–958.

Rathod, V., Doloi, B. & Bhattacharyya, B., 2014. Experimental investigations into machining accuracy and surface roughness of microgrooves fabricated by electrochemical micromachining. *Proceedings of the Institution of Mechanical Engineers, Part B: Journal of Engineering Manufacture*, pp.1–22.

READE, Magnesium Diboride / Magnesium Boride Powder (MgB2) from READE. Available at: http://www.reade.com/products/7-boride-compounds-powder/297-magnesium-diboride-powder-mgb2-magnesium-boride-powder-magnesium-boride-pieces-magnesium-boride-single-crystal-magnesium-boride-targets-magnesium-diboride-pieces-magnesium-diboride-single-crystal [Accessed January 27, 2015].

Richardson, T.J. & De Jonghe, L.C., 1990. Acoustic emission study of microcracking in 123-type ceramic superconductors. *Journal of Materials Research*, 5(10), pp.2066–2074.

Saravanan, D., Arularasu, M. & Ganesan, K., 2012. A study on electrochemical micromachining of super duplex stainless steel for biomedical filters. *ARPN Journal of Engineering and Applied Sciences*, 7(5), pp.517–523.

Sato, A., 1962. Method of machining semiconductors. , pp.1–3.

Savage-Smith, E., 2000. The practice of surgery in Islamic lands: myth and reality. *Social history of medicine : the journal of the Society for the Social History of Medicine / SSHM*, 13(2), pp.307–321.

Schuster, R. et al., 2000. Electrochemical Micromachining. *Science*, 289, pp.98–101.

Semiconductor, No Titl. *Dictionary.com*. Available at: http://www.dictionary.com/browse/semiconductor.

Sharma, S., Jain, V.K. & Shekhar, R., 2002. Electrochemical drilling of inconel superalloy with acidified sodium chloride electrolyte. *International Journal of Advanced Manufacturing Technology*, 19(7), pp.492–500.

Shriver, D.F. et al., 2006. Semiconductor Chemistry. In *Inorganic Chemistry*. Oxford: W. H. Freeman and Company, pp. 588–642.

Da Silva Neto, J.C., Da Silva, E.M. & Da Silva, M.B., 2006. Intervening variables in electrochemical machining. *Journal of Materials Processing Technology*, 179(1-3), pp.92–96.

De Silva, A.K.M., Altena, H.S.J. & McGeough, J.A., 2003. Influence of Electrolyte Concentration on Copying Accuracy of Precision-ECM. *CIRP Annals - Manufacturing Technology*, 52(1), pp.165–168.

Simon, P. & Ihlemann, J., 1996. Machining of submicron structures on metals and semiconductors by ultrashort UV-laser pulses. *Applied Physics A-Materials Science & Processing*, 63(5), pp.505–508.

Singh, D. et al., 2008. Development of Electrochemical Micromachining (ECMM) Setup. , pp.1–130. Available at: https://www.academia.edu/1407899/Development_of_Electrochemical_ Micromachining_Table_Top_Machine_Set_Up [Accessed February 10, 2015].

Sjöström, T. & Su, B., 2011. Micropatterning of titanium surfaces using electrochemical micromachining with an ethylene glycol electrolyte. *Materials Letters*, 65(23-24), pp.3489–3492.

Skoczypiec, S., 2011. Research on ultrasonically assisted electrochemical machining process. *International Journal of Advanced Manufacturing*

Technology, 52(5-8), pp.565–574.

Smets, N. et al., 2010. Time averaged calculations in Pulse Electrochemical Machining, using a strongly non-linear model. *Journal of Applied Electrochemistry*, 40(7), pp.1395–1405.

Spieser, A., 2015. *Development of an Electrochemical Micromachining (µECM) machine*. Brunel University.

Stafford, R.J., 2003. High Field MRI : Technology, Applications, Safety and Limitations. , pp.1–5.

Statista, 2014. Global Electronics Industry - market size by country. *Welt-Elektromarkt - Ausblick bis 2015*. Available at: http://www.statista.com/statistics/268398/market-size-of-the-global-electronics-industry-by-country/.

Sun, J.J., Taylor, E.J. & Srinivasan, R., 2001. MREF-ECM process for hard passive materials surface finishing. *Journal of Materials Processing Technology*, 108(3), pp.356–368.

Tandon, S. et al., 1990. Experimental Investigations into Electrochemical Spark Machining of Composites. *Precision Engineering*, 12(4), pp.227–238.

Technische Universitat Munchen, 2015. An introduction to semiconductors. Available at: http://www.wsi.tum.de/Institute/Scientificbackground/AnIntroductiontoSemiconductors/tabid/65/Default.aspx [Accessed January 20, 2016].

Tian, Z. et al., 1992. Confined etchant layer technique for two-dimensional lithography at high resolution using electrochemical scanning tunnelling microscopy. *Faraday Discussions*, 94(i), p.37. Available at: http://xlink.rsc.org/?DOI=fd9929400037.

Trimmer, A.L. et al., 2003. Single-step electrochemical machining of complex

nanostructures with ultrashort voltage pulses. *Applied Physics Letters*, 82(19), pp.3327–3329.

Vian, C.J.B., Birkin, P.R. & Leighton, T.G., 2010. Cluster Collapse in a Cylindrical Cell: Correlating Multibubble Sonoluminescence, Acoustic Pressure, and Erosion. *The Journal of Physical Chemistry C*, 114(39), pp.16416–16425.

Vita Needle Company, HYPODERMIC TUBE GAUGE CHART. Available at: http://www.vitaneedle.com/hypodermic-tube-gauge-chart.htm [Accessed July 31, 2015].

Vortex Business Solutions, 2013. Superconductor Week. Available at: http://www.superconductorweek.com/what-is-superconductivity [Accessed January 20, 2015].

Wagner, T., 2002. *High Rate Electrochemical Dissolution of Iron- Based Alloys in NaCl and NaNO3 Electrolytes*. Universitat Stuttgart.

Walton, D.J., 2002. Sonoelectrochemistry – the application of ultrasound to electrochemical systems. *Arkivoc*, 3, pp.198–218.

Wang, M. et al., 2010. Electrochemical machining of the spiral internal turbulator. *International Journal of Advanced Manufacturing Technology*, 49(9-12), pp.969–973.

Wang, Y. et al., 2010. Development of a Soft-Computer Numerical Control System for Micro-Electrochemical Machining. *American Journal of Nanotechnology*, 1(2), pp.51–55.

Wang, Y. et al., 2013. The Needle With Lancet Point: Geometry for Needle Tip Grinding and Tissue Insertion Force. *Journal of Manufacturing Science and Engineering*, 135(4), p.041010.

Wendt, H. & Kreysa, G., 2013. *Electrochemical Engineering: Science and Technology in Chemical and Other Industries*, Springer Science &

Business Media.

Wika, S.F., 2012. Pitting and Crevice Corrosion of Stainless Steel under Offshore Conditions. , (July), p.79.

Wu, M.K. et al., 1987. superconductivity at 93 K in a new mixed phase Y-Ba-Cu-O compound system at ambient pressure. *Physical Review Letters*, 58(9), pp.908–910.

Wu, X. et al., 2013. Modelling of the liquid membrane electrochemical etching of a nano-tip. *International Journal of Advanced Manufacturing Technology*, 69(1-4), pp.723–729.

Xu, K. et al., 2015. Study of Surface Roughness in Wire Electrochemical Micro Machining. *Journal of Materials Processing Technology*, 222, pp.103–109.

Yeager, E., 1953. Ultrasonic Waves and Electrochemistry. I. A Survey of the Electrochemical Applications of Ultrasonic Waves. *The Journal of the Acoustical Society of America*, 25(3), pp.443–455.

Zeng, Z. et al., 2012. A study of micro-EDM and micro-ECM combined milling for 3D metallic micro-structures. *Precision Engineering*, 36(3), pp.500–509.

Zhang, P.F. et al., 2008. Mechanical Drilling Processes for Titanium Alloys: a Literature Review. *Machining Science and Technology*, 12(4), pp.417–444.

Zhang, Y., 2010. *Investigation Into Current Efficiency for Pulse Electrochemical Machining of Nickel Alloy*. University of Nebraska - Lincoln. Available at: http://digitalcommons.unl.edu/imsediss/2.

Zhang, Z. et al., 2011. A Micro-machining system based on electrochemical dissolution of material. *Russian Journal of Electrochemistry*, 47(7), pp.819–824.

Zhu, D. & Xu, H.Y., 2002. Improvement of electrochemical machining accuracy by using dual pole tool. *Journal of Materials Processing Technology*, 129(1-3), pp.15–18.